USGS
science for a changing world

Land Subsidence Along the California Aqueduct in West-Central San Joaquin Valley, California, 2003–10

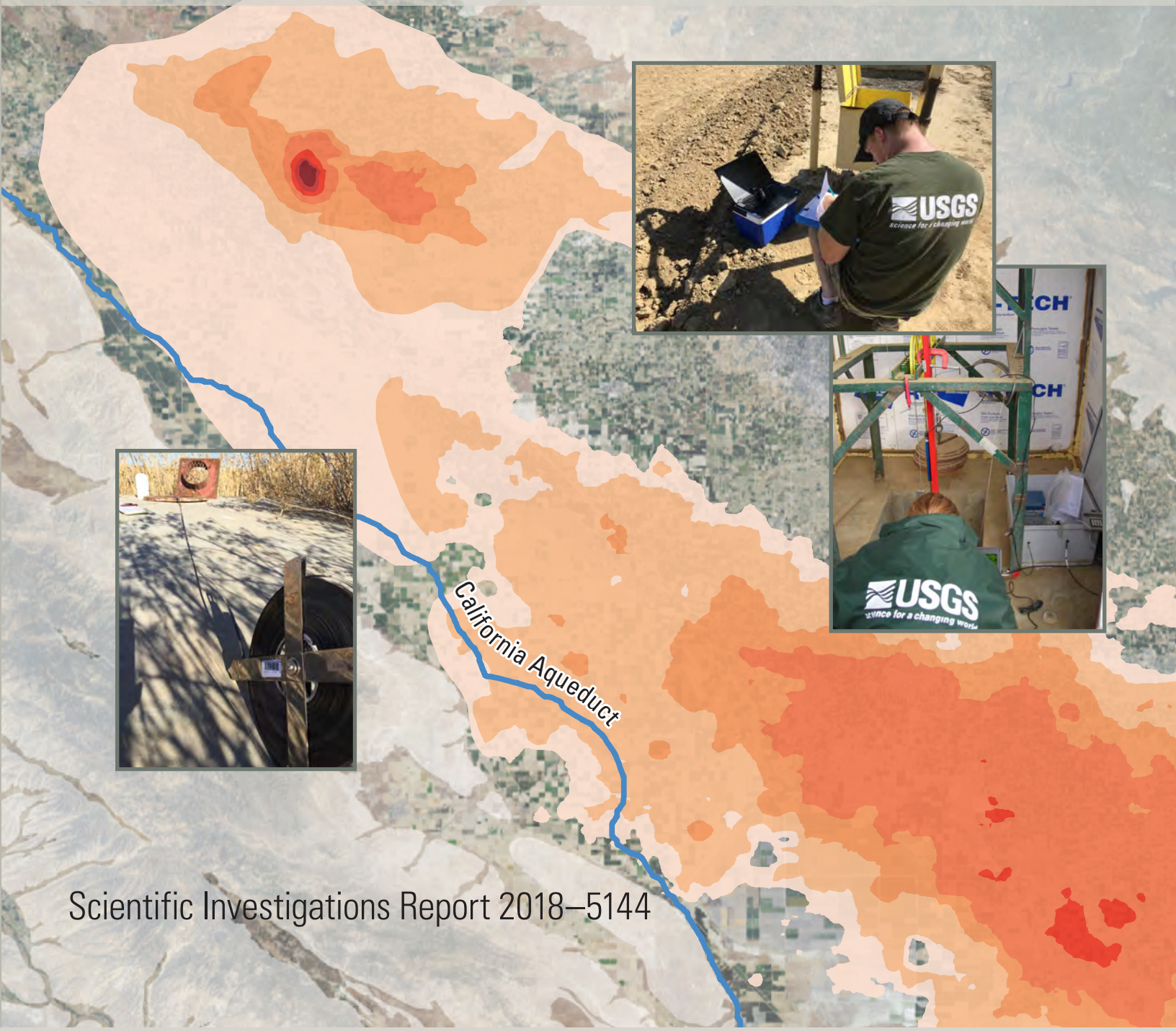

Scientific Investigations Report 2018–5144

U.S. Department of the Interior
U.S. Geological Survey

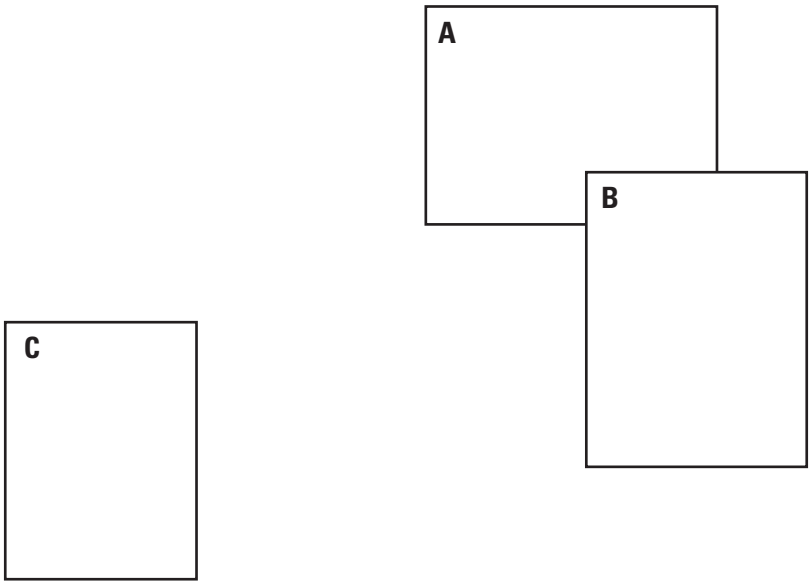

FRONT COVER:

A: Photograph showing U.S. Geological Survey (USGS) scientist inspecting well 12S/12E-16H5. Photograph by Michelle Sneed, USGS, 2018.

B: Photograph showing USGS scientist inspecting extensometer/well 20S/18E-6D1. Photograph by Claudia Faunt, USGS, 2012.

C: Photograph showing groundwater-level measurement using a calibrated steel tape at well 14S/15E-5J1. Photograph by Michelle Sneed, USGS, 2017.

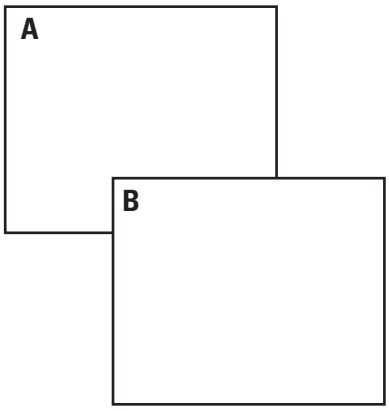

BACK COVER:

A: Photograph showing the California Aqueduct. Photograph by Michelle Sneed, USGS, 2015.

B: Photograph showing the California Aqueduct. Photograph by Michelle Sneed, USGS, 2017.

Land Subsidence Along the California Aqueduct in West-Central San Joaquin Valley, California, 2003–10

By Michelle Sneed, Justin T. Brandt, and Mike Solt

Prepared in cooperation with the California Department of Water Resources

Scientific Investigations Report 2018–5144

U.S. Department of the Interior
U.S. Geological Survey

U.S. Department of the Interior
RYAN K. ZINKE, Secretary

U.S. Geological Survey
James F. Reilly II, Director

U.S. Geological Survey, Reston, Virginia: 2018

Suggested citation:
Sneed, M., Brandt, J.T., and Solt, M., 2018, Land subsidence along the California Aqueduct in west-central San Joaquin Valley, California, 2003–10: U.S. Geological Survey Scientfic Investigations Report 2018–5144, 67 p., https://doi.org/10.3133/sir20185144.

ISSN 2328-0328 (online)

Acknowledgments

This study was done in cooperation with the California Department of Water Resources; the authors gratefully acknowledge their support and assistance during this study. We thank the University NAVSTAR (Navigation Satellite Timing and Ranging) Consortium (UNAVCO) for allowing free access to continuous Global Positioning System data. Radar data used to produce the interferograms shown in this report were acquired by the European Space Agency and the Japanese Aerospace Exploration Agency and distributed by Western North America Interferometric Synthetic Aperture Radar Consortium, GeoEarthScope, and the Alaska Synthetic Aperture Radar Facility for purposes of research and development. Geodetic surveys along Highways 152 and 198 were done by the California Department of Transportation and the National Geodetic Survey. The Global Positioning System surveys along the California Aqueduct were done by the California Department of Water Resources. Extensometer data from 13S/15E-31J17 (Fordel) and water-level data from wells 13S/15E-31J3 and 13S/15E-31J6 were provided by Luhdorff and Scalmanini Consulting Engineers. Extensometer and water-level data from other sites were obtained from the U.S. Geological Survey and California Department of Water Resources databases and Westlands Water District.

Contents

Contents—Continued

Figures

Figures—Continued

Figures—Continued

Tables

Conversion Factors

International System of Units to U.S. customary units

Multiply	By	To obtain
	Length	
millimeter (mm)	0.03937	inch (in.)
meter (m)	3.281	foot (ft)
kilometer (km)	0.6214	mile (mi)
meter (m)	1.094	yard (yd)
	Area	
square kilometer (km^2)	247.1	acre
square kilometer (km^2)	0.3861	square mile (mi^2)
	Flow rate	
millimeter per year (mm/yr)	0.03937	inch per year (in/yr)

Temperature in degrees Celsius (°C) may be converted to degrees Fahrenheit (°F) as

$$°F = (1.8 \times °C) + 32.$$

Datums

Horizontal coordinate information is referenced to the North American Datum of 1983 (NAD 83). Vertical coordinate information is referenced to the World Geodetic System of 1984 (WGS 84). Altitude, as used in this report, refers to distance above the vertical datum.

Abbreviations

ALOS	Advanced Land Observing Satellite
CCID	Central California Irrigation District
CGPS	continuous Global Positioning System
DMC	Delta-Mendota Canal
DWR	California Department of Water Resources
ENVISAT	Environmental Satellite
ESA	European Space Agency
FWA	Friant Water Authority
GPS	Global Positioning System
InSAR	Interferometric Synthetic Aperture Radar
ISRO	Indian Space Research Organization
MODIS	Moderate Resolution Imaging Spectroradiometer
NASA	National Aeronautics and Space Administration
NAVSTAR	Navigation Satellite Timing and Ranging
PBO	Plate Boundary Observatory
PS	persistent scatterer
Reclamation	Bureau of Reclamation
SAR	Synthetic Aperture Radar
SGMA	Sustainable Groundwater Management Act
SLDMWA	San Luis and Delta-Mendota Water Authority
UNAVCO	University Navigation Satellite Timing and Ranging Consortium
USGS	U.S. Geological Survey

Well-Numbering System

Wells are identified and numbered according to their location in the rectangular system for the subdivision of public lands. Identification consists of the township number, north or south; the range number, east or west; and the section number. Each section is divided into sixteen 40-acre tracts lettered consecutively (except I and O), beginning with "A" in the northeast corner of the section and progressing in a sinusoidal manner to "R" in the southeast corner. Within the 40-acre tract, wells are sequentially numbered in the order they are inventoried. The final letter refers to the base line and meridian. In California, there are three base lines and meridians: Humboldt (H), Mount Diablo (M), and San Bernardino (S). All wells in the study area are referenced to the Mount Diablo base line and meridian (M). Well numbers consist of 15 characters and follow the format 001S004E10B002M. In this report, well numbers are abbreviated and written 1S/4E-10B2. The following diagram shows how the number for well 001S004E10B002M is derived.

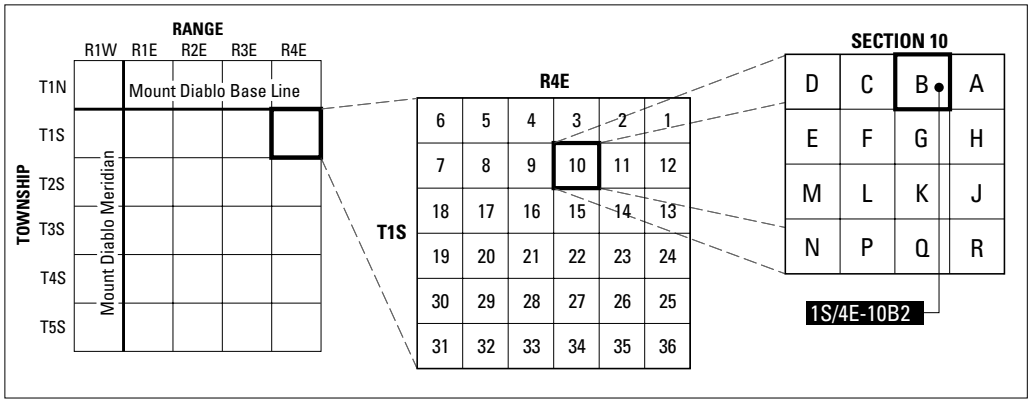

Land Subsidence Along the California Aqueduct in West-Central San Joaquin Valley, California, 2003–10

By Michelle Sneed, Justin T. Brandt, and Mike Solt

Abstract

Extensive groundwater withdrawal from the unconsolidated deposits in the San Joaquin Valley caused widespread aquifer-system compaction and resultant land subsidence from 1926 to 1970—locally exceeding 8.5 meters. The importation of surface water beginning in the early 1950s through the Delta-Mendota Canal and in the early 1970s through the California Aqueduct resulted in decreased groundwater pumping, recovery of water levels, and a reduced rate of compaction in some areas of the San Joaquin Valley. However, drought conditions during 1976–77, 1987–92, and drought conditions and operational reductions in surface-water deliveries during 2007–10 decreased surface-water availability, causing pumping to increase, water levels to decline, and renewed compaction. Land subsidence from this compaction has reduced freeboard and flow capacity of the California Aqueduct, Delta-Mendota Canal, and other canals that deliver irrigation water and transport floodwater.

The U.S. Geological Survey, in cooperation with the California Department of Water Resources, assessed more recent land subsidence near a 145-kilometer reach of the California Aqueduct in the west-central part of the San Joaquin Valley as part of an effort to minimize future subsidence-related damages to the California Aqueduct. The location, magnitude, and stress regime of land-surface deformation during 2003–10 were determined by using data and analyses associated with extensometers, Global Positioning System surveys, Interferometric Synthetic Aperture Radar, spirit-leveling surveys, and groundwater wells. Comparison of continuous Global Positioning System, shallow-extensometer, and groundwater-level data indicated that most of the compaction in this area took place beneath the Corcoran Clay, the primary regional confining unit. The integration of measurements strengthens confidence in individual measurement methods and provides the information at spatial and temporal scales that water managers need to design and implement groundwater sustainability plans in compliance with California's Sustainable Groundwater Management Act.

Measurements of land-surface deformation during 2003–10 indicated that the parts of the California Aqueduct closest to the Coast Ranges in the west-central part of the San Joaquin Valley were fairly stable or minimally subsiding on an annual basis; some areas show seasonal periods of subsidence and uplift that resulted in little or no longer-term elevation loss. Many groundwater levels in these areas did not reach historical lows during 2003–10, indicating that deformation nearest the Coast Ranges was likely primarily elastic.

Land-surface deformation measurements indicated that some parts of the California Aqueduct that traverse farther from the Coast Ranges toward the valley center subsided. Some parts of the California Aqueduct subsided locally, but generally the California Aqueduct is within part of a 12,000-square-kilometer area affected by 25 millimeters or more of subsidence during 2008–10, with maxima in Madera County, south of the town of El Nido near the San Joaquin River and the Eastside Bypass (540 millimeters), and in Tulare County, west of the town of Pixley (345 millimeters). Interferometric Synthetic Aperture Radar-derived subsidence maps for various periods during 2003–10 show that the area of maximum active subsidence (that is, the largest rates of subsidence) shifted from its historical (1926–70) location southwest of the town of Mendota to these areas nearer the valley center. Calculations indicated that the subsidence rate doubled in 2008 in parts of the study area. Water levels declined during 2007–10 in many shallow and deep wells in the most rapidly subsiding areas, where water levels in many deep wells reached their historical lows, indicating that subsidence measured during this period was largely inelastic.

Continued groundwater-level and land-subsidence monitoring in the San Joaquin Valley is important because (1) operational- and drought-related reductions in surface-water deliveries since 1976 have resulted in increased groundwater pumping and associated water-level declines and land subsidence, (2) land use and associated pumping continue to change throughout the valley, and (3) subsidence management is stipulated in the Sustainable Groundwater Management Act. The availability of surface water remains uncertain; even during record-setting precipitation years, such as 2010–11, water deliveries fell short of requests and groundwater pumping was required to meet the irrigation demand. In some areas, the infrastructure is not available to supply surface water, and groundwater is the only source of water. Because of the expected continued demand for water and the limitations and uncertainty of surface-water supplies, groundwater pumping and associated land subsidence remains a concern. Spatially detailed information on land subsidence is needed to minimize future subsidence-related damages to the California Aqueduct and other infrastructure in the San Joaquin Valley, as well as alterations to natural resources such as stream gradients, water depths, and water temperatures. The integration of data on land-surface elevation, subsurface deformation, and water levels—particularly continuous measurements—enables the analysis of aquifer-system response to groundwater pumping, which in turn, enables estimation of the preconsolidation head and calculation of aquifer-system storage properties. This information can be used to improve numerical model simulations of groundwater flow and aquifer-system compaction and allow for consideration of land subsidence in the evaluation of water resource management alternatives and compliance with the Sustainable Groundwater Management Act.

Introduction

The San Joaquin Valley (valley) is a 400-kilometer (km) long, broad structural trough constituting the southern two-thirds of the Central Valley of California. The alluvium-filled valley averages 65 km in width and covers 26,000 square kilometers (km^2), excluding the rolling foothills of the Sierra Nevada, Tehachapi Mountains, and the Coast Ranges that skirt the valley on three sides. The study area includes the west-central part of the valley from near Oro Loma on the north to Kettleman City on the south, but necessarily includes adjacent areas owing to the regional nature of subsidence (fig. 1).

The extensive withdrawal of groundwater from the unconsolidated alluvial deposits has caused widespread land subsidence—locally exceeding 8.5 meters (m) between 1926 and 1970 (Poland and others, 1975; fig. 2) and reaching 9 m by 1981 (Ireland, 1986). Long-term groundwater-level declines can result in a vast one-time release of "water of compaction" from compacting silt and clay layers (aquitards), which causes land subsidence (Galloway and others, 1999). Land subsidence from groundwater pumping began in the mid-1920s (Poland and others, 1975; Bertoldi and others, 1991; Galloway and Riley, 1999), and by 1970, about half of the San Joaquin Valley, or about 13,500 km^2, was affected by land subsidence of more than 0.3 m (Poland and others, 1975; fig. 2).

Surface-water imports from the Central Valley Project's Delta-Mendota Canal (DMC) since the early 1950s and the State Water Project's California Aqueduct since the early 1970s resulted in a decrease of groundwater pumping, which was accompanied by a steady recovery of water levels and a reduced rate of compaction in the western part of the valley. During the droughts of 1976–77 and 1987–92 (California Department of Water Resources, 1998), diminished deliveries of imported surface water prompted increased pumping of groundwater to meet irrigation demands. This increased groundwater pumping resulted in water-level declines and periods of renewed compaction. Following each of these droughts, recovery to pre-drought water levels was rapid, and compaction virtually ceased (fig. 3; Swanson, 1998; Galloway and others, 1999).

During 2007–10, groundwater pumping again increased because of reduced Central Valley Project and State Water Project surface-water deliveries. Surface-water deliveries through the Central Valley Project were limited to 10–75 percent of requested supplies for agricultural and urban contractors in the San Joaquin Valley; deliveries through the State Water Project were limited to 35–60 percent of requested supplies for agricultural, municipal, industrial, and environmental uses during this period. The climatic drought was terminated by the near-average 2009–10 winter; however, 2010 Central Valley Project surface-water deliveries were still 45–75 percent of that requested in the San Joaquin Valley, and State Water Project surface-water deliveries were 50 percent of requested amounts (accessed December 2, 2015, at https://www.usbr.gov/mp/cvo/vungvari/water_allocations_historical.pdf; accessed July 5, 2018, at http://wdl.water.ca.gov/swpao/deliveries.cfm). Replenishment of depleted surface reservoirs was a primary cause of reduced deliveries in 2010. Because aquifer systems respond to increased pumping regardless of the reason for the increase, this drought period is referred to as 2007–10 in this report. Groundwater levels declined during 2007–10 in response to this increased pumping, approaching or surpassing historical low levels in some areas, such as at well 13S/15E-31J6 near Mendota, which reinitiated compaction in some areas, as shown at continuous Global Positioning System (CGPS) station P304 (fig. 4).

Following the historically wet winter of 2010–11, Central Valley Project and State Water Project surface-water deliveries in 2011 were still only 80 percent of requested supplies for agricultural contractors (accessed July 5, 2018, at https://www.usbr.gov/mp/cvo/vungvari/water_allocations_historical.pdf; accessed July 5, 2018, at http://wdl.water.ca.gov/swpao/deliveries.cfm), indicating that substantial groundwater pumping could continue during dry and wet climatic conditions.

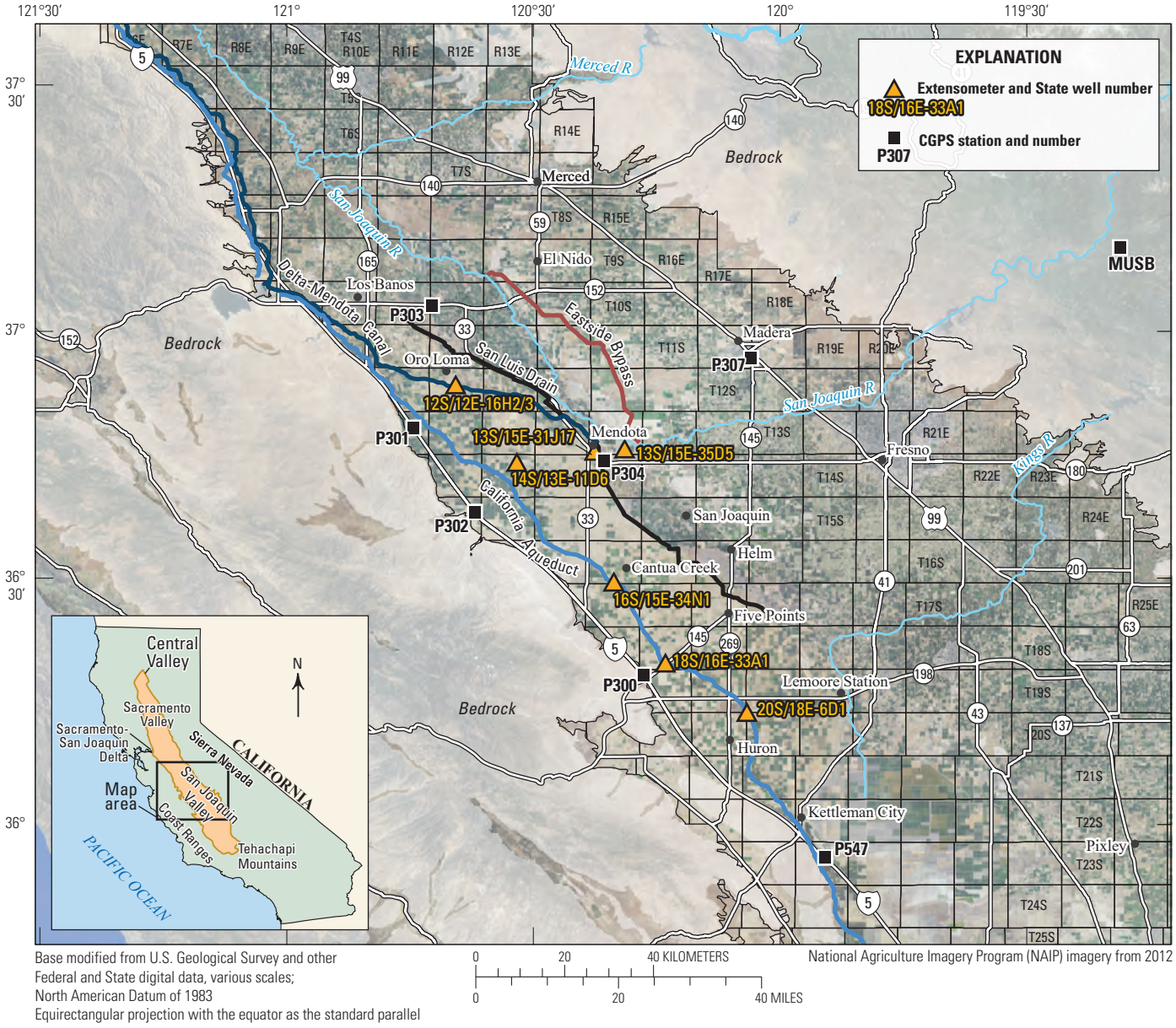

Figure 1. Location and geographic features of the study area and the locations of selected continuous Global Positioning System (CGPS) stations and extensometers, San Joaquin Valley, California.

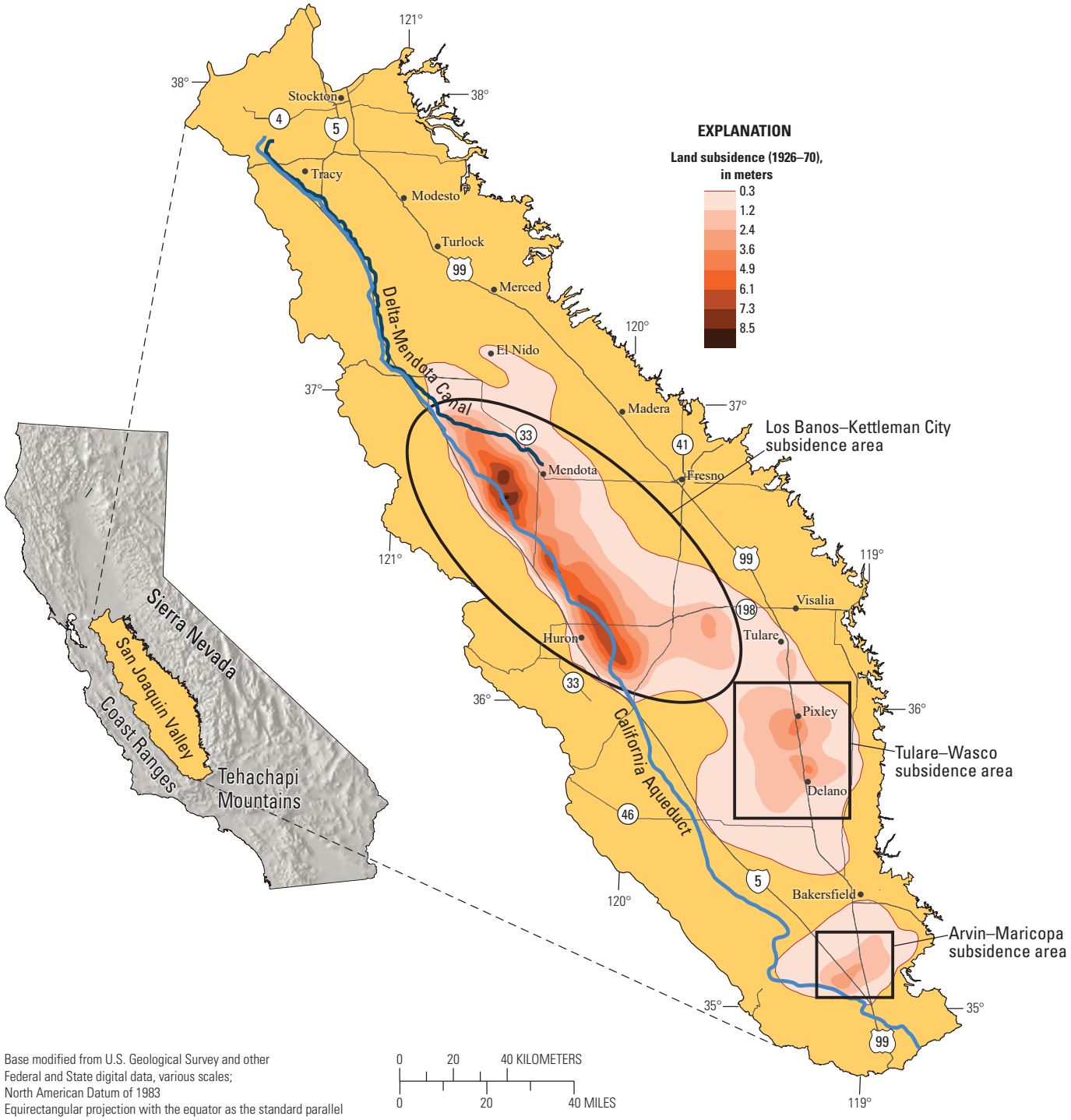

Figure 2. Land subsidence in the San Joaquin Valley, California, 1926–70 (modified from Ireland and others, 1984).

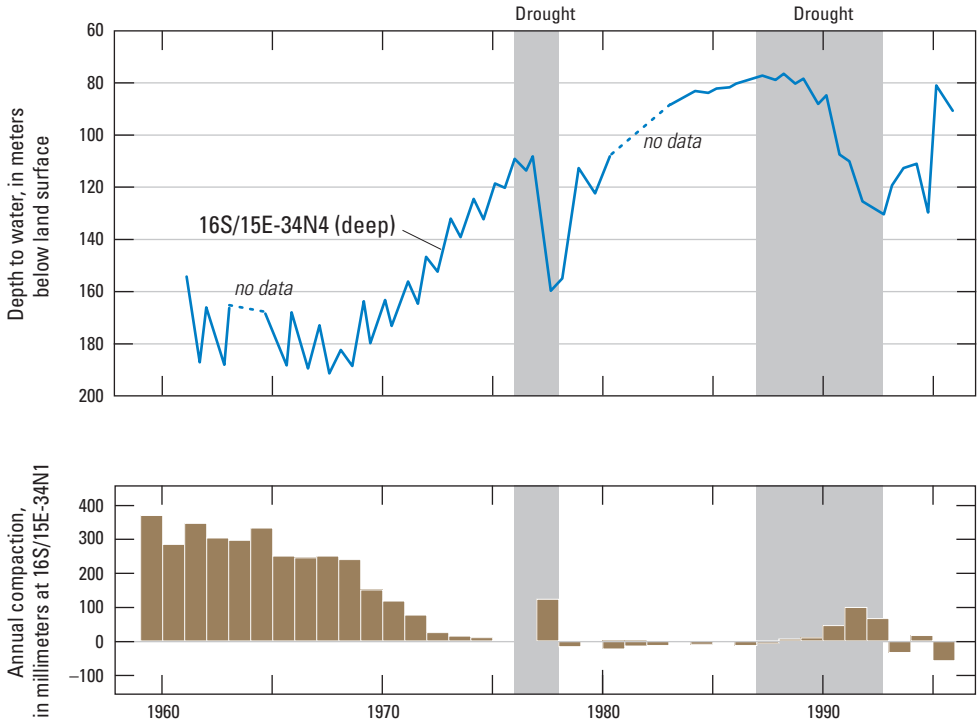

Figure 3. Water levels and annual compaction in observation well 16S/15E-34N4 and extensometer 16S/15E-34N1, respectively, near Cantua Creek, San Joaquin Valley, California, 1959–95 (modified from Swanson, 1998; Galloway and others, 1999). The periods shaded represent calendar years affected by increased pumping because of drought periods. See figure 1 for location.

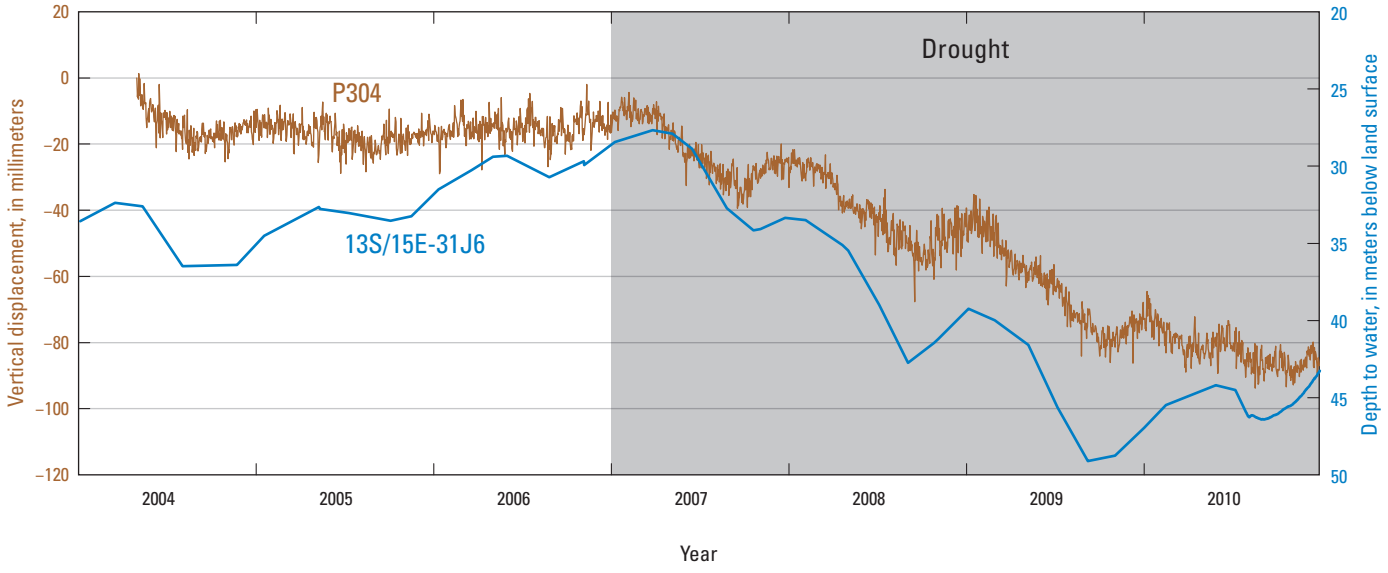

Figure 4. Discretely measured water levels in well 13S/15E-31J6, screened below the Corcoran Clay Member of the Tulare Formation, and daily vertical displacement at continuous Global Positioning System (CGPS) station P304 near Mendota, California, 2004–10. Well 13S/15E-31J6 data before May 1, 2010, were obtained from Luhdorff and Scalmanini Consulting Engineers (Debbie Cannon, Luhdorff and Scalmanini Consulting Engineers, written commun., 2013), and well 13S/15E-31J6 data after May 1, 2010, were obtained from the U.S. Geological Survey (accessed July 5, 2018, at https://waterdata.usgs.gov/ca/nwis/nwis). Station P304 daily data were obtained from the University NAVSTAR (Navigation Satellite Timing and Ranging) Consortium. The period shaded represents calendar years affected by increased pumping during 2007–10. Negative values of vertical displacement indicate relative subsidence and positive values indicate relative uplift.

Groundwater pumping that results in renewed compaction and land subsidence could cause serious operational, maintenance, and construction-design problems for the California Aqueduct, the Delta-Mendota Canal, and other water-delivery and flood-control canals in the San Joaquin Valley. Subsidence has reduced the flow capacity of several canals that deliver irrigation water to farmers and transport floodwater out of the valley. For example, several parts of the California Aqueduct, managed by the California Department of Water Resources (DWR), and canals managed by the San Luis and Delta-Mendota Water Authority (SLDMWA), the Central California Irrigation District (CCID), and the Friant Water Authority (FWA) have had reduced freeboard and structural damages that have required millions of dollars to repair, and more repairs are expected in the future (Bob Martin, SLDMWA, oral commun., 2010; Chris White, CCID, oral commun., 2010; David Rennie, DWR, written commun., 2014; Doug DeFlitch, FWA, written commun., 2017). When surface water has been plentiful such as during 2017, the reduced conveyance capacities of canals owing to subsidence may hinder the ability to deliver it, as has occurred in the Friant-Kern Canal (Doug DeFlitch, Friant Water Authority, written commun., 2017, accessed July 27, 2017, at http://www.recorderonline.com/news/friant-kern-canal-sinking-raising-concerns/article_e6a64238-6e8c-11e7-a789-13522266756d.html).

Purpose and Scope

In 2009, the U.S. Geological Survey (USGS), in cooperation with the California Department of Water Resources (DWR), initiated a study to assess land subsidence near the California Aqueduct (Aqueduct) in the west-central San Joaquin Valley as part of an effort to minimize future subsidence-related damages to the Aqueduct. The purpose of this report is to present the status of land subsidence, compaction, and water-level trends along the Aqueduct and adjacent areas in the west-central San Joaquin Valley from 2003 through 2010. Measured groundwater-level changes during 2003–10 were examined and compared with measurements of compaction and land subsidence to evaluate their relation, including determinations of stress-strain regimes (elastic or inelastic). Updated water-level, compaction, and subsidence data are presented in a historical context.

The focus of this report is subsidence caused by water-level decline and consequent compaction of aquifer systems, which is the dominant mechanism of subsidence in the valley. However, it is possible that a small portion of the subsidence discussed in this report was caused by one or more additional processes, including hydrocompaction of moisture-deficient deposits above the water table, fluid withdrawal from oil and gas fields, and deep-seated tectonic movements (Galloway and others, 1999).

Subsidence-related data and analyses presented in this report include Global Positioning System (GPS) data, spirit-leveling surveys, extensometer data, and Interferometric Synthetic Aperture Radar (InSAR) analyses. The GPS and spirit-leveling survey data were collected by many parties at various spatial and temporal scales. The extensometer data were collected by the USGS, DWR, SLDMWA, and Luhdorff and Scalmanini Consulting Engineers. The InSAR maps showing land-surface deformation for various time spans were generated by the USGS.

Description of Study Area

The San Joaquin Valley of California covers about 26,000 km^2 and represents the southern part of the Central Valley. Centrally located in California, the San Joaquin Valley is bounded by the Sacramento–San Joaquin Delta and Sacramento Valley on the north, the Sierra Nevada on the east, the Tehachapi Mountains on the south, and the Coast Ranges on the west (fig. 1). Generally, the land surface has very low relief; its configuration is the result of millions of years of alluvial and fluvial deposition of sediments derived from the bordering mountain ranges and deposited by the San Joaquin River and its tributaries. Most of the valley lies close to sea level, but elevation increases along the valley margins; along the eastern edge, the land surface is about 150 m above sea level, and most of the western boundary ranges from 15 to 110 m above sea level (Faunt, 2009). The geographic area of focus in this report is where the California Aqueduct traverses the west-central San Joaquin Valley, from about Oro Loma to Kettleman City (fig. 1). The area of focus contains several population centers, the largest of which are the cities of Mendota (population of 11,000) and Huron (population of 6,700), and many smaller communities are distributed throughout the region (accessed January 2, 2018, at https://www.census.gov/quickfacts/fact/table/US/PST045217). More than two-thirds of the region is dominated by agricultural land uses, including permanent and seasonal crops.

Climate in the study area is arid to semiarid and is characterized by hot, dry summers and damp, mild winters, when the area frequently is covered by a ground fog known regionally as “tule fog.” Precipitation during an average year ranges from 125 to 250 millimeters (mm; PRISM Climate Group, 2006). Dramatic deviations from average climatic conditions are manifested as droughts or floods, with most of the San Joaquin Valley prone to flooding. About 85 percent of the precipitation falls during November through April, half of it during December through February on average (PRISM Climate Group, 2006).

Surface water is used in the San Joaquin Valley when it is available; essentially all natural flows in area streams are diverted for agricultural and municipal use (Moore and others, 1990; Faunt, 2009). The valley also relies heavily on groundwater, which accounts for about 30 percent of the annual supply for agricultural and urban purposes (California Department of Water Resources, 2003; Faunt, 2009).

Percentages of surface water and groundwater that constitute the annual supply are not well understood in the study area; however, results from the Central Valley Hydrologic Model indicated that during periods of drought, the groundwater usage constitutes at least half of the annual supply and as much as about 90 percent after several drought years (Faunt, 2009).

Previous Land-Subsidence Studies

Land subsidence in the San Joaquin Valley was documented in the many reports generated as part of the cooperative subsidence program during 1956–86 by the USGS and the DWR. These reports include the widely cited USGS Professional Paper Series 437 A–I (Bull, 1964; Lofgren and Klausing, 1969; Bull, 1972; Bull, 1975; Bull and Miller, 1975; Bull and Poland, 1975; Lofgren, 1975; Poland and others, 1975; Ireland and others, 1984), collectively referred to as "the Poland Reports," after Dr. Joseph F. Poland, who led the program, and USGS Professional Paper Series 497 A–E and G (Meade, 1964; Meade, 1967; Johnson and others, 1968; Meade, 1968; Riley, 1970; Miller and others, 1971). An additional report was published as part of the proceedings from the "Dr. Joseph F. Poland Symposium on Land Subsidence," held in 1995; this report (Swanson, 1998) provides a brief update of land subsidence in the San Joaquin Valley from the early 1980s through 1995, when subsidence data collection in the valley was sharply reduced; the downscaled monitoring effort focused on selected extensometers and surveys along the California Aqueduct and other important canals.

The previous reports described three areas of subsidence: (1) Los Banos–Kettleman City, (2) Tulare-Wasco, and (3) Arvin-Maricopa (fig. 2). This report focuses on an area very similar to the Los Banos–Kettleman City area, but includes areas to the east, in the vicinities of Madera and Pixley. A report describing hydraulic and mechanical properties affecting groundwater flow and aquifer-system compaction in the San Joaquin Valley (Sneed, 2001) was produced to constrain the WESTSIM model by the Bureau of Reclamation (Reclamation), which was used to evaluate potential land subsidence under selected hydrologic conditions (Quinn and Faghih, 2008). Subsidence detected using InSAR analysis was described for selected areas and periods during the 1990s (Brandt and others, 2005). Reports by Williamson and others (1989) and Faunt (2009) documented numerical models of the hydrologic landscape and groundwater flow in the Central Valley, which also incorporated subsidence observations to constrain subsidence simulations. A report by Sneed and others (2013) documented subsidence along the Delta-Mendota Canal in the northern part of the San Joaquin Valley during 2003–10; the southern study-area extent of that report overlaps the northern study-area extent of this report. Luhdorff and Scalmanini Consulting Engineers and others (2014) summarized much of the subsidence findings in the San Joaquin Valley as part of a larger body of work summarizing subsidence knowledge in California. Farr and others (2015; 2016) released preliminary progress reports describing the InSAR analyses used to map subsidence in the San Joaquin Valley, including parts of the California Aqueduct for periods during 2007–16.

Hydrogeologic Framework

This section describes the hydrogeologic framework of the San Joaquin Valley. A description of the geology and aquifer system is given along with a summary of groundwater dynamics and land subsidence. A more detailed discussion of the geology of the Central Valley is given by Page (1986).

Geology and Aquifer System

The San Joaquin Valley is a major northwest-southeast structural trough formed as a down-warping fore-arc basin. Throughout Late Cretaceous (Mesozoic Era) and Tertiary (Cenozoic Era) Periods of geologic time, thousands of meters of shallow-water marine sediments were deposited in this basin. Overlying these marine deposits are continental deposits of late Cenozoic age. In aggregate, these marine and continental deposits thicken from east to west and from north to south. At the extreme southwestern part of the study area, the thickness of sediments reaches about 14,000 m (Wentworth and others, 2012).

The valley was formed chiefly by tectonic movement during the late Cenozoic (late Tertiary and Quaternary Periods) that included westward tilting of the Sierra Nevada block. Quaternary deformation has been principally along the southern and western borders of the valley, where the marine and continental rocks are tightly faulted and folded and the stream terraces are conspicuously elevated (Lofgren, 1976).

The sediments of the San Joaquin Valley compose an aquifer system comprising unconfined, semi-confined, and confined aquifers. Three distinct aquifers exist in much of the study area (fig. 5). In downward succession, these include (1) unconfined to semi-confined fresh water in alluvial deposits overlying a widespread lacustrine confining bed—the Corcoran Clay Member of the Tulare Formation (referred to in this report as the Corcoran Clay); (2) an extensive reservoir of fresh water confined beneath the Corcoran Clay in alluvial and lacustrine deposits; and (3) a body of saline water, contained primarily in marine sediments, that underlies the freshwater throughout the area (Page, 1986).

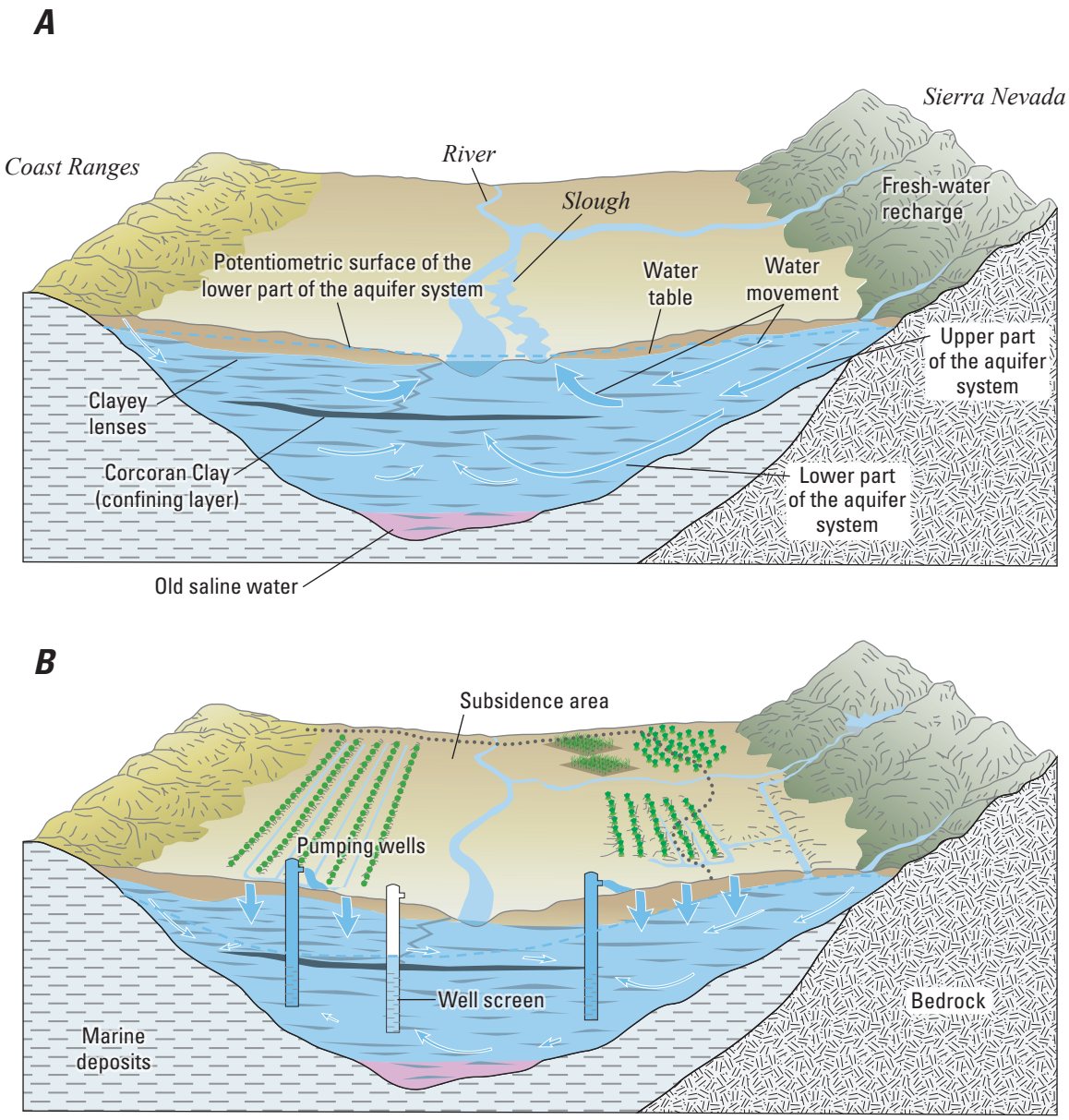

Figure 5. Relation of the Corcoran Clay Member of the Tulare Formation to younger and older alluvium and aquifers and groundwater-flow regimes in the San Joaquin Valley, California, for *A*, pre-development, and *B*, post-development (modified from Belitz and Heimes, 1990; Galloway and others, 1999; Faunt, 2009).

Numerous lenses of fine-grained sediments, which are highly compressible and account for nearly all aquifer-system compaction and resultant land subsidence, are distributed throughout the San Joaquin Valley and generally constitute more than 50 percent of the total thickness of the valley fill (Williamson and others, 1989). Generally, these lenses are not vertically extensive or laterally continuous; an exception is the Corcoran Clay, which was deposited during the Pleistocene when as much as 17,100 km^2 of the San Joaquin Valley was inundated by lakes (Page and Bertoldi, 1983; Farrar and Bertoldi, 1988). This diatomaceous clay is a low-permeability, areally extensive, lacustrine deposit (Johnson and others, 1968) that is as much as 60 m thick (Davis and others, 1959; Page, 1986).

Groundwater Levels and Movement

Groundwater levels and movement have responded to changes in the groundwater budget associated with development (fig. 5). Prior to development, natural discharge from the aquifer system was in a long-term dynamic equilibrium with natural recharge, and longer-term changes in groundwater storage were negligible (Planert and Williams, 1995). Groundwater from recharge areas along mountain fronts flowed downward and laterally toward the valley trough, where it flowed upward to areas of discharge along rivers and marshes (fig. 5*A*; Planert and Williams, 1995; Faunt, 2009). Precipitation that fell on the valley floor that was not consumed by evapotranspiration infiltrated and followed a similar path. During the early years of groundwater development, wells drilled into the deep aquifer in low-lying areas near rivers and marshes flowed by artesian pressure, owing to higher hydraulic head in the confined parts of the aquifer system (Faunt, 2009).

Well depths in the San Joaquin Valley are determined by the locations of permeable aquifer materials and by the local groundwater quality. In some areas, for example, wells are screened in lower parts of the aquifer system because of low-permeability materials and (or) poor-quality water in overlying parts of the aquifer system (Planert and Williams, 1995). The construction of thousands of irrigation wells, many of which have long intervals of screened casing, has increased the hydraulic connections between zones in the aquifer system compared to the predevelopment flow regime (Bertoldi and others, 1991). Where these wells are open above and below the Corcoran Clay, flow occurs through the boreholes between the unconfined, semi-confined, and confined parts of the aquifer system.

Groundwater withdrawal and the lowering of hydraulic heads in the confined parts of the aquifer system, by as much as about 150 m, have reversed the predevelopment flow regime between the upper and lower parts of the aquifer system in many areas (Bull and Miller, 1975; Poland and others, 1975; Ireland and others, 1984; Williamson and others, 1989; Galloway and Riley, 1999; Faunt, 2009). Furthermore, by the 1960s, irrigation had become the dominant source of recharge; this recharge generally maintained or raised the water table, resulting in increased downward flow in the system. Groundwater-level measurements and simulations (Faunt, 2009) indicated that seasonal fluctuations in the confined part of the aquifer system exceeded 100 m in places, whereas those at the water table generally were less than 1.5 m.

Surface-water imports began in the early 1950s using the DMC, and in the early 1970s using the California Aqueduct, which resulted in significantly reduced reliance on groundwater in some areas. The combined effect of increased availability of imported surface water and decreased groundwater pumping was a large-scale, rapid recovery of the water levels in the confined part of the aquifer system (fig. 3; Faunt, 2009). In some parts of the western San Joaquin Valley, groundwater levels in the confined part of the aquifer system recovered to pre-1960 levels, whereas groundwater levels in the unconfined system remained fairly high. Since the early 1970s, this water-level recovery has been interrupted primarily during periods when surface-water deliveries were curtailed because of climatic drought, such as during 1976–77, 1987–92, and 2007–10, or when additional operational requirements were implemented. During these periods, groundwater levels declined quickly with the onset of pumping, partly because of reduced aquifer-system storage capacity, which is described in the section "Mechanics of Pumping-Induced Land Subsidence" (figs. 3, 4; Faunt, 2009). A detailed history of changes in groundwater levels and movement is reported in Faunt (2009).

Land Subsidence

The extensive withdrawal of groundwater from the unconsolidated deposits of the San Joaquin Valley has caused widespread land subsidence—locally exceeding 8.5 m between 1926 and 1970 (fig. 2; Poland and others, 1975) and reaching 9 m by 1981 (Ireland, 1986). Long-term groundwater-level declines can result in a vast one-time release of "water of compaction" from compacting silt and clay interbeds (aquitards) and confining units, which causes land subsidence (Galloway and others, 1999). Several other types of subsidence have occurred in the San Joaquin Valley, including subsidence related to the hydrocompaction of moisture-deficient deposits above the water table, subsidence related to fluid withdrawal from oil and gas fields, subsidence caused by deep-seated tectonic movements, and subsidence caused by the oxidation of peat soils that is a major factor in the Sacramento–San Joaquin Delta. However, aquifer-system compaction caused by groundwater pumpage, the focus of this report, has caused the largest magnitude and areal extent of land subsidence in the San Joaquin Valley (Poland and others, 1975; Ireland and others, 1984; Farrar and Bertoldi, 1988; Bertoldi and others, 1991; Galloway and Riley, 1999). The San Joaquin Valley has been called "The largest human alteration of the Earth's surface" (Galloway and Riley, 1999).

Land subsidence from groundwater pumping began in the mid-1920s (Poland and others, 1975; Bertoldi and others, 1991; Galloway and Riley, 1999), and by 1970, there had been more than 0.3 m of land subsidence in about half of the San Joaquin Valley, or about 13,500 km^2 (Poland and others, 1975). The San Joaquin Valley contains three principal areas of subsidence caused by groundwater withdrawals as defined in the Poland Reports: (1) 6,215 km^2 in the Los Banos–Kettleman City area, (2) 3,680 km^2 in the Tulare-Wasco area, and (3) 1,815 km^2 in the Arvin-Maricopa area (Poland and others, 1975; Thomas and Phoenix, 1976; Ireland and others, 1984; fig. 2). The study area for this report is most similar to the Los Banos–Kettleman City area but extends eastward toward Madera and Pixley because of the regional nature of the subsidence. Leveling surveys and extensometer data indicated that most compaction has occurred below the bottom of the Corcoran Clay and that even the deepest extensometers have measured only a portion of the total land subsidence (Lofgren, 1961; Ireland and others, 1984). In the Los Banos–Kettleman City area, hydraulic head declines of more than 120 m in the confined part of the aquifer system caused the inelastic (permanent) compaction of the clayey beds, yielding a one-time release of "water of compaction"; this resulted in 9 m of land subsidence during 1926–81 and an associated loss of aquifer-system storage and storage capacity (Poland and others, 1975; Ireland and others, 1984; Ireland, 1986; Galloway and Riley, 1999). This one-time release of water of compaction was substantial; it is estimated that by the mid-1970s, about one-third of the volume of water pumped from storage in this area came from compaction of fine-grained beds (Poland and others, 1975; Williamson and others, 1989; Faunt, 2009). Although the largest body of clay is the Corcoran Clay, a relatively insignificant volume of water has been released from storage in the Corcoran Clay (Faunt, 2009), likely because of its large thickness and low permeability.

Subsidence was greatly slowed or arrested in the Los Banos–Kettleman City area after the importation of surface water (particularly through the California Aqueduct beginning in the early 1970s) and subsequent recovery of groundwater levels. The droughts of 1976–77, 1987–92, and 2007–10 resulted in diminished deliveries of imported water, increased pumping, rapid lowering of groundwater levels, and re-initiation of subsidence (figs. 3, 4; Swanson, 1998; Galloway and Riley, 1999; Sneed and others, 2013).

In addition to the loss of water and aquifer-system storage capacity from inelastic compaction, surficial environments such as wetlands and riparian corridors, generally found in the topographically lowest parts of the landscape, also can be affected by subsidence. Differential subsidence can alter stream gradients, water depths, and water temperatures, and can cause channel migration toward subsiding areas; wetlands could vanish or emerge in new locations. Although these effects have caused some concern, most of the attention regarding subsidence-related damages in the San Joaquin Valley has focused on engineered structures, including aqueducts, levees, dams, roads, bridges, pipelines, and well casings (Galloway and Riley, 1999; Luhdorff and Scalmanini Consulting Engineers and others, 2014). Important and expensive damages and repairs include the loss of conveyance capacity in canals that deliver water or remove floodwaters; the realignment of canals as their constant gradient becomes variable; the raising of infrastructure such as canal check stations, levees, and dams; and the releveling of furrowed fields, many of which are laser-leveled for maximum irrigation efficiency. (A check station is a structure built to control the water-surface level and flow in a canal).

The effects of a sag in a channel profile are increased flow velocity in the upstream end, decreased velocity in the middle, and loss of flow capacity immediately downstream of the sag. If the channel is unlined, such as the Eastside Bypass and the lower reaches of the DMC, or is a natural waterway, erosion may occur in the upstream end and deposition may occur in the subsided area. If the sag is deep, filling the channel with water to the top of the levee in the sag will not raise the water level enough to maintain the flow capacity downstream of the subsided reach. Owing to these sags in natural and engineered waterways, subsidence has increased the potential for, and severity of, flooding in low lying areas (Bertoldi, 1989; Faunt, 2009).

Mechanics of Pumping-Induced Land Subsidence

Land subsidence attributed to groundwater pumping occurs in many aquifer systems that are, at least in part, composed of unconsolidated fine-grained sediments and have undergone extensive groundwater development (Poland, 1984). The relation between changes in pore-fluid pressure and compression of the aquifer system is based on the principle of effective stress (Terzaghi, 1925):

$$\sigma_e = \sigma_T - \rho \quad (1)$$

where

σ_e is the effective or intergranular stress,
σ_T is the total stress or geostatic load, and
ρ is the pore-fluid pressure (fig. 6).

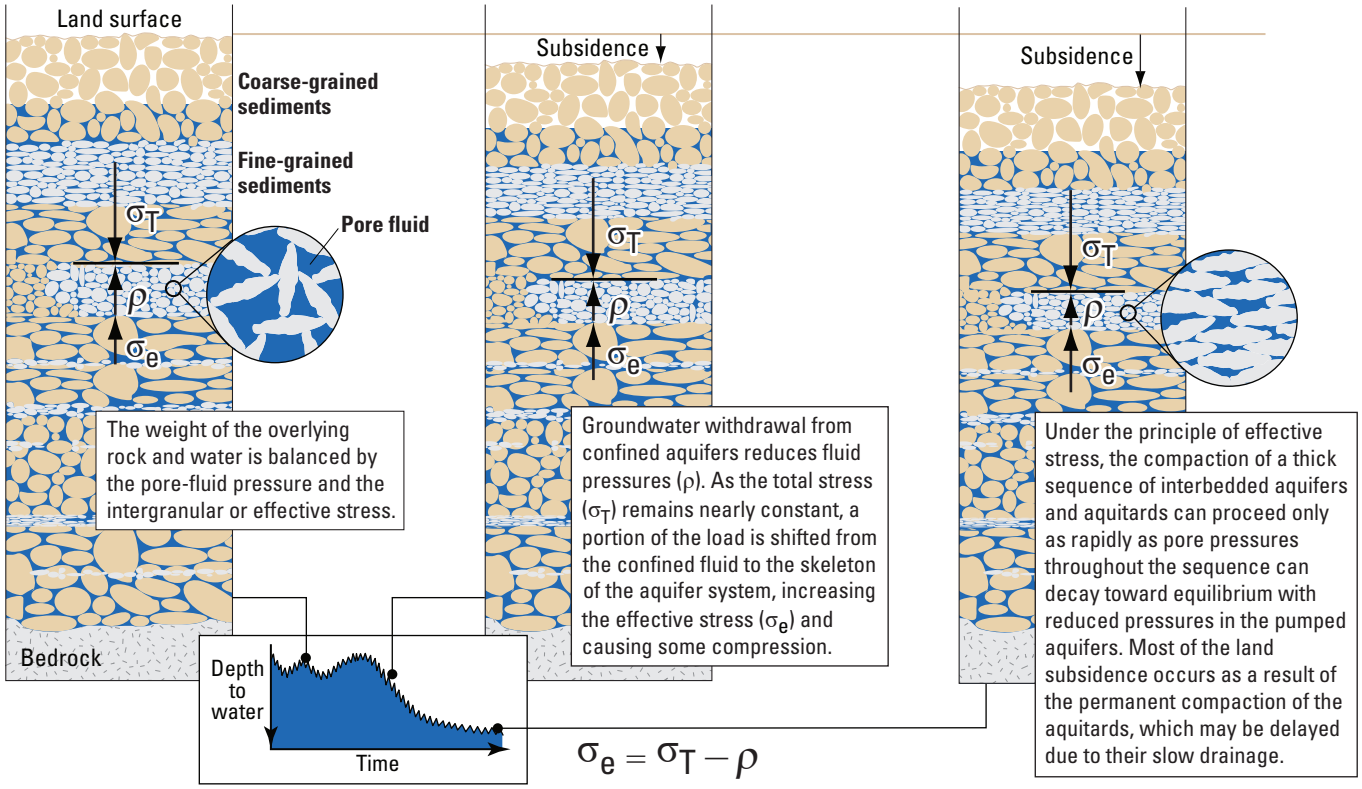

Figure 6. Principle of effective stress, as applied to land subsidence. Land subsidence as a result of a decrease in pore-fluid pressure (ρ) and resultant increase in effective stress (σ_e) exerted on a horizontal plane located at depth below land surface in fine-grained material under conditions of total stress (σ_T) in a one-dimensional, fluid-saturated geologic medium (modified from Galloway and others, 1999).

The pore structure of a sedimentary aquifer system is supported by the granular skeleton of the aquifer system and the pore-fluid pressure of the groundwater that fills the intergranular pore space (Meinzer, 1928). If total stress remains constant and groundwater is withdrawn in quantities that result in reduced pore-fluid pressures and water-level declines, the reduction of the pore-fluid pressure support increases the intergranular stress, or effective stress, on the granular skeleton. A change in effective stress deforms the skeleton: an increase in effective stress compresses it, and a decrease in effective stress causes it to expand. This deformation is sometimes inelastic (permanent), resulting in vertical compaction of the aquifer system, a permanent reduction in aquifer-system storage capacity, and land subsidence (fig. 6). An aquifer-system skeleton consisting of primarily fine-grained sediments, such as silt and clay, is much more compressible than one consisting of primarily coarse-grained sediments, such as sand and gravel. Inelastic compaction of coarse-grained sediment is generally negligible (Ireland and others, 1984; Hanson, 1989; Sneed and Galloway, 2000).

Aquifer-system deformation is elastic (recoverable) if the stress imposed on the skeleton is smaller than any previous maximum effective stress (Terzaghi, 1925). The largest historical effective stress imposed on the aquifer system—sometimes the result of the lowest groundwater level—is the "preconsolidation stress," and the corresponding (lowest) groundwater level is the "preconsolidation head" (Leake and Prudic, 1991). If the effective stress exceeds the preconsolidation stress, the pore structure of the granular matrix of the fine-grained sediments is rearranged as water drains; this new configuration results in a reduction of pore volume (reduced aquifer-system storage capacity) and, thus, inelastic compaction of the aquifer system. Furthermore, the compressibility of the fine-grained sediments constituting the aquitards, and any resulting compaction under stresses exceeding the preconsolidation stress, is 20 to more than 100 times greater than under stresses less than the preconsolidation stress (Riley, 1998).

For a developed aquifer system with an appreciable thickness of fine-grained sediments, a significant part of the total compaction can be residual compaction (Sneed and Galloway, 2000), which is compaction that occurs in thick aquitards as heads in the aquitards equilibrate with heads in the adjacent aquifers (Terzaghi, 1925). The simple compaction model mentioned earlier does not account for delayed drainage from low-permeability fine-grained sediments such as this. Depending on the thickness and the vertical hydraulic diffusivity of a thick aquitard, fluid-pressure equilibration—and thus compaction—lags behind pressure (or hydraulic head) declines in the adjacent aquifers; associated compaction can require decades or centuries to approach completion (Sneed and Galloway, 2000). Thus, if the aquifer head declines below the previous lowest level for a relatively short period, the preconsolidation head in the aquitard is not necessarily reset to the new low value (fig. 3; Phillips and others, 2003). In practice, because heads in aquitards cannot be measured without disrupting the native diffusivity (inserting a sensor would release the pressure), heads in aquitards only can be estimated, simulated, or deduced by observed changes in the relationship of compaction and groundwater levels measured in the adjacent aquifer. When compaction is observed to substantially increase per unit decline in groundwater level, then the preconsolidation stress in the aquitard likely was exceeded.

The time constant of an aquitard, τ, is the time required for about 93 percent of the excess pore pressure to dissipate, and therefore about 93 percent of the ultimate compaction to occur, following an instantaneous increase in stress. The time constant is directly proportional to the inverse of the vertical hydraulic diffusivity, and for a doubly draining aquitard, to the square of the half-thickness of the aquitard:

$$\tau = S_s' \left(b'/2\right)^2 / K_v' \qquad (2)$$

where

S_s' is the specific storage of the aquitard,
b' is the aquitard thickness,
K_v' is the vertical hydraulic conductivity of the aquitard, and
S_s'/K_v' is the inverse of the vertical hydraulic diffusivity (Riley, 1969).

Ireland and others (1984) estimated that the time constants for aquifer systems at 15 sites in the San Joaquin Valley ranged from 5 to 1,350 years. Terzaghi (1925) described this delay in his theory of hydrodynamic consolidation. Numerical modeling based on Terzaghi's theory has been used to simulate complex histories of compaction caused by known water-level fluctuations (Helm, 1978; Hanson, 1989; Sneed and Galloway, 2000).

The concepts reviewed in this section collectively form the aquitard-drainage model, which provides the theoretical basis of many subsidence studies related to the production of groundwater, oil, and gas. For a review of the history of the aquitard-drainage model, see Holzer (1998); for a more complete description of aquifer-system compaction, see Poland (1984); and for a review and selected case studies of land subsidence caused by aquifer-system compaction in the United States, see Galloway and others (1999).

Measurements and Methods

In this report, measurements of land-surface elevations, aquifer-system compaction, and groundwater levels are presented, interpreted, and integrated to improve understanding of the processes responsible for land-surface elevation changes. The sources of original data and processing techniques (if any) are described in this section; data are presented, interpreted, and integrated in the "Land Subsidence, Aquifer-System Compaction, and Groundwater Levels" section.

Land-Surface Elevation and Elevation Change

Land-surface elevation and change in elevation were measured at selected locations or along transportation and water-conveyance routes using InSAR, CGPS, and geodetic (GPS and spirit-level) survey methods by agencies and groups including USGS, DWR, California Department of Transportation (Caltrans), National Geodetic Survey, University NAVSTAR (Navigation Satellite Timing and Ranging) Consortium (UNAVCO), and various private contractors.

Interferometric Synthetic Aperture Radar (InSAR)

Interferometric Synthetic Aperture Radar is a satellite-based remote sensing technique that can detect centimeter-level ground-surface deformation under favorable conditions over hundreds of square kilometers at a spatial resolution (pixel size) of 90 m or better (Bawden and others, 2003). Synthetic Aperture Radar (SAR) imagery is produced by reflecting radar signals off a target area and measuring the two-way travel time back to the satellite. Synthetic Aperture Radar imagery has two components: amplitude and phase. The amplitude is the radar signal intensity returned to the satellite and depends on the varying reflective properties that delineate features of the landscape such as roads, mountains, structures, and other features. The phase component is proportional to the line-of-sight distance from the ground to the satellite (range) and is the component used to measure land-surface displacement (subsidence or uplift).

There are two primary forms of interferometric processing: conventional and persistent scatterer (PS) InSAR. The conventional InSAR technique uses two SAR images of the same area taken at different times and differences the phase component of the SAR signal, resulting in maps called interferograms that show relative ground-elevation change (range change) between the two SAR acquisition dates. If the ground has moved away from the satellite (subsidence), a more distal phase portion of the waveform is reflected back to the satellite. Conversely, if the ground has moved closer to the satellite (uplift), a more proximal phase portion of the waveform is reflected back to the satellite (Sneed and Brandt, 2013). The phase difference, or shift, between the two SAR images is then calculated relative to a selected reference point for each pixel within the image extent.

The PS InSAR technique is similar to the conventional technique, but it usually requires 20 or more SAR images that are processed simultaneously to determine, in part, the amplitude variance of all the SAR images at each pixel. Pixels that have relatively high variance in amplitude (often associated with differing plant-growth stages, tillage, or other relatively short-term changes at or near the ground surface) among the many SAR images are filtered from the dataset, resulting in a dataset containing "persistent" pixels, or pixels with relatively low variance in amplitude. The phase difference is then calculated in a manner identical to that of conventional InSAR, except that the differential phase is calculated only for each persistent pixel, rather than for every pixel within the image extent. A differential phase regression model is then calculated for selected interferometric pairs, which defines a linear dependence of interferometric phase on the difference in satellite geometry of the two SAR images composing the interferometric pair. This linear relationship leads to a digital elevation model height correction factor (Werner and others, 2003; Strozzi and others, 2005).

The InSAR signal quality depends partly on topography, satellite-orbit geometry, atmospheric artifacts, ground cover, land-use practices, time span of the interferogram, and other factors. Areas with high topographic relief can result in blocked radar signals (shadows), which is not a problem in the topographically flat San Joaquin Valley. Strict satellite-orbit control is required for successful application of the InSAR technique because repeat satellite passes must view the same point on the ground from very similar positions and angles to minimize topographic effects (parallax). The parallax effect is typically minimized by selecting SAR images for interferometric processing for which the perpendicular baseline, or horizontal distance between two satellite passes, is less than about 200 m (Sneed and Brandt, 2013).

The principal sources of error in the InSAR method applied to the San Joaquin Valley result from atmospheric artifacts and agricultural land-use practices (related to ground cover), both of which have deleterious effects on interferograms. Atmospheric artifacts are caused by non-uniform atmospheric water vapor in the form of clouds and tule fog; water vapor slows the radar signal, causing a phase shift that can lead to erroneous deformation interpretations (Zebker and others, 1997). Agricultural land-use practices, including the tilling, plowing, or flooding of farm fields, cause large and non-uniform changes in the amplitude and phase components of radar signals reflected back to the satellite. The non-uniform phase changes can result in spatially decorrelated (randomized) interferograms that cannot be interpreted. Interferograms spanning long periods (generally 2 or more years) often have poor signal quality because more non-uniform change is likely to have occurred in urban and non-urban areas (Sneed and Brandt, 2013). The PS InSAR technique is less affected by the land-use and time-span dependent effects because pixels with relatively high variance in amplitude are removed early in the processing, leaving only the relatively "good" quality pixels for processing.

Atmospheric artifacts can be identified by using independent interferograms and can be removed by stacking interferograms, and time-span dependent errors can be reduced by stacking interferograms. The term "independent interferograms" refers to two or more interferograms that do not share a common SAR image. When apparent ground motion is detected in a single interferogram, or in a set of interferograms that share a common SAR image, then the apparent motion is likely an artifact of atmospheric phase delay or other error source within the common SAR image. When the pixel-by-pixel range displacements of two or more interferograms are added to create a "stacked interferogram," a cloud in one SAR image may not affect the total displacement measured by the stacked interferogram. For example, when two interferograms are generated from three SAR images, the area with a cloud in the common SAR image will have apparent increased range in the first interferogram and decreased range in the second interferogram. When these two interferograms are added (stacked) together, the equal and opposite apparent deformation will be canceled out. Stacking also is beneficial in reducing time-span dependent errors. Stacking two or more interferograms that span shorter periods, which have less timespan-dependent errors, can result in more spatially correlated longer-term interferograms.

For this study, SAR data acquired between July 2003 and January 2010 from the European Space Agency's (ESA) Environmental Satellite (ENVISAT) and the Japanese Aerospace Exploration Agency's Advanced Land Observing Satellite (ALOS) were used for InSAR analysis (table 1). For this period, the side-looking C-band (56-mm wavelength) ENVISAT satellite orbited the Earth on a 35-day repeat cycle with a vertical resolution as small as 5 mm. The L-band (240-mm wavelength) ALOS satellite orbited the Earth on a 46-day repeat cycle with a vertical resolution as small as 20 mm. Although an interferogram produced from data collected by the longer-wavelength Phased Array L-band Synthetic Aperture Radar (PALSAR) instrument aboard ALOS is less sensitive to atmosphere and agricultural land-use changes than the shorter-wavelength Advanced Synthetic Aperture Radar instrument aboard ENVISAT, it also is about four times less sensitive to range changes, or deformation (Sandwell and others, 2008). These two datasets are referred to as ALOS and ENVISAT data, respectively, throughout the remainder of this report. The lower sensitivity of ALOS data permitted application of the conventional InSAR processing technique to these data, and the greater sensitivity to atmospheric conditions and agricultural land uses of ENVISAT interferometry required processing with the PS InSAR technique. Interferograms processed using PS InSAR methods also were restricted to about a 1-year time span or less to reduce time-span-dependent errors, whereas the ALOS data were restricted to time spans of about 3 years or less (table 1). ALOS and ENVISAT datasets were used to leverage the greater spatial correlation afforded by ALOS with the greater measurement resolution afforded by ENVISAT.

Two primary methods were used to evaluate InSAR image quality for this study. First, a visual spatial correlation analysis of each image was done to qualify image quality. For ALOS data, the entire image was analyzed visually to qualify spatial correlation. For ENVISAT data, the mountainous areas were analyzed visually for spatial correlation because the high density of persistent scatterer pixels in mountainous areas facilitated detection of spatial decorrelation compared to the low density of persistent scatterers on the valley floor, and because fewer potential sources of artifacts exist in mountainous areas compared to the valley floor. When the InSAR imagery was determined to be spatially decorrelated or otherwise degraded in the fairly stable mountainous areas, it was considered likely that the valley floor also was spatially decorrelated, and the image was either rejected or only conditionally accepted for analysis. Second, visible spectrum imagery from the Moderate Resolution Imaging Spectroradiometer (MODIS) instrument aboard the National Aeronautics and Space Administration (NASA) TERRA and AQUA satellites was used to make qualitative assessments of atmospheric moisture throughout the study area on each day of the ENVISAT SAR acquisition. This was a fairly simple means to identify clouds or fog over the study area and to reject, accept, or conditionally accept the ENVISAT imagery, which can be greatly affected by such conditions. The MODIS data were not used to evaluate the ALOS images because ALOS imagery is much less degraded from atmospheric moisture because of its much longer wavelength.

A total of 29 ENVISAT SAR images from track 435, extending from about Oro Loma to Kettleman City (fig. 7), were acquired and processed using the PS INSAR technique to produce 127 interferograms. Of these interferograms, 26 were of sufficient quality for analysis, with time spans ranging from 35 to 350 days between July 3, 2003, and May 22, 2008 (table 1). Additionally, six ENVISAT SAR images from track 163, extending from about Madera to south of Kettleman City (fig. 7), were previously acquired and processed using the PS InSAR technique to produce five interferograms that were used for this study (https://ca.water.usgs.gov/projects/central-valley/land-subsidence-san-joaquin-valley.html). These five interferograms had time spans ranging from 70 to 350 days between January 19, 2008, and January 23, 2010 (table 1).

Ordinary kriging was applied to PS InSAR data to interpolate ground-surface-elevation change between the persistent pixels identified by using the PS InSAR technique. The kriged data were then used to interpret PS InSAR data at selected locations such as extensometers, CGPS stations, and geodetic monuments used for geodetic surveys. To improve kriging computational run times, the volume of PS InSAR data was reduced by removing data points in the mountainous areas and by systematically selecting a subset of the original points on the basis of spatial location; the subset size was arbitrarily set at 1 percent of the points generated by the original PS InSAR processing. The R statistical software (R Development Core Team, 2008) was used to calculate the interpolated values and assess the degree of spatial autocorrelation. Semivariance was modeled using a spherical model with a lag distance of 500 m; a sill of 1,000, which describes the upper bound of semivariance; a range of 3,000 m, which describes the distance at which the semivariance value achieves 95 percent of the sill (the distance at which the data are no longer exhibiting spatial autocorrelation); and the nugget effect of 1, which represents a discontinuity of the semivariogram present at the origin due to micro-scale spatial variance and/or sampling/measurement errors. A spherical model was fit to the estimated semivariogram to optimize the output of the deformation values generated by the kriging calculations. The ordinary kriging calculations were then applied to a predefined grid by using the log of the PS InSAR values and the semivariogram parameters to calculate interpolated range-change values every 500 m. For a description of kriging theory, see the literature on geostatistics, such as Isaaks and Srivastava (1989).

Table 1. Interferograms interpreted for this report.

[See appendix 1 for selected interferograms used in time-series and stacked interferograms shown in this report. **Abbreviations**: ALOS, Advanced Land Observing Satellite; ENVISAT, Environmental Satellite, mm/dd/yyyy, month/day/year; no., number; SAR, synthetic aperture radar; —, not applicable]

Index no.	Track	First SAR acquisition (mm/dd/yyyy)	Second SAR acquisition (mm/dd/yyyy)	Time span of SAR pair, in days	Appendix figure no.
ENVISAT interferograms					
*1	T435	07/03/2003	05/13/2004	315	1–1
*2	T435	05/13/2004	11/04/2004	175	1–2
3	T435	05/13/2004	12/09/2004	210	—
4	T435	09/30/2004	11/04/2004	35	—
5	T435	09/30/2004	03/24/2005	175	—
*6	T435	11/04/2004	01/13/2005	70	1–3
7	T435	12/09/2004	02/17/2005	70	—
*8	T435	01/13/2005	03/24/2005	70	1–4
9	T435	02/17/2005	02/02/2006	350	—
10	T435	12/29/2005	03/09/2006	70	—
11	T435	02/02/2006	03/09/2006	35	—
12	T435	02/02/2006	05/18/2006	105	—
*13	T435	03/09/2006	01/18/2007	315	1–5
14	T435	04/13/2006	05/18/2006	35	—
15	T435	05/18/2006	10/05/2006	140	—
16	T435	05/18/2006	02/22/2007	280	—
17	T435	06/22/2006	07/27/2006	35	—
18	T435	08/31/2006	10/05/2006	35	—
19	T435	08/31/2006	01/18/2007	140	—
20	T435	10/05/2006	02/22/2007	140	—
*21	T435	01/18/2007	11/29/2007	315	1–6
22	T435	10/25/2007	11/29/2007	35	—
23	T435	10/25/2007	01/03/2008	70	—
24	T435	11/29/2007	01/03/2008	35	—
*25	T435	11/29/2007	04/17/2008	140	1–7
*26	T435	04/17/2008	05/22/2008	35	1–8
*27	T163	01/19/2008	06/07/2008	140	1–9
*28	T163	06/07/2008	05/23/2009	350	1–10
*29	T163	05/23/2009	08/01/2009	70	1–11
*30	T163	08/01/2009	11/14/2009	105	1–12
*31	T163	11/14/2009	01/23/2010	70	1–13
ALOS interferograms					
32	T219-Central	01/05/2007	02/20/2007	46	—
33	T219-North	01/05/2007	01/13/2010	1104	—
34	T219-North	05/23/2007	11/23/2007	184	—
35	T219-North	05/23/2007	01/08/2008	230	—
36	T219-North	05/23/2007	01/13/2010	966	—
37	T219-Central	11/23/2007	01/08/2008	46	—
38	T219-South	11/23/2007	01/08/2008	46	—
39	T219-North	11/23/2007	02/23/2008	92	—
40	T219-Central	11/23/2007	02/23/2008	92	—
41	T219-South	11/23/2007	02/23/2008	92	—
42	T219-North	11/23/2007	04/09/2008	138	—
43	T219-South	11/23/2007	04/09/2008	138	—
44	T219-North	11/23/2007	01/13/2010	782	—
45	T219-North	01/08/2008	02/23/2008	46	—
46	T219-Central	01/08/2008	02/23/2008	46	—
47	T219-South	01/08/2008	02/23/2008	46	—
48	T219-North	01/08/2008	04/09/2008	92	—
49	T219-Central	01/08/2008	04/09/2008	92	—
50	T219-South	01/08/2008	04/09/2008	92	—
**51	T219-North	01/08/2008	01/13/2010	736	1–14
52	T219-North	02/23/2008	04/09/2008	46	—
53	T219-Central	02/25/2009	04/12/2009	46	—
54	T219-South	02/25/2009	04/12/2009	46	—

*The ENVISAT image was used in time series.

**The ALOS image was used in time series (only in Oro Loma–Madera area).

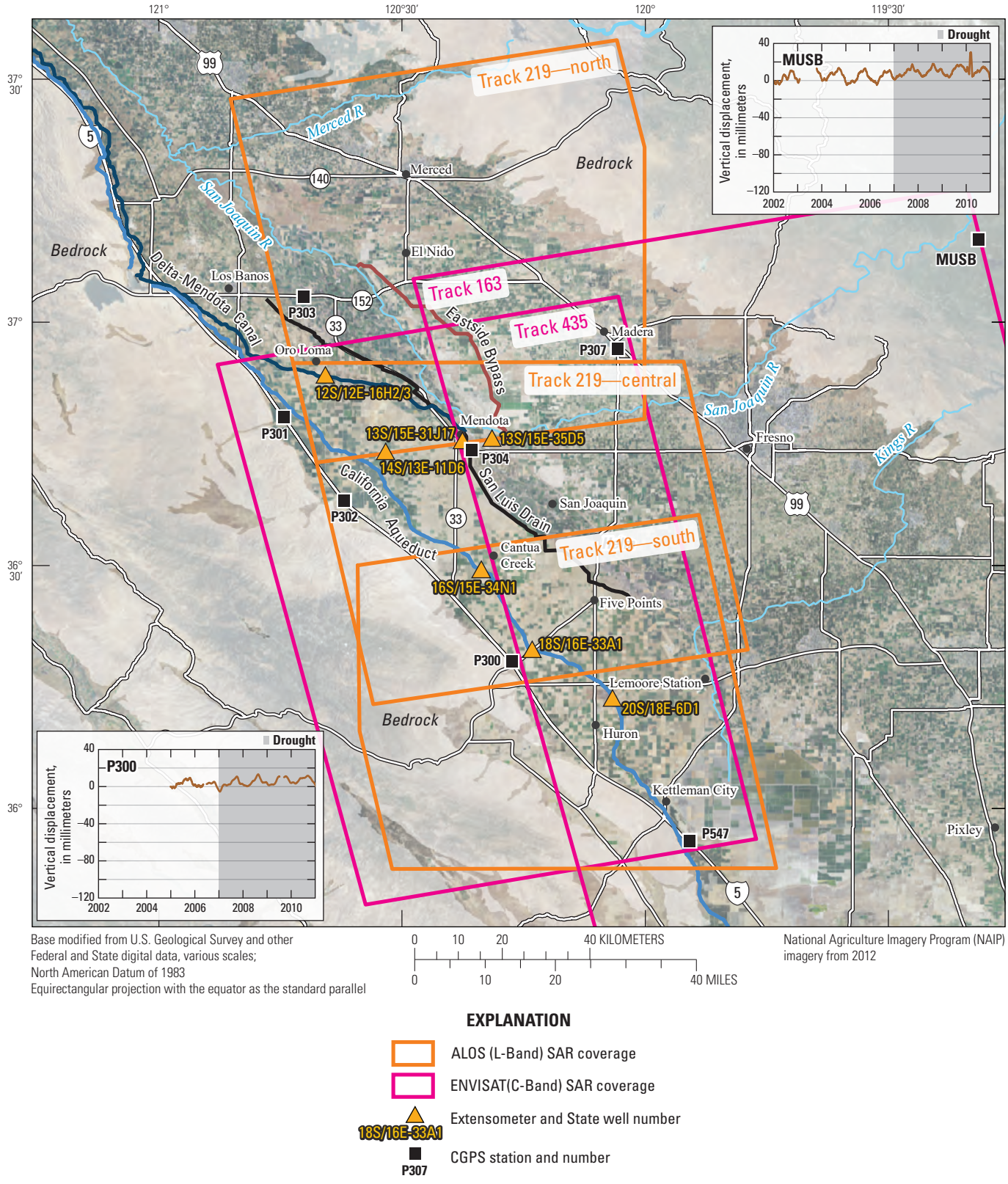

Figure 7. Locations of continuous Global Positioning System (CGPS) stations and extents of Environmental Satellite (ENVISAT) and Advanced Land Observing Satellite (ALOS) Synthetic Aperture Radar (SAR) coverage, San Joaquin Valley, California. Extents of ENVISAT SAR coverage were obtained from the European Space Agency, and the extents of ALOS SAR coverage were obtained from the Japanese Aerospace Exploration Agency.

A total of 36 ALOS SAR images on track 219 (fig. 7), extending from about Merced to Kettleman City, were acquired and processed using the conventional InSAR technique to produce 173 interferograms. Of these interferograms, 23 were of sufficient quality for analysis, with time spans ranging from 46 to 1,104 days between January 5, 2007, and January 13, 2010 (table 1). One of these interferograms (January 8, 2008–January 13, 2010; index number 51 in table 1) was used to define maximum subsidence locations near El Nido, where ENVISAT and geodetic survey data were not available. Additionally, this ALOS interferogram was combined with a stacked image generated from ENVISAT track-163 data (January 19, 2008–January 23, 2010; appendix 1), and selected ENVISAT track-299 and ALOS track-220 data presented in Sneed and others (2013), to produce a subsidence map for 2008–10 that covers the entire valley floor from about Merced to Bakersfield.

A subset of the 26 available ENVISAT interferograms from track 435 was used for time-series generation, stacking, or both to produce interferograms that span seasonal and annual periods between July 3, 2003, and May 22, 2008, to allow for deformation analysis for shorter and longer periods (index numbers 1–26 in table 1; appendix 1). Interferogram selection criteria to generate the time-series graphs were based on the land-surface elevation peaks (early in the year) and troughs (early fall) shown by some CGPS data (fig. 8), which can be combined to show year-to-year elevation changes. However, because of limited data availability that was further restricted by image quality, these peaks and troughs likely were not captured by the interferograms, possibly resulting in conservative estimates of seasonal, and therefore, longer-term elevation changes. ENVISAT interferograms from track 163 (index numbers 27–31 in table 1), previously processed for a different study (accessed July 31, 2017, at https://ca.water.usgs.gov/projects/central-valley/land-subsidence-san-joaquin-valley.html), were stacked, and the resulting image was used to extend time series through 2010. One ALOS interferogram (January 8, 2008–January 13, 2010; index number 51 in table 1) was used to extend the 2003–08 time series generated using ENVISAT track-435 data for the El Nido area, where subsequent ENVISAT data were not available. All of the 2003–10 time series generated from InSAR results and presented have a data gap during March 24, 2005–March 9, 2006. Additionally, time series for the Oro Loma–Madera area have a period of data overlap during January 8, 2008–May 22, 2008 (135 days), whereas time series for all other areas have a period of data overlap during January 19, 2008–May 22, 2008 (124 days). Any deformation that may have occurred during periods of data gaps or overlaps in the time series or stacks was not estimated.

Continuous Global Positioning System Network

The CGPS data for this study were obtained from the UNAVCO Plate Boundary Observatory (PBO) network of continuously operating GPS stations. The PBO is the geodetic component of UNAVCO, a consortium of research institutions whose focus is measuring vertical and horizontal plate boundary deformation across the North American and Pacific Plates in the western United States using high-precision measurement techniques. Daily CGPS position time series were downloaded from the PBO website (accessed August 4, 2017, at http://pbo.unavco.org/) using the North America 2008 Reference Frame. Day-to-day CGPS height solutions varied by as much as about 35 mm, likely owing to variable atmospheric conditions, random walk noise, and other effects not directly related to land-surface-elevation change (Zerbini and others, 2001; Williams and others, 2004; Langbein, 2008). To minimize this high-frequency noise and to enable better correlation between changes in GPS heights and InSAR range-change measurements, a 31-day moving average was applied to the CGPS data (fig. 8; Sneed and others, 2013). The removal of the fairly large day-to-day variations in GPS heights minimized potential error without removing long-term (figs. 8*A–C*) or seasonal (figs. 8*B*, *C*) deformation trends and permitted more meaningful comparison with InSAR results. In addition to comparing the CGPS height data to range-change measurements from PS InSAR results, the locations of the fairly stable CGPS stations P300 and MUSB also were used as the selected reference points to calculate the relative range changes of the PS InSAR data from ENVISAT track 435 and track 163, respectively (fig. 7). Data from five other CGPS stations were used for InSAR results comparison and error analysis. Of the eight CGPS stations included in this study, seven were constructed using the deep-drilled braced style, which is the most stable style. The eighth CGPS station, P300, was constructed using a concrete pillar fastened to an underlying massive outcrop with cemented reinforcing rods (accessed December 21, 2017, at http://kb.unavco.org/kb/article/unavco-resources-gnss-station-monumentation-104.html).

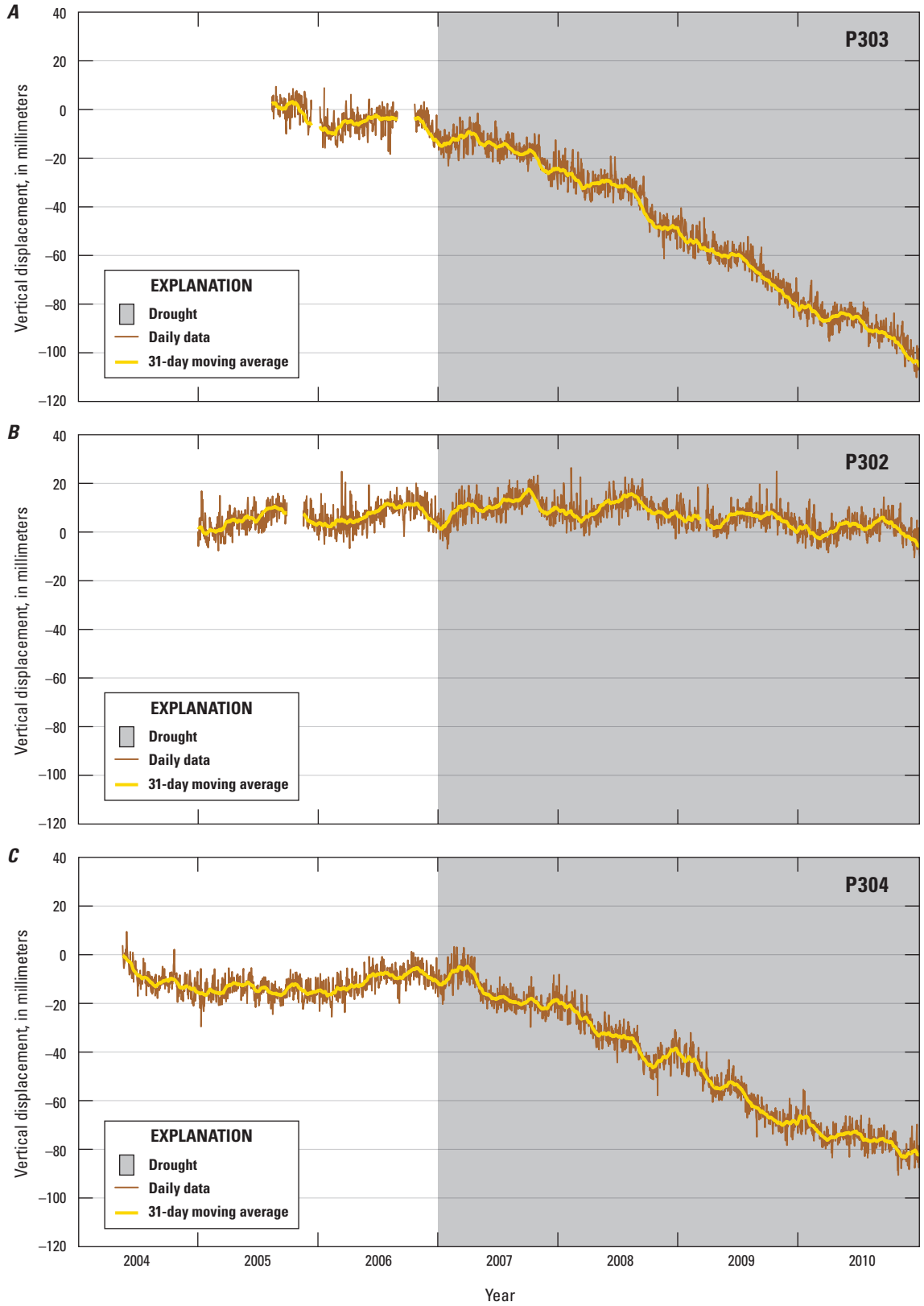

Figure 8. Daily and averaged (31-day moving) continuous Global Positioning System (CGPS) vertical displacement data from three selected CGPS stations in the San Joaquin Valley, California, which are representative of *A*, long-term-dominated displacement with little seasonal displacement (P303); *B*, seasonally dominated displacement with little long-term displacement (P302); and *C*, long-term and seasonal displacement (P304). These CGPS data were obtained from the University Navigation Satellite Timing and Ranging (NAVSTAR) Consortium. Negative values of vertical displacement indicate relative subsidence, and positive values indicate relative uplift. See figure 7 for locations.

Geodetic (Global Positioning System and Spirit-Level) Surveys

Published and unpublished data from previously completed GPS and spirit-level surveys (hereafter termed geodetic surveys when both methods are used to compute elevation change) in the study area were obtained and used for analysis of land-surface change for this study. Published subsidence contours of a large part of the San Joaquin Valley from 1926–70, constructed using topographic maps and spirit-level surveys (Poland and others, 1975), were used to compare areas of historical subsidence to areas of more recent subsidence. Elevation data for selected geodetic monuments (bench marks) along Highway 198 surveyed during the late 1950s to the early 1960s and 2004, and along Highway 152 surveyed in 1972, 1988, and 2004 (National Geodetic Survey, variously dated), were used to compute changes in elevation between the survey dates (Marti Ikehara, National Geodetic Survey, written commun., 2012). Similarly, elevation data for selected geodetic monuments along the California Aqueduct surveyed in 2000 and in 2009 were used to compute changes in elevation between the surveys (Forrest Smith, California Department of Water Resources, written commun., 2009).

Aquifer-System Compaction Measurements Using Borehole Extensometers

Borehole extensometers were used at selected locations in the study area, for various periods, to monitor aquifer-system compaction; monitoring entities included the USGS, DWR, SLDMWA, CCID, Luhdorff and Scalmanini Consulting Engineers, and others. For a detailed description about extensometer construction and measurement of aquifer-system compaction, see Lofgren (1961), Poland (1984), and Freeman (1996). A short summary is provided here.

A total of 35 extensometers were monitored in the San Joaquin Valley, with most of the monitoring occurring in the 1950s and 1960s, and very little occurring since the early 1980s (Sneed and others, 2013). The extensometers were constructed to indicate changes in aquifer-system thickness of specific depth intervals and thus to discriminate the compaction of the materials in definite depth zones (Inter-Agency Committee on Land Subsidence in the San Joaquin Valley, 1958). When this study was initiated in 2009, six extensometers were being actively monitored in the study area: 13S/15E-31J17 (Fordel), 13S/15E-35D5 (Yearout), 12S/12E-16H2/3 (Oro Loma Deep/Oro Loma Shallow), 14S/13E-11D6 (Panoche), and 20S/18E-6D1 (Rasta; fig. 9). Oro Loma Deep, Panoche, and Rasta are anchored below the Corcoran Clay (greater than 264 m below land surface), whereas Fordel, Yearout, and Oro Loma Shallow are anchored above or near the top of the Corcoran Clay (less than 150 m below land surface); consequently, only a small fraction of the total aquifer-system thickness is monitored by these shallower extensometers. The two Oro Loma extensometers, Panoche, and Rasta are cable extensometers, and the Yearout extensometer is a free-standing pipe extensometer built in the 1950s and 1960s. The Fordel extensometer is a counter-weighted pipe extensometer constructed in Mendota; data collection began in 1999. The cable in Oro Loma Shallow broke in late 2012 such that the extensometer is no longer operational; the others were still operational in 2018.

To increase the number of active monitoring locations and (or) to improve the frequency, precision, and depth range of aquifer-system compaction measurements, four cable-type extensometers (fig. 9) were refurbished: 12S/12E-16H2 (Oro Loma Deep, 305-m depth), 14S/13E-11D6 (Panoche, 414-m depth), 18S/16E-33A1 (DWR Yard, 314-m depth), and 20S/18E-6D1 (Rasta, 264-m depth). The refurbishment of the four selected extensometers was completed in early 2012. Since then (and through the publication date of this report), the sites have been maintained by USGS personnel who download the data, make manual dial-gauge and water-level measurements for quality control, and adjust equipment. The details of the refurbishment and preliminary data collected at the refurbished extensometer sites are presented in Sneed and others (2013). The preliminary data presented in Sneed and others (2013) have been revised; the revised data from these sites are available from the USGS National Water Information System (accessed August 20, 2013, at http://waterdata.usgs.gov/ca/nwis/nwis; table 2).

The relative contribution of compaction to subsidence at definite depth intervals in an aquifer system can be delimited at locations where the measurements of land subsidence and aquifer-system compaction are co-located. This occurs where two or more extensometers at different depths are co-located, or at locations where one or more extensometers is co-located with repeat land-surface elevation measurements, such as those derived from repeat leveling surveys, GPS observations (including continuous), and InSAR analysis. Land-subsidence calculations are based on measurements from or near land surface (in the case of CGPS or geodetic surveys, the depth of the CGPS antenna mount or geodetic monument anchor, which generally is less than 9-m below land surface) and represent the deformation from the entire subsurface geologic column. Because extensometers are anchored at a specific depth, the aquifer-system compaction measurement is specific to a depth interval (Poland, 1984). In general, the determination of compacting depth intervals determined from multi-depth measurements at a few specific locations cannot be extended to other locations in the valley because of variability in groundwater use, depth of extraction, and aquifer-system structure and composition (heterogeneity), and because numerous wells screened across confining units (particularly the Corcoran Clay) have created preferential flow, further altering the hydraulic head distribution in the aquifer system.

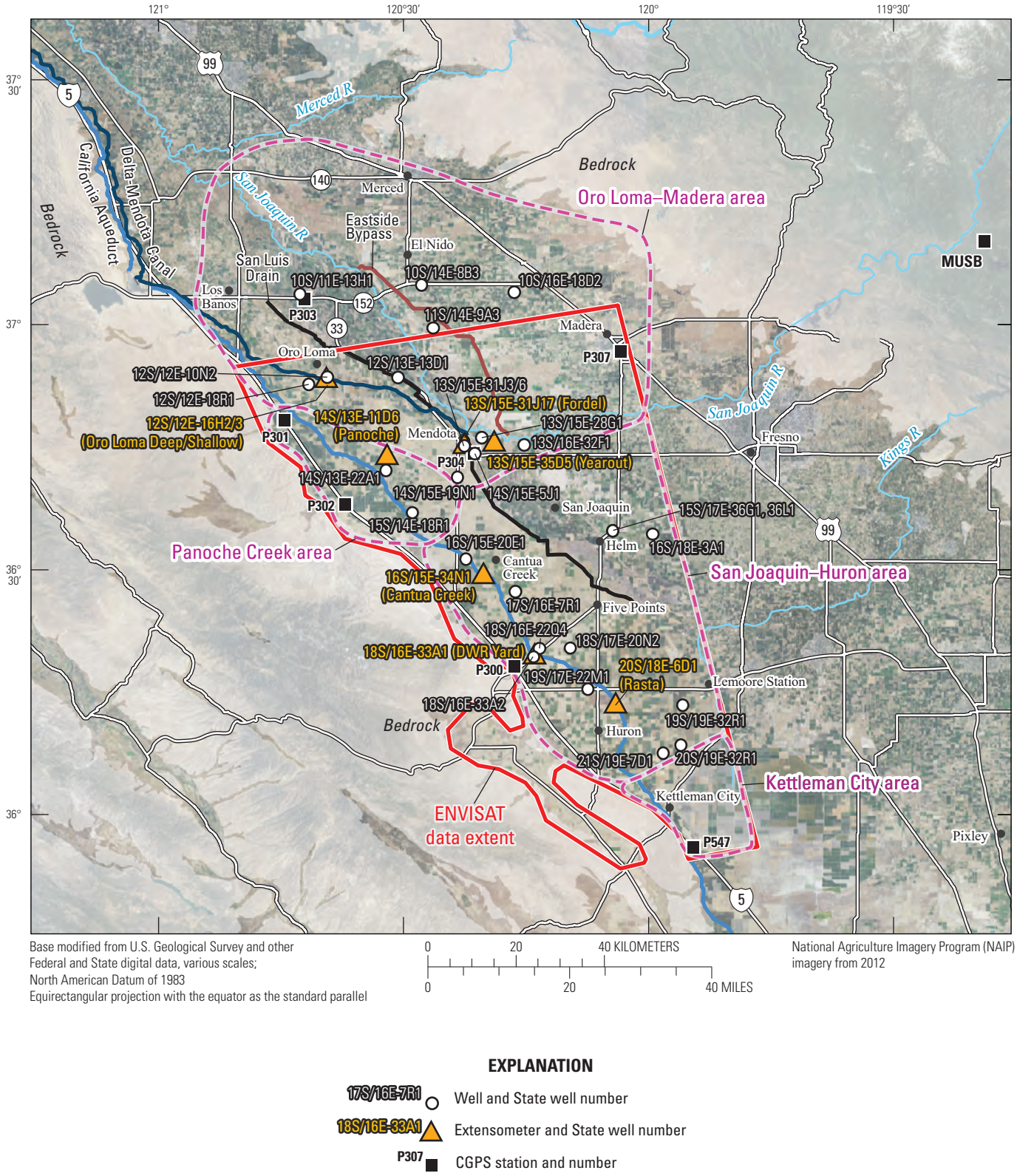

Base modified from U.S. Geological Survey and other Federal and State digital data, various scales; North American Datum of 1983 Equirectangular projection with the equator as the standard parallel

National Agriculture Imagery Program (NAIP) imagery from 2012

EXPLANATION

17S/16E-7R1 — Well and State well number

18S/16E-33A1 — Extensometer and State well number

P307 — CGPS station and number

Figure 9. Selected extensometers, continuous Global Positioning System (CGPS) stations, wells used to generate groundwater hydrographs, extent of Environmental Satellite (ENVISAT) data, and four areas of subsidence as defined in this study, San Joaquin Valley, California. See table 2 for information and data links for the extensometers and wells. DWR, California Department of Water Resources.

Table 2. Data sources and selected characteristics for groundwater wells and extensometers used in this report, San Joaquin Valley, California.

[DWR, California Department of Water Resources; LSCE, Luhdorff and Scalmanini Consulting Engineers; USGS, U.S. Geological Survey; WWD, Westlands Water District; —, not applicable]

State well number	Site identification number (USGS)	Nickname	Well depth (meters)[1]	Well category[2]	Data source	Link to data source	Link to additional records
010S011E13H001M	370351120422801	—	51	Shallow	DWR	http://www.water.ca.gov/waterdatalibrary/groundwater/hydrographs/brr_hydro.cfm?CFGRIDKEY=30426	https://nwis.waterdata.usgs.gov/ca/nwis/inventory/?site_no=370351120422801&agency_cd=USGS
010S014E08B003M	370500120274002	—	94	Deep	DWR	http://www.water.ca.gov/waterdatalibrary/groundwater/hydrographs/brr_hydro.cfm?CFGRIDKEY=32360	https://nwis.waterdata.usgs.gov/ca/nwis/inventory/?site_no=370500120274002&agency_cd=USGS
010S016E18D002M	370407120161601	—	150	Deep	DWR	http://www.water.ca.gov/waterdatalibrary/groundwater/hydrographs/brr_hydro.cfm?CFGRIDKEY=30142	https://nwis.waterdata.usgs.gov/ca/nwis/inventory/?site_no=370407120161601&agency_cd=USGS
011S014E09A003M	365944120261201	—	74	Shallow	DWR	http://www.water.ca.gov/waterdatalibrary/groundwater/hydrographs/brr_hydro.cfm?CFGRIDKEY=33790	https://nwis.waterdata.usgs.gov/ca/nwis/inventory/?site_no=365944120261201&agency_cd=USGS
012S012E10N002M	365340120390902	—	—	Inferred deep	DWR	http://www.water.ca.gov/waterdatalibrary/groundwater/hydrographs/brr_hydro.cfm?CFGRIDKEY=32009	https://nwis.waterdata.usgs.gov/ca/nwis/inventory/?site_no=365340120390902&agency_cd=USGS
012S012E16H002M[3]	365325120391501	Oro Loma Deep	305	—	DWR/USGS	https://ca.water.usgs.gov/land_subsidence/california-subsidence-resources.php	https://nwis.waterdata.usgs.gov/ca/nwis/inventory/?site_no=365325120391501&agency_cd=USGS
012S012E16H003M[3]	365325120391502	Oro Loma Shallow	107	—	DWR/USGS	https://ca.water.usgs.gov/land_subsidence/california-subsidence-resources.php	https://nwis.waterdata.usgs.gov/ca/nwis/inventory/?site_no=365325120391502&agency_cd=USGS
012S012E18R001M	365301120413701	—	6	Shallow	DWR	http://www.water.ca.gov/waterdatalibrary/groundwater/hydrographs/brr_hydro.cfm?CFGRIDKEY=32218	https://nwis.waterdata.usgs.gov/ca/nwis/inventory/?site_no=365301120413701&agency_cd=USGS
012S013E13D001M	—	—	—	Inferred shallow	DWR	http://www.water.ca.gov/waterdatalibrary/groundwater/hydrographs/brr_hydro.cfm?CFGRIDKEY=33958	—
013S015E28G001M	—	—	—	Inferred shallow	DWR	http://www.water.ca.gov/waterdatalibrary/groundwater/hydrographs/brr_hydro.cfm?CFGRIDKEY=32438	—
013S015E31J003M	364521120222001	—	126	Shallow	LSCE	—	https://nwis.waterdata.usgs.gov/ca/nwis/inventory/?site_no=364521120222001&agency_cd=USGS
013S015E31J006M	364518120222001	—	151	Deep	LSCE/USGS	https://nwis.waterdata.usgs.gov/ca/nwis/inventory/?site_no=364518120222001&agency_cd=USGS	http://www.water.ca.gov/waterdatalibrary/groundwater/hydrographs/brr_hydro.cfm?CFGRIDKEY=37957
013S015E31J017M[4]	364518120222401	Fordel	141	—	LSCE	https://ca.water.usgs.gov/land_subsidence/california-subsidence-resources.php	https://nwis.waterdata.usgs.gov/ca/nwis/inventory/?site_no=364518120222401&agency_cd=USGS

Table 2. Data sources and selected characteristics for groundwater wells and extensometers used in this report, San Joaquin Valley, California.—Continued

[DWR, California Department of Water Resources; LSCE, Luhdorff and Scalmanini Consulting Engineers; USGS, U.S. Geological Survey; WWD, Westlands Water District; —, not applicable]

State well number	Site identification number (USGS)	Nickname	Well depth (meters)[1]	Well category[2]	Data source	Link to data source	Link to additional records
013S015E35D005M[5]	364536120184301	Yearout	134	—	USGS	https://ca.water.usgs.gov/land_subsidence/california-subsidence-resources.php	https://nwis.waterdata.usgs.gov/ca/nwis/inventory/?site_no=364536120184301&agency_cd=USGS
013S016E32F001M	364528120150201	—	112	Shallow	DWR	http://www.water.ca.gov/waterdatalibrary/groundwater/hydrographs/brr_hydro.cfm?CFGRIDKEY=31955	https://nwis.waterdata.usgs.gov/ca/nwis/inventory/?site_no=364528120150201&agency_cd=USGS
014S013E11D006M[3]	364358120314906	Panoche	414	—	DWR/USGS	https://ca.water.usgs.gov/land_subsidence/california-subsidence-resources.php	https://nwis.waterdata.usgs.gov/ca/nwis/inventory/?site_no=364358120314906&agency_cd=USGS
014S013E22A001M	364219120315401	—	427	Deep	WWD	—	https://nwis.waterdata.usgs.gov/ca/nwis/inventory/?site_no=364219120315401&agency_cd=USGS; http://www.water.ca.gov/waterdatalibrary/groundwater/hydrographs/brr_hydro.cfm?CFGRIDKEY=14219
014S015E05J001M	364422120210601	—	67	Shallow	LSCE	https://nwis.waterdata.usgs.gov/ca/nwis/inventory/?site_no=364422120210601&agency_cd=USGS	https://nwis.waterdata.usgs.gov/ca/nwis/inventory/?site_no=364422120210601&agency_cd=USGS
014S015E19N001M	364128120231101	—	315	Deep	DWR/USGS	http://www.water.ca.gov/waterdatalibrary/groundwater/hydrographs/brr_hydro.cfm?CFGRIDKEY=15795	https://nwis.waterdata.usgs.gov/ca/nwis/inventory/?site_no=364128120231101&agency_cd=USGS
015S014E18R001M	—	—	—	Inferred shallow	DWR	http://www.water.ca.gov/waterdatalibrary/groundwater/hydrographs/brr_hydro.cfm?CFGRIDKEY=34252	—
015S017E36G001M	363503120033501	—	95	Shallow	DWR	http://www.water.ca.gov/waterdatalibrary/groundwater/hydrographs/brr_hydro.cfm?CFGRIDKEY=14409	https://nwis.waterdata.usgs.gov/ca/nwis/inventory/?site_no=363503120033501&agency_cd=USGS
015S017E36L001M	363458120034101	—	83	Shallow	DWR	http://www.water.ca.gov/waterdatalibrary/groundwater/hydrographs/brr_hydro.cfm?CFGRIDKEY=32241	https://nwis.waterdata.usgs.gov/ca/nwis/inventory/?site_no=363458120034101&agency_cd=USGS
016S015E20E001M	363126120220901	—	—	Inferred shallow	WWD	—	https://nwis.waterdata.usgs.gov/ca/nwis/inventory/?site_no=363126120220901&agency_cd=USGS; http://www.water.ca.gov/waterdatalibrary/groundwater/hydrographs/brr_hydro.cfm?CFGRIDKEY=25953
016S015E34N001M[3]	362913120195801	Cantua Creek	610	—	DWR/USGS	https://ca.water.usgs.gov/land_subsidence/california-subsidence-resources.php	https://nwis.waterdata.usgs.gov/ca/nwis/inventory/?site_no=362913120195801&agency_cd=USGS

Table 2. Data sources and selected characteristics for groundwater wells and extensometers used in this report, San Joaquin Valley, California.—Continued

[DWR, California Department of Water Resources; LSCE, Luhdorff and Scalmanini Consulting Engineers; USGS, U.S. Geological Survey; WWD, Westlands Water District; —, not applicable]

State well number	Site identification number (USGS)	Nickname	Well depth (meters)[1]	Well category[2]	Data source	Link to data source	Link to additional records
016S018E03A001M	—	—	—	Inferred shallow	DWR	http://www.water.ca.gov/waterdatalibrary/groundwater/hydrographs/brr_hydro.cfm?CFGRIDKEY=20276	—
017S016E07R001M	362729120160701	—	555	Deep	DWR	http://www.water.ca.gov/waterdatalibrary/groundwater/hydrographs/brr_hydro.cfm?CFGRIDKEY=35915	https://nwis.waterdata.usgs.gov/ca/nwis/inventory/?site_no=362729120160701&agency_cd=USGS
018S016E22Q004M	—	—	—	Inferred shallow	WWD	—	http://www.water.ca.gov/waterdatalibrary/groundwater/hydrographs/brr_hydro.cfm?CFGRIDKEY=25434
018S016E33A001M[3]	361935120134501	DWR Yard	314	—	DWR/USGS	https://ca.water.usgs.gov/land_subsidence/california-subsidence-resources.php	https://nwis.waterdata.usgs.gov/ca/nwis/inventory/?site_no=361935120134501&agency_cd=USGS
018S016E33A002M	—	—	—	Inferred shallow	DWR	http://www.water.ca.gov/waterdatalibrary/groundwater/hydrographs/brr_hydro.cfm?CFGRIDKEY=18445	—
018S017E20N002M	362033120092301	—	558	Deep	DWR/USGS	http://www.water.ca.gov/waterdatalibrary/groundwater/hydrographs/brr_hydro.cfm?CFGRIDKEY=39038	https://nwis.waterdata.usgs.gov/ca/nwis/inventory/?site_no=362033120092301&agency_cd=USGS
019S017E22M001M	361533120071301	—	629	Deep	DWR/USGS	http://www.water.ca.gov/waterdatalibrary/groundwater/hydrographs/brr_hydro.cfm?CFGRIDKEY=18046	https://nwis.waterdata.usgs.gov/ca/nwis/inventory/?site_no=361533120071301&agency_cd=USGS
019S019E32R001M	—	—	—	Inferred shallow	WWD	—	http://www.water.ca.gov/waterdatalibrary/groundwater/hydrographs/brr_hydro.cfm?CFGRIDKEY=25541
020S018E06D001M[3]	361334120035101	Rasta	264	—	DWR/USGS	https://ca.water.usgs.gov/land_subsidence/california-subsidence-resources.php	https://nwis.waterdata.usgs.gov/ca/nwis/inventory/?site_no=361334120035101&agency_cd=USGS
020S019E32R001M	—	—	—	Inferred shallow	DWR	http://www.water.ca.gov/waterdatalibrary/groundwater/hydrographs/brr_hydro.cfm?CFGRIDKEY=24771	—
021S019E07D001M	—	—	—	Inferred deep	DWR	http://www.water.ca.gov/waterdatalibrary/groundwater/hydrographs/brr_hydro.cfm?CFGRIDKEY=22411	—

[1]Data source is USGS National Water Information System.

[2]Depth relative to the Corcoran Clay. See section "Water Levels" for full description of well categories.

[3]Extensometer, cable type.

[4]Extensometer, counterweighted-pipe type.

[5]Extensometer, free-standing-pipe type.

Water Levels

Groundwater levels and groundwater-level changes in the study area were evaluated using water-level hydrographs from 27 wells spread throughout the study area (fig. 9). Measurements of groundwater levels in wells in the study area were obtained from USGS (accessed July 5, 2018, https://waterdata.usgs.gov/ca/nwis/nwis) and DWR databases (accessed July 5, 2018, http://wdl.water.ca.gov/waterdatalibrary/groundwater/index.cfm), and from the Westlands Water District (Dennis Loyd, Westlands Water District, written commun., 2013; table 2). These data were compared graphically to assess the correlation (or lack thereof) between vertical changes in land surface and changes in groundwater levels for selected areas along the California Aqueduct and adjacent areas to the east. Hydrographs were selected to represent the hydrologic conditions above and below the Corcoran Clay by determining (or deducing) the depth of the well screen(s) relative to the depth of the Corcoran Clay. In this report, wells for which depths were known were categorized as either above the Corcoran Clay (shallow) or below the Corcoran Clay (deep). For wells with unknown depths, water-level elevations from those wells were compared to those from nearby wells with known depths. If a correlation between the water levels from wells with known and unknown depths could be made with a high degree of confidence, the well was categorized as "inferred shallow" or "inferred deep," accordingly. In areas where multiple wells were present, representative hydrographs were selected based on availability of construction information, location, similarity to hydrographs from nearby wells, measurement frequency, and period of record. Wells with screened intervals above and below the Corcoran Clay were not (knowingly) used.

Land Subsidence, Aquifer-System Compaction, and Groundwater Levels

The PS InSAR and conventional interferograms and CGPS, extensometer, and geodetic-survey data show that during 2003–10, some areas in the study area had significant land-surface elevation changes, and others were relatively stable. A combination of individual and stacked interferograms, and CGPS, extensometer, and geodetic-survey data, were used to examine the characteristics of shorter- and longer-term deformation. For this report, "shorter-term" refers to periods of less than 1 year, and "longer-term" refers to periods of 1 year or longer. Following the calculation of PS InSAR range-change data relative to a selected reference point (P300 for ENVISAT track 435 or MUSB for ENVISAT track 163), the interferograms were interpreted for five other CGPS stations to analyze InSAR-measurement quality and precision (fig. 10). This comparative analysis showed that nearly all of the interferogram-derived range-change values used for time-series analyses were within 10 mm of the vertical displacement values calculated from the CGPS measurements. This indicated a resolution of the InSAR data of 10 mm or better. Note that three of the five CGPS stations shown in figure 10 (P301, P302, and P547) are on the fringes of the valley (fig. 9) where the aquifer system is fairly thin and bedrock is shallow; measurements from these stations may include vertical displacement unrelated to aquifer-system compaction such as that associated with plate-margin tectonics or crustal loading and (or) unloading (Borsa and others, 2014).

Selected PS InSAR interferograms are presented to show detailed land-surface deformation patterns along the California Aqueduct and adjacent areas (fig. 11; appendix 1) using ENVISAT track-435 data for the period 2003–08 (table 1). A stacked interferogram created from five ENVISAT track-163 interferograms for the period January 19, 2008, to January 23, 2010 (appendix figs. 1–9 to 1–13), was combined with the ALOS interferogram for January 8, 2008, to January 13, 2010 (appendix fig. 1–14); the results were then contoured to show valley-wide land-deformation patterns for 2008–10 (fig. 12). Data from three extensometers and geodetic-surveys along the California Aqueduct are presented and compared to the InSAR results. Geodetic-survey data along Highways 152 and 198 are presented for historical context.

Groundwater levels were compared to land-subsidence patterns and timing to help determine the relationship of land-surface deformation to changes in groundwater levels. Groundwater-level data are useful in the interpretation of subsidence data; however, groundwater levels generally represent a fairly small thickness of the aquifer system (according to the screened interval), whereas aquifer-system compaction and subsidence data generally represent a large aggregate thickness of the aquifer system. Available groundwater-level and elevation measurements generally did not coincide in space, time, or both, so a detailed analysis comparing particular water-level changes (stresses) and associated elevation changes (strains) was not possible. Instead, the paired data were analyzed in a broader context to determine if the preconsolidation stress threshold was surpassed during 2003–10 and, by extension, if measured deformation was likely elastic or inelastic during this period.

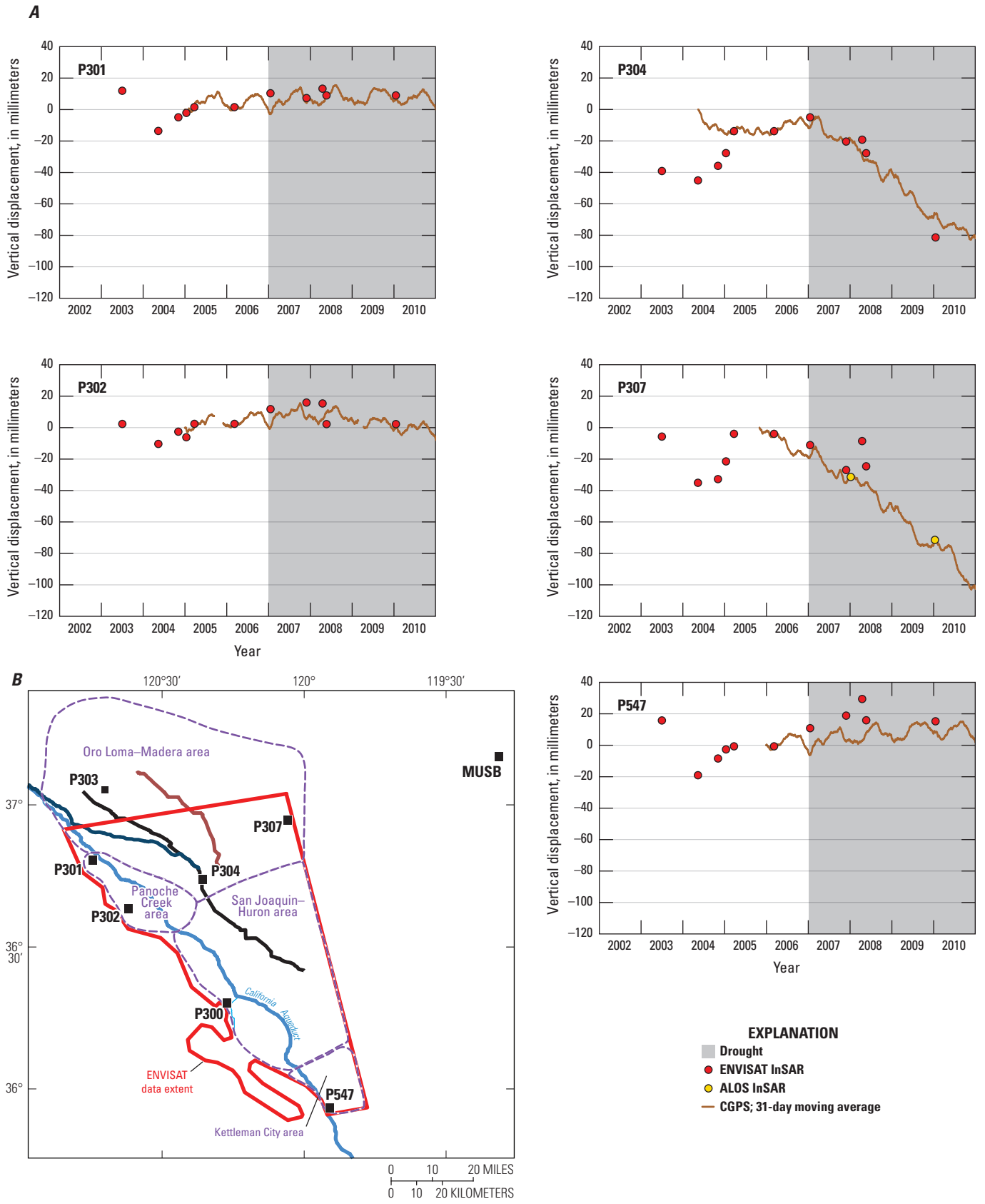

Figure 10. *A*, Continuous Global Positioning System (CGPS) and Interferometric Synthetic Aperture Radar (InSAR) time series at five CGPS stations in the San Joaquin Valley, California, for periods during 2003–10. Data from the Environmental Satellite (ENVISAT) and the Advanced Land Observing Satellite (ALOS) were used for the InSAR time series. The CGPS data were obtained from the University Navigation Satellite Timing and Ranging (NAVSTAR) Consortium. *B*, Map showing locations of CGPS stations. See appendix 1 and table 1 for interferograms used to construct the time series.

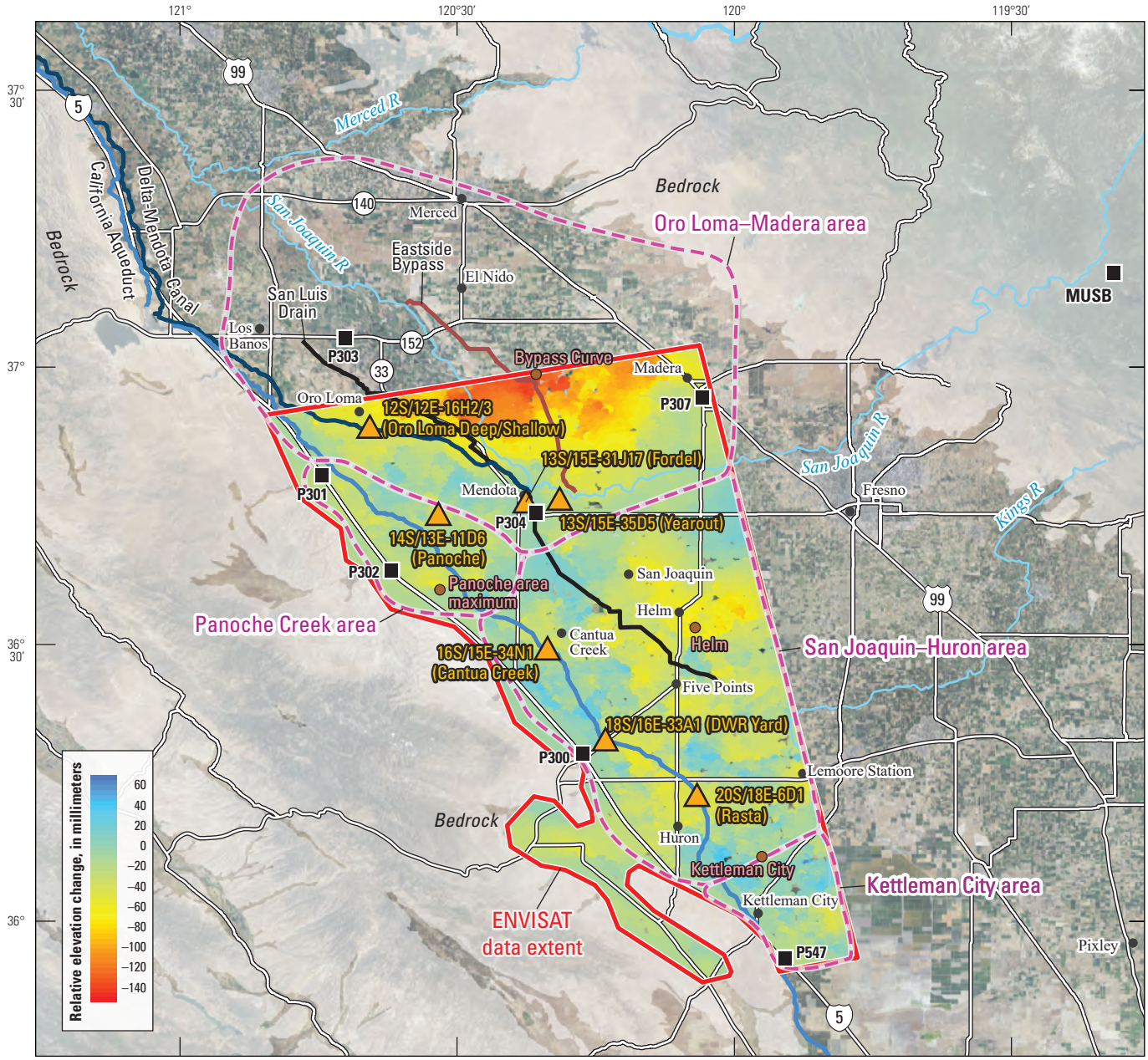

Base modified from U.S. Geological Survey and other Federal and State digital data, various scales; North American Datum of 1983 Equirectangular projection with the equator as the standard parallel

National Agriculture Imagery Program (NAIP) imagery from 2012

EXPLANATION

PS InSAR derived elevation change
July 3, 2003–May 22, 2008

Extensometer and State well number
18S/16E-33A1

CGPS station and number
P307

InSAR-derived local maximum and name
Helm

Figure 11. Elevation changes for the extent of Environmental Satellite (ENVISAT) track 435, interpreted from stacked persistent scatterer Interferometric Synthetic Aperture Radar (PS InSAR) interferograms for July 3, 2003–May 22, 2008, locations of selected extensometers and continuous Global Positioning System (CGPS) stations, and four areas of subsidence as defined in this study, San Joaquin Valley, California. Negative values of elevation change indicate subsidence, and positive values indicate uplift. See appendix figures 1–1 to 1–8 for the individual interferograms used to produce this stacked interferogram. DWR, California Department of Water Resources.

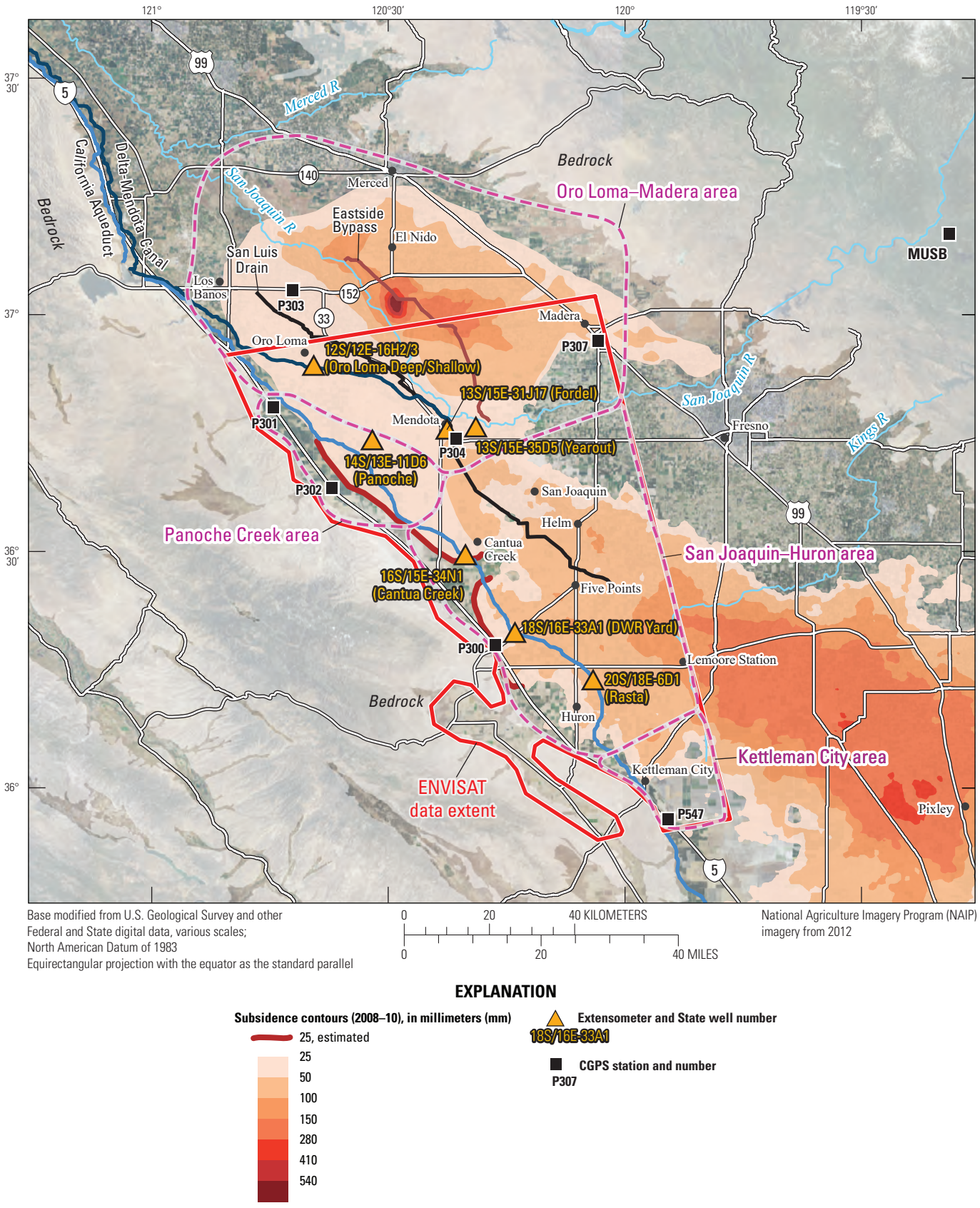

Base modified from U.S. Geological Survey and other Federal and State digital data, various scales; North American Datum of 1983 Equirectangular projection with the equator as the standard parallel

0 20 40 KILOMETERS
0 20 40 MILES

National Agriculture Imagery Program (NAIP) imagery from 2012

EXPLANATION

Subsidence contours (2008–10), in millimeters (mm)

- 25, estimated
- 25
- 50
- 100
- 150
- 280
- 410
- 540

Extensometer and State well number
18S/16E-33A1

CGPS station and number
P307

Figure 12. Subsidence contours derived from Environmental Satellite (ENVISAT) and Advanced Land Observing Satellite (ALOS) data for January 2008–January 2010, locations of selected continuous Global Positioning System (CGPS) stations, and four areas of subsidence as defined in this study, San Joaquin Valley, California. See appendix figures 1–9 to 1–14 for the individual interferograms used to produce the contours. DWR, California Department of Water Resources.

Patterns of Land Subsidence, Compaction, and Groundwater Levels During 2003–10

The study area has been subdivided into four areas generally based on similar land-deformation patterns along the Aqueduct during 2000–10 derived from geodetic surveys and InSAR results. From north to south, the areas are (1) Oro Loma–Madera (El Nido), (2) Panoche Creek, (3) San Joaquin–Huron, and (4) Kettleman City (fig. 11). The Oro Loma–Madera area is characterized by large magnitudes of subsidence during 2008–10 centered north of the study area, near El Nido (fig. 12). Although the largest magnitudes are distant from the Aqueduct, the Aqueduct is included in the regional subsidence bowl centered near El Nido. The Panoche Creek area generally is characterized by smaller subsidence magnitudes compared to the Oro Loma–Madera area; however, subsidence magnitudes along the Aqueduct are similar. The San Joaquin–Huron area is characterized by larger magnitudes of subsidence along the Aqueduct compared to the Panoche Creek area. Subsidence in the San Joaquin–Huron area is related to the large magnitudes of subsidence centered east of the Aqueduct near Pixley (fig. 12). The Kettleman City area is characterized by fairly minor subsidence along the Aqueduct. For each of the four areas, land subsidence and compaction information derived from InSAR, extensometer, CGPS station, and geodetic survey results are described and followed by descriptions of groundwater levels. All of the available information is then integrated to conceptualize depth intervals and stress regimes of aquifer-system compaction for each area.

Oro Loma–Madera (El Nido)

The Oro Loma–Madera area includes the communities of Oro Loma, Los Banos, Madera, Merced, Mendota, and El Nido; extensometers 12S/12E-16H2 (Oro Loma Deep), 12S/12E-16H3 (Oro Loma Shallow), 13S/15E-31J17 (Fordel), and 13S/15E-35D5 (Yearout); and CGPS stations P303, P304, and P307 (figs. 9, 11). Groundwater levels in the large Oro Loma–Madera area were examined using hydrographs from 13 wells near 4 selected areas of interest: El Nido/Bypass Curve, Oro Loma extensometers, CGPS P303, and Mendota, where the Fordel and Yearout extensometers and CGPS P304 are located (fig. 9).

Subsidence and Aquifer-System Compaction

The Oro Loma–Madera area is part of a large subsidence feature centered south of the town of El Nido that is evident in interferograms for periods during 2003–04 and 2006–10 (figs. 11, 12; appendix 1). Land-surface elevation changes interpreted from the ALOS interferogram for January 8, 2008–January 13, 2010, indicated subsidence of 25 mm or more over 3,100 km^2 in the central part of the San Joaquin Valley, extending about 80 km west-east from near Interstate 5 and the Aqueduct to east of California Highway 99, and 40 km north-south, from about Merced to about Mendota (fig. 12; Sneed and Phillips, 2012; Sneed and others, 2013). The maximum subsidence shown in the ALOS interferogram was more than 540 mm, or about 270 millimeters per year (mm/yr), between the San Joaquin River and Eastside Bypass, about 10 km south of El Nido (fig. 12; appendix fig. 1–14). The center of the subsidence maximum is obscured either by decorrelation from ground disturbance or an unresolvable steep subsidence gradient (large differences in subsidence magnitude in the small area; appendix fig. 1–14). Available ENVISAT data did not cover the area of maximum subsidence shown by ALOS but did capture the southern part of the main subsidence bowl (fig. 11; appendix 1). A 7-year time series was constructed for Bypass Curve (where the ENVISAT and ALOS datasets overlap), about 10 km southeast of the ALOS maximum, by combining ENVISAT interferograms from track 435 (July 3, 2003–May 22, 2008; appendix figs. 1–1 to 1–8) and the ALOS interferogram for January 8, 2008–January 13, 2010, shown in appendix figure 1–14 (fig. 13*A*). The total measured elevation change during the period July 3, 2003–January 13, 2010, was about 340 mm of subsidence—45 mm of subsidence during the period July 3, 2003–November 4, 2004; no subsidence during the period November 4, 2004–March 24, 2005; 75 mm of subsidence during the period March 9, 2006–November 29, 2007; and 220 mm of subsidence during the period November 29, 2007–January 13, 2010 (fig. 13*A;* appendix 1). The rate of subsidence in the Bypass Curve area was about 35 mm/yr during 2003–04, increased to about 45 mm/yr during 2006–07, and again increased to about 100 mm/yr during 2008–10. Subsidence calculations from GPS surveys done in 2008 and 2010 by the DWR corroborated the high InSAR-derived rate during that period, and biannual GPS surveys during 2011–16 by Reclamation indicated that the high rate of subsidence continued (accessed July 5, 2018, at http://www.restoresjr.net/science/subsidence-monitoring/). Additionally, results of a previous study that used interferograms from ENVISAT to calculate deformation rates for selected locations in this subsidence area indicated that subsidence rates doubled around May 2008 (Sneed and others, 2013).

There are no extensometers near the area of maximum active subsidence, but four extensometers are situated along the southern and southwestern margins of the subsidence bowl (figs. 11, 12). Of the four extensometers—12S/12E-16H2 (Oro Loma Deep), 12S/12E-16H3 (Oro Loma Shallow), 13S/15E-31J17 (Fordel), and 13S/15E-35D5 (Yearout)—only Oro Loma Deep is anchored below the Corcoran Clay. Measurements from the Oro Loma extensometers were not taken during 2000–08; however, InSAR time series at the Oro Loma site indicated subsidence of about 55 mm between 2003 and 2010 (fig. 13*A*). The Fordel extensometer indicated periods of compaction and expansion between 2002 and 2010, resulting in about 2 mm of net compaction (fig. 14). Yearout data are not presented in this report because the anchor depth is very similar to that of the nearby Fordel extensometer, which has higher-quality and temporally denser data.

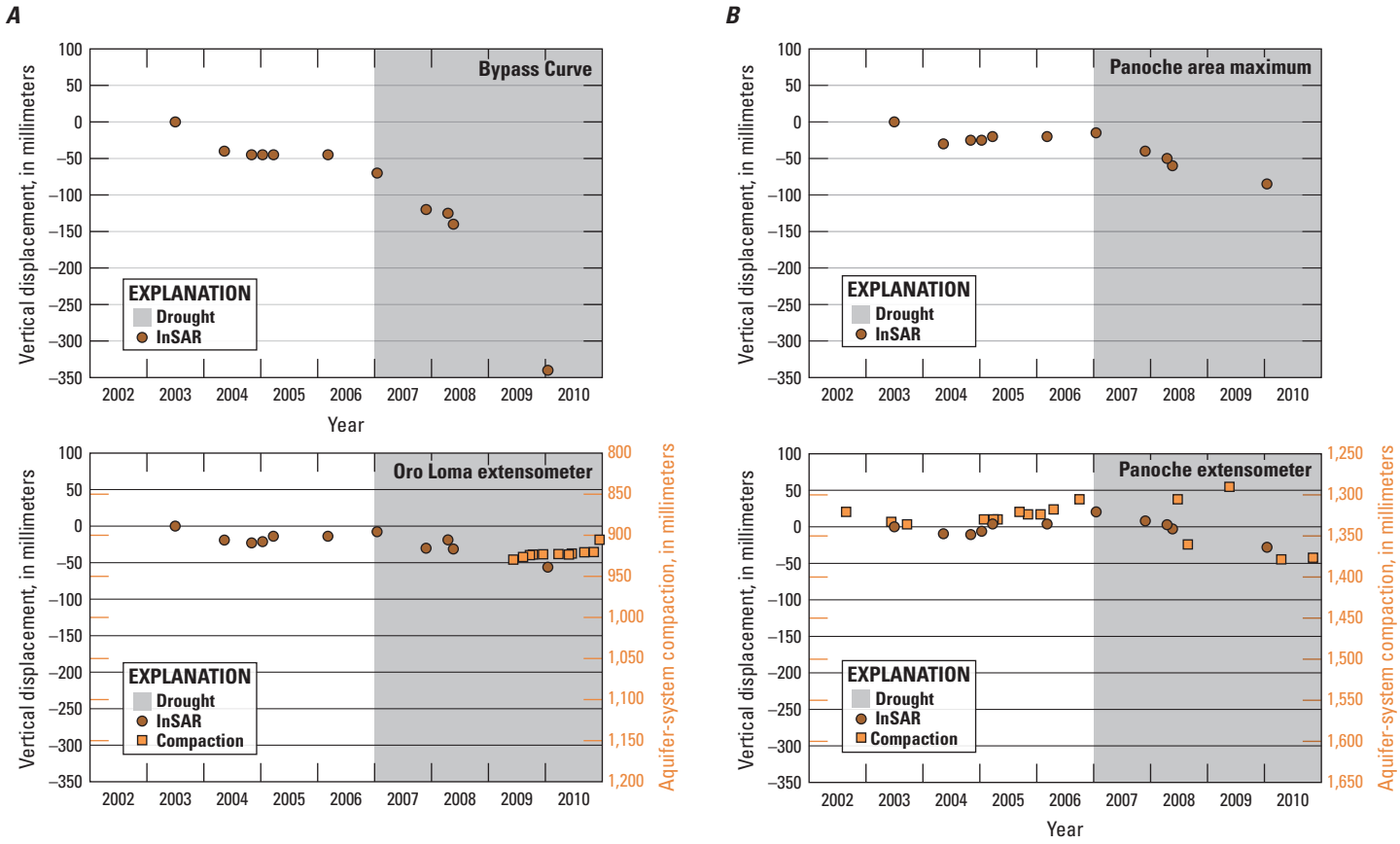

Figure 13. Time series of vertical displacement of land surface and aquifer-system compaction for 2003–10 derived from Interferometric Synthetic Aperture Radar (InSAR) analysis and extensometer data, respectively, in *A*, Area 1: Oro Loma–Madera (El Nido) area—the location of local maximum subsidence (Bypass Curve) and the location of the Oro Loma extensometer site; *B*, Area 2: Panoche Creek area—the location of local maximum subsidence and the location of the Panoche extensometer site; *C*, Area 3: San Joaquin–Huron area—the location of local maximum subsidence near Helm, the location of regional maximum subsidence near Pixley, and the locations of 16S/15E-34N1 (Cantua Creek), 18S/16E-33A1 [California Department of Water Resources (DWR) Yard], and 20S/18E-6D1 (Rasta) extensometer sites; and *D*, Area 4: Kettleman City area—the location of local maximum subsidence north of Kettleman City, San Joaquin Valley, California. Negative values of vertical displacement indicate relative subsidence, and positive values indicate relative uplift. Larger values of aquifer-system compaction indicate increased compaction, and smaller values indicate decreased compaction. See appendix 1 for the individual interferograms used to produce the time series. See table 2 for extensometer information and data links.

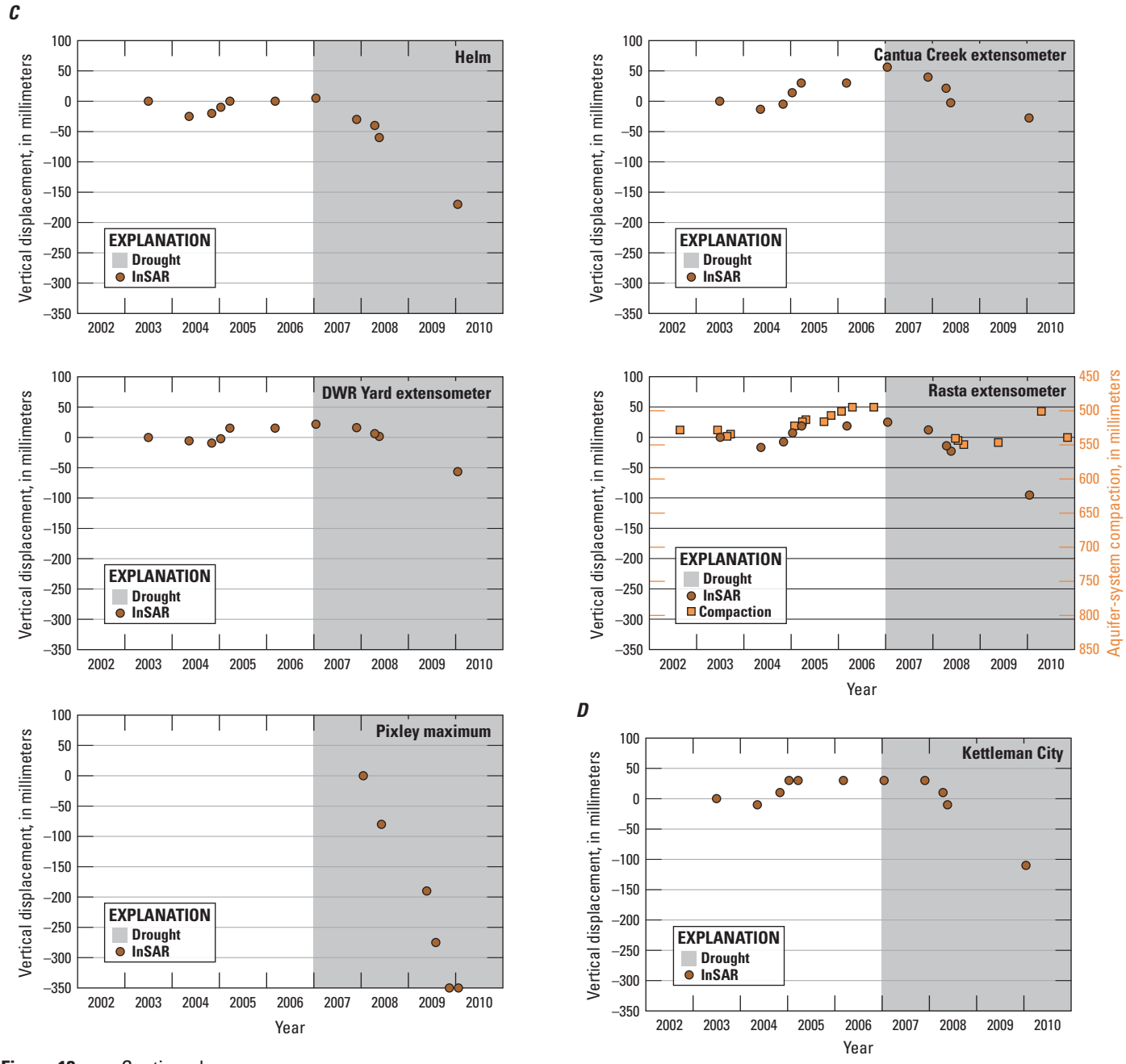

Figure 13. —Continued

There are no CGPS stations near the area of maximum active subsidence, but three stations are situated along the margins of the subsidence bowl (figs. 11, 12). The CGPS data from P307 (fig. 10), near Madera, and from P303 (fig. 8*A*), east of Los Banos on Highway 152, indicated subsidence of about 100 mm between 2005 and 2010—a rate of about 20 mm/yr. Continuous Global Positioning System stations P307 and P303 also showed seasonally variable rates; P307 showed small amounts of uplift during winter seasons, whereas P303 showed less seasonal variation, such that subsidence slowed or ceased during some shorter-term periods—mostly during fall and winter (figs. 8, 10). The CGPS stations P307 and P303 showed subsidence rate increases of about 50 percent after about May 2008. The CGPS data from P304 (fig. 10), near Mendota, showed about 80 mm of subsidence between mid-2004 and 2010, with nearly all of it (70 mm) occurring after 2006, at a fairly steady rate of about 20 mm/yr. The CGPS station P304 also showed seasonally variable rates, including small amounts of uplift during fall and winter seasons, which were most pronounced between 2007 and 2010 (figs. 10, 14). Comparison of 2004–10 data from the Fordel (13S/15E-31J17) extensometer (anchored near the top of the Corcoran Clay) and CGPS P304 indicated that about 91 percent of the aquifer-system compaction occurred below the top of the Corcoran Clay (fig. 14).

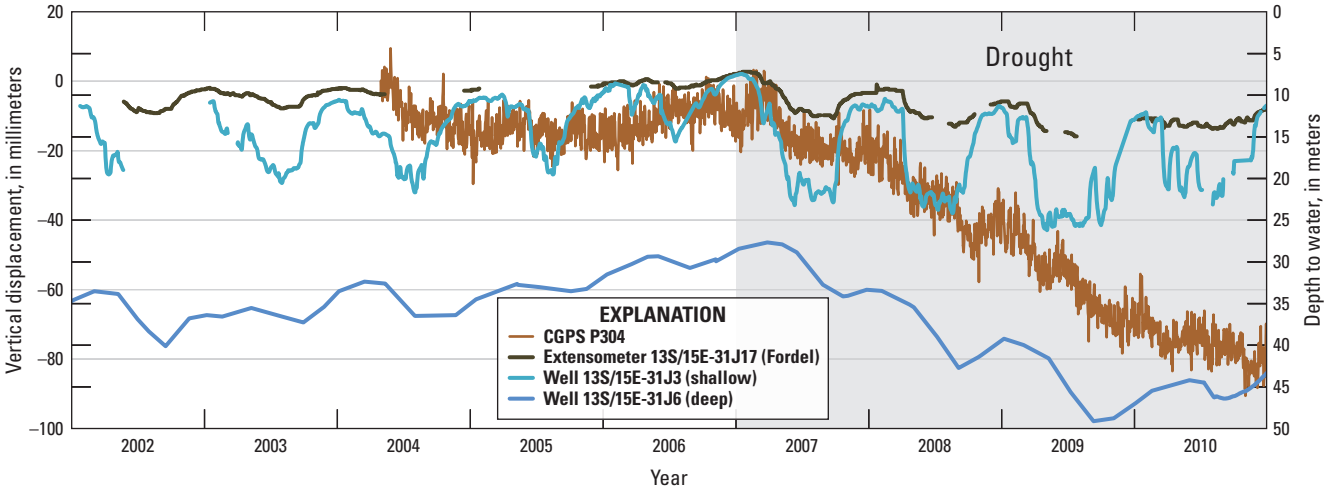

Figure 14. Vertical displacement (aquifer-system compaction) measured by the Fordel (13S/15E-31J17) extensometer (anchored near the top of the Corcoran Clay), vertical displacement at continuous Global Positioning System (CGPS) station P304, and water levels for shallow well 13S/15E-31J3 and for deep well 13S/15E-31J6 near Mendota, California, 2002–10. The period shaded represents calendar years affected by increased pumping during and after the climatic drought of 2007–09. Fordel and 13S/15E-31J3 data were obtained from Luhdorff and Scalmanini Consulting Engineers (Debbie Cannon, Luhdorff and Scalmanini Consulting Engineers, written commun., 2013); 13S/15E-31J6 data before May 1, 2010, were obtained from Luhdorff and Scalmanini Consulting Engineers (Debbie Cannon, Luhdorff and Scalmanini Consulting Engineers, written commun., 2013); and other water-level data were obtained from the U.S. Geological Survey (accessed July 5, 2018, at https://waterdata.usgs.gov/ca/nwis/nwis). The P304 data were obtained from the University Navigation Satellite Timing and Ranging (NAVSTAR) Consortium (accessed July 5, 2018, at http://www.unavco.org/instrumentation/networks/status/pbo/overview/P304). Negative values of vertical displacement indicate relative subsidence, and positive values indicate relative uplift. See table 2 for information and data links for the extensometer and wells.

A comparison of results from geodetic surveys along the California Aqueduct by the DWR between 2000 and 2009, and InSAR results from 2003 to 2010 along the 13-km reach of the Aqueduct in this area, generally indicated similar areal patterns of subsidence and stability (figs. 15*A*, *D*). The InSAR results generally showed larger magnitudes of subsidence along the Aqueduct than indicated by the geodetic data, except for a few-kilometer reach. The geodetic surveys in that reach indicated as much as about 170 mm of subsidence at a single location, which was larger by more than a factor of two relative to nearby surveyed locations. These surveying data indicated a very large subsidence gradient in this area (fig. 15*D*). Implications of high subsidence gradients for infrastructure are discussed in the section "Effects of Land Subsidence on Infrastructure." Although a coincident area of subsidence was indicated from 2003 to 2010 InSAR analysis, the maximum magnitude was much less (about 40 mm). The difference in magnitudes could be caused by (1) different periods of the datasets, (2) the comparison of point-specific geodetic surveying data and areally averaged or estimated InSAR data that represent a much larger area than the Aqueduct itself, (3) instability of the geodetic monument, (4) errors in the InSAR or survey data, or (5) a combination of these factors.

Groundwater Levels

Groundwater levels in the large Oro Loma–Madera area were examined using hydrographs from 13 wells near 4 selected areas of interest (figs. 9, 11): El Nido/Bypass Curve, Oro Loma extensometers, CGPS P303, and Mendota (CGPS P304 and Fordel extensometer). In the area south of El Nido, the center of the large subsidence bowl previously discussed, and near Bypass Curve (figs. 11, 12), the hydrographs from shallow (11S/14E-9A3) and deep (10S/16E-18D2, 10S/14E-8B3) wells showed seasonal fluctuations as large as about 12 m superimposed on longer periods of declines and recoveries associated with climatic conditions (fig. 16*A*). Water levels in these three wells declined during the 1976–77, 1987–92, and 2007–10 drought periods and had variable recoveries post-drought. Water levels in shallow well 11S/14E-9A3 recovered to levels near or above pre-drought levels after the 1976–77 and 1987–92 drought periods. Deep wells 10S/16E-18D2 and 10S/14E-8B3 recovered near or above pre-drought levels after 1976–77 but did not recover to pre-drought levels after the 1987–92 drought period. The historically lowest groundwater levels in the shallow aquifer were measured during the 1987–92 drought period, whereas the historically lowest groundwater levels in the deep aquifer were measured during the 2007–10 drought period (fig. 16*A*).

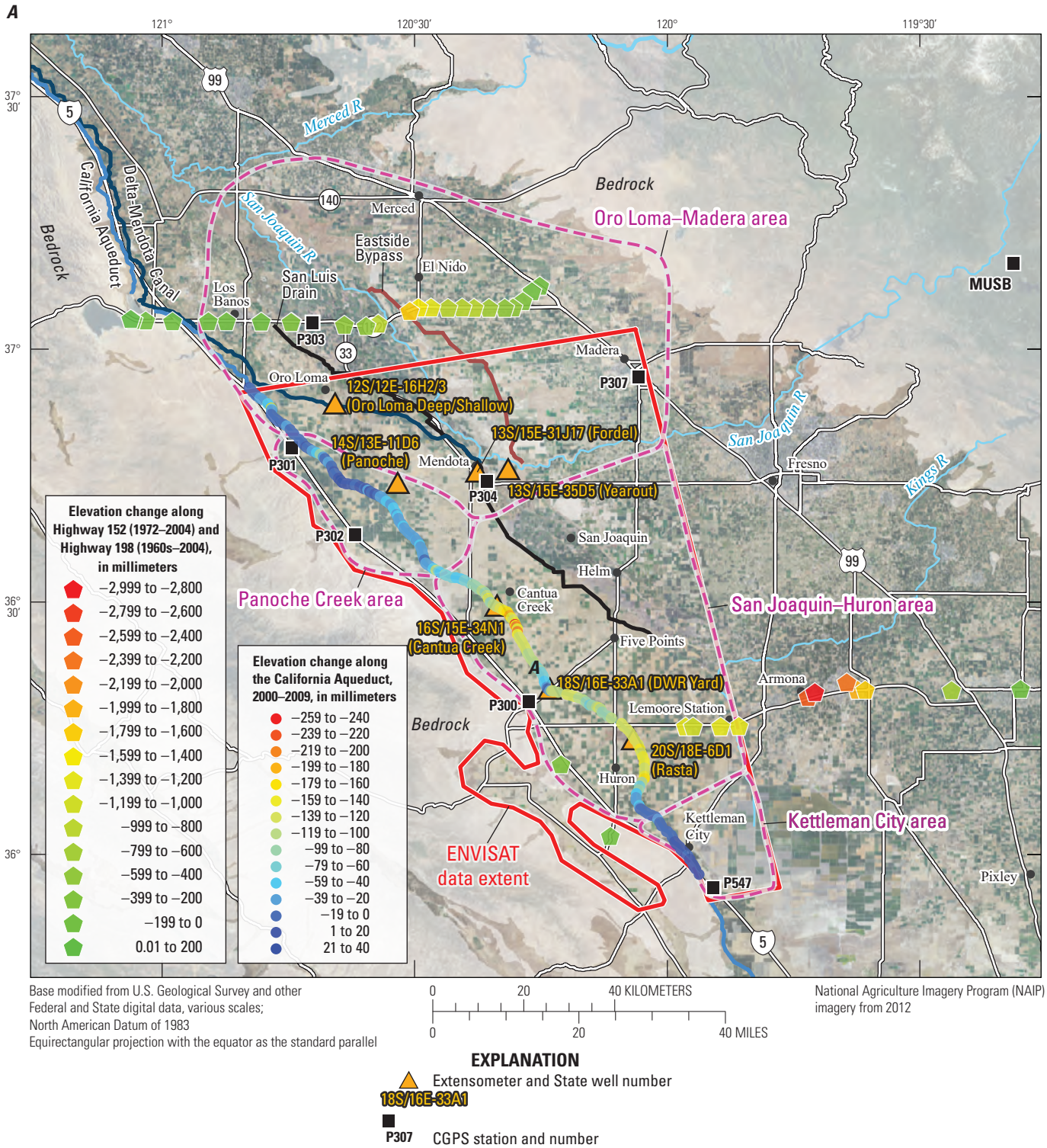

Figure 15. *A*, Locations and results of geodetic surveys completed along Highways 152 and 198 and along the California Aqueduct and locations of selected extensometers and continuous Global Positioning System (CGPS) stations, and extent of Environmental Satellite (ENVISAT) data; *B*, elevation changes computed from repeat geodetic surveys along Highway 152 (1972–88 and 1972–2004); *C*, elevation changes computed from repeat geodetic surveys along Highway 198 (1960s–2004); and *D*, comparison of Interferometric Synthetic Aperture Radar (InSAR)-derived elevation changes (2003–10) and geodetic-surveying-derived elevation changes (2000–09) along the California Aqueduct. Subsidence data along Highways 152 and 198 were computed from National Geodetic Survey elevations (Marti Ikehara, National Geodetic Survey, written commun., 2012). Subsidence data along the California Aqueduct were obtained from the California Department of Water Resources (DWR; Forrest Smith, California Department of Water Resources, written commun., 2009). Negative values of elevation change indicate subsidence, and positive values indicate uplift.

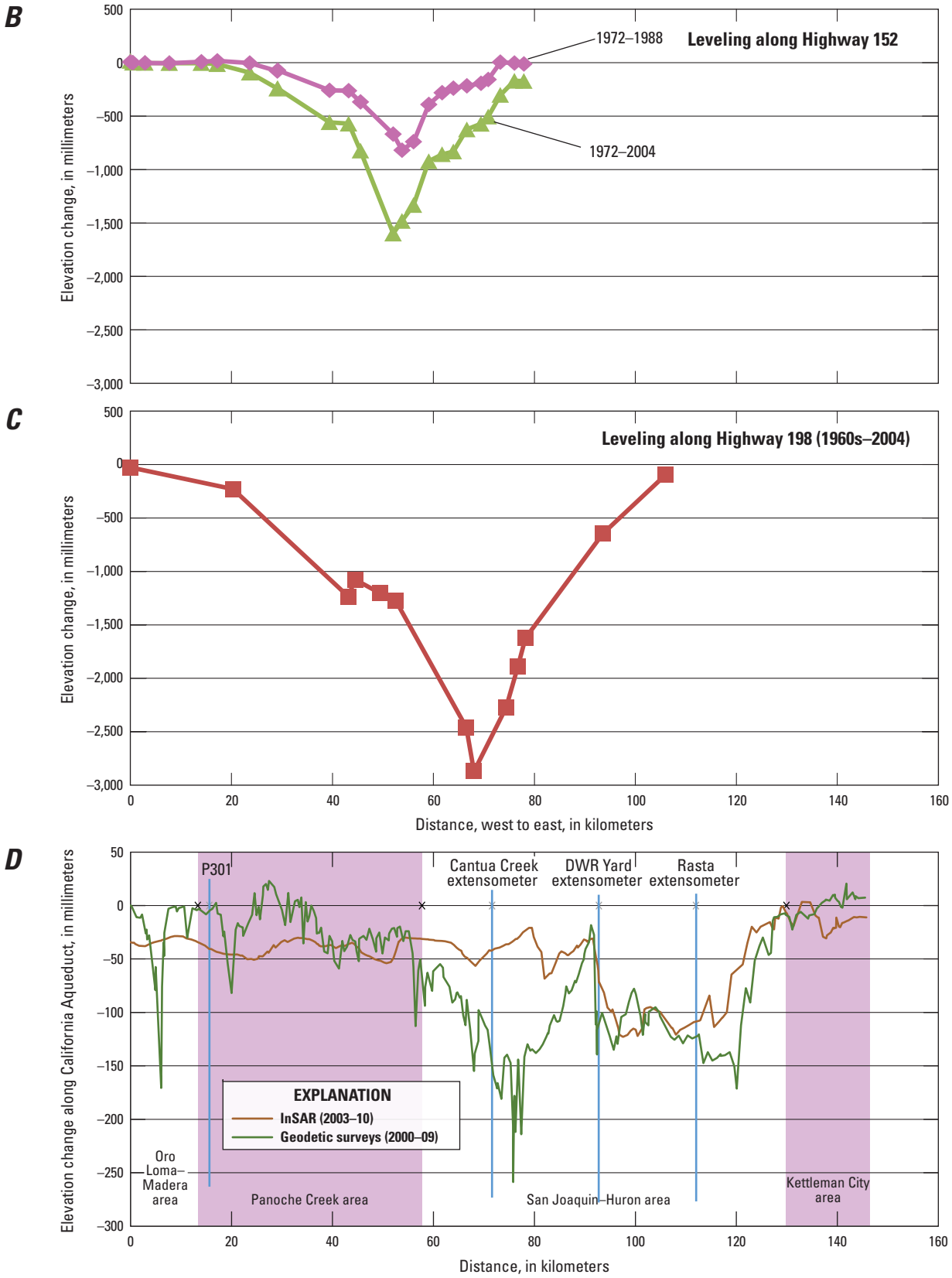

Figure 15. —Continued

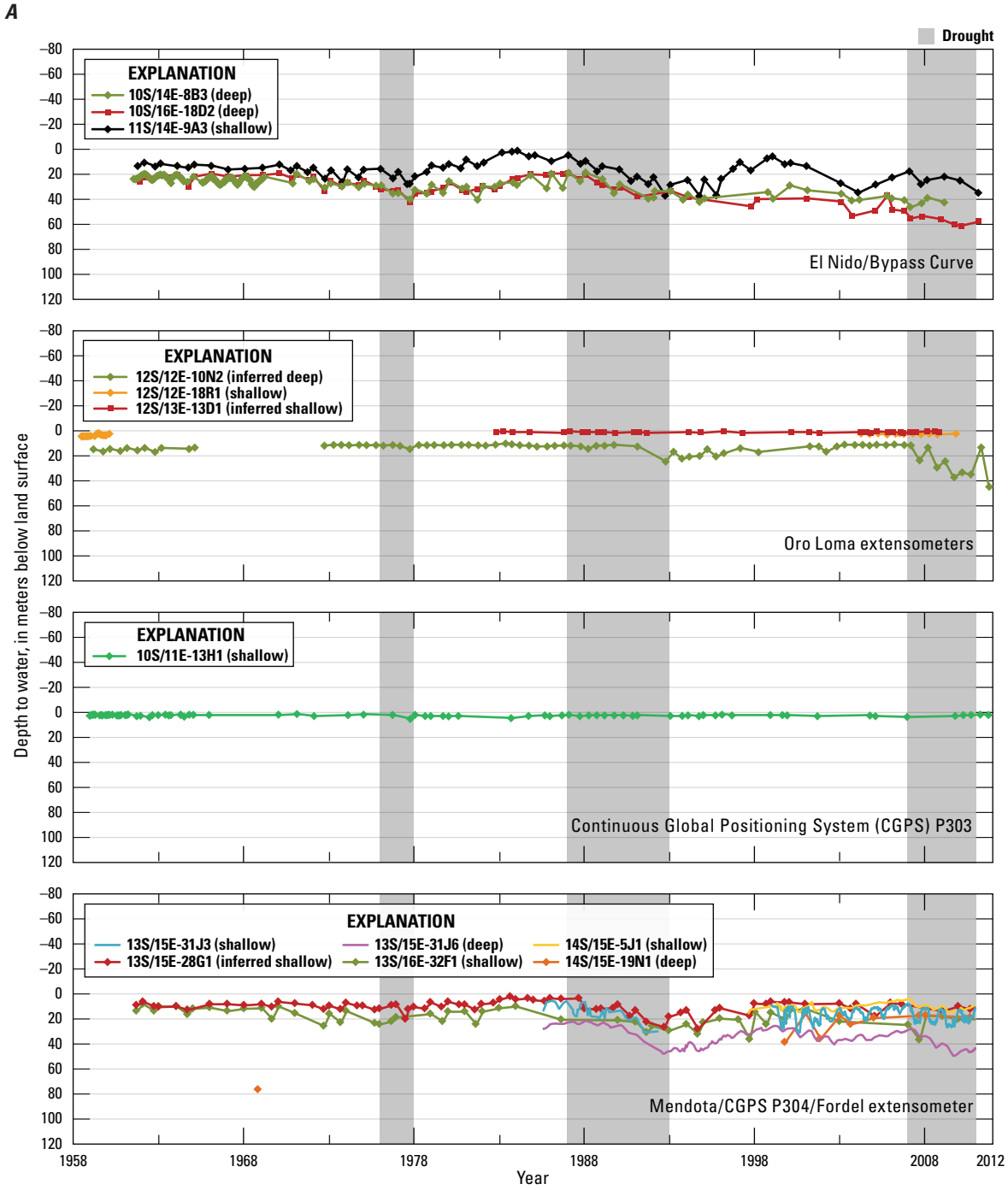

Figure 16. Measurements of water levels in wells in the *A*, Oro Loma–Madera area; *B*, Panoche Creek area; *C*, San Joaquin–Huron area; and *D*, Kettleman City area. The periods shaded represent calendar years affected by increased pumping as a result of drought periods. A break in the hydrograph line indicates a data gap of at least 5 years. Water-level data were obtained from California Department of Water Resources (accessed July 5, 2018, at http://wdl.water.ca.gov/waterdatalibrary/groundwater/index.cfm) and U.S. Geological Survey (accessed July 5, 2018, at https://waterdata.usgs.gov/ca/nwis/nwis) databases, and from Luhdorff and Scalmanini Consulting Engineers (Debbie Cannon, Luhdorff and Scalmanini Consulting Engineers, written commun., 2013). See figure 9 for well locations and table 2 for well information and data links.

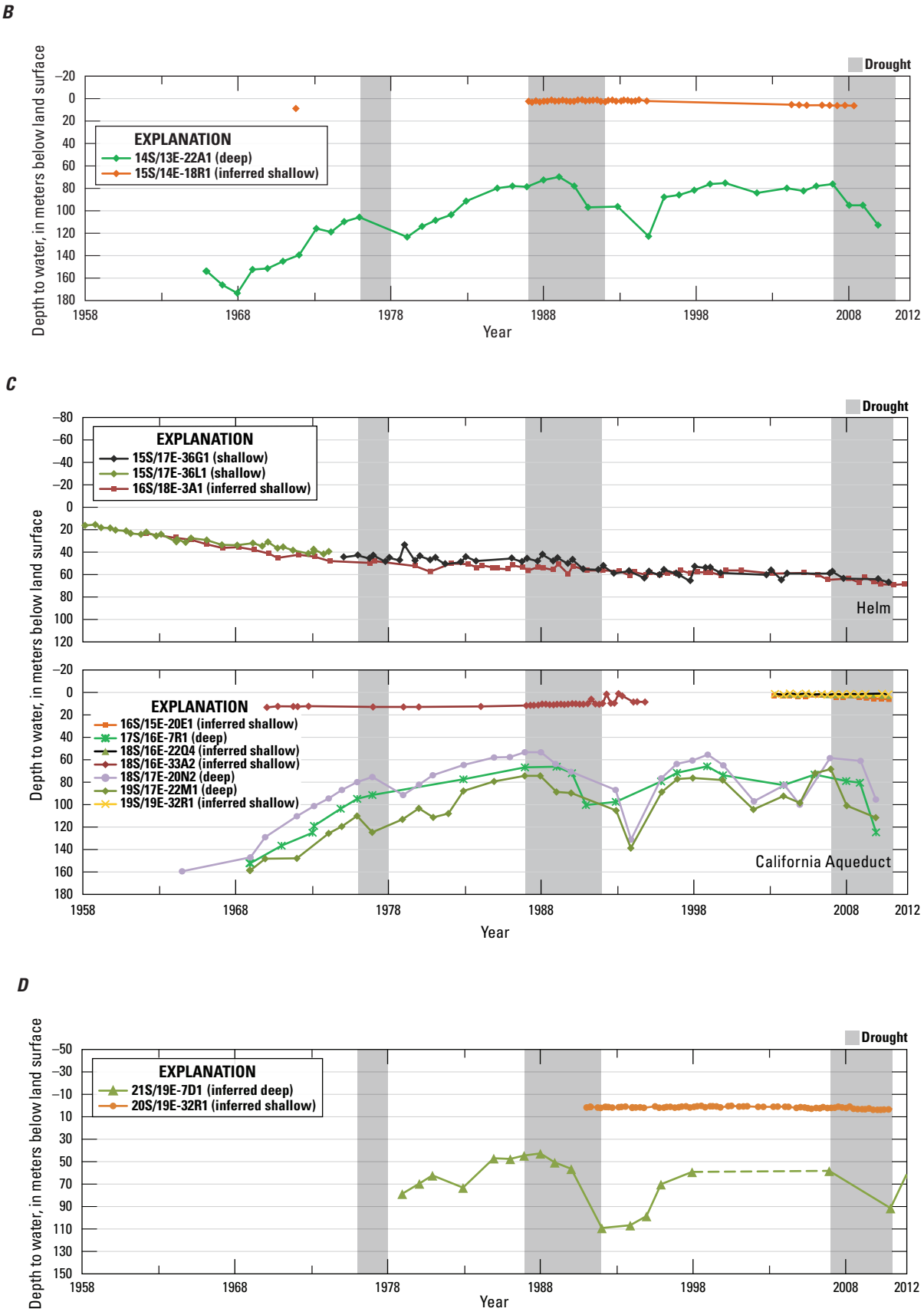

Figure 16. —Continued

Water levels near the Oro Loma extensometers were examined using the hydrographs from wells 12S/12E-18R1, 12S/13E-13D1, and 12S/12E-10N2 (fig. 16*A*). Groundwater levels measured in shallow or inferred shallow wells 12S/12E-18R1 and 12S/13E-13D1 showed small seasonal fluctuations superimposed on fairly stable water levels during their respective periods of record (fig. 16*A*). Groundwater levels in deep wells, such as inferred deep well 12S/12E-10N2, showed seasonal fluctuations that varied in magnitude between the late 1950s and 2010 (fig. 16*A*). There were longer-term trends of water-level stability throughout the record, except during, or just after, the three drought periods, when water levels declined then subsequently recovered; the historically lowest water levels were measured during the 2007–10 drought period and were about 12 m lower than the previous historical low in 1992.

Continuous Global Positioning System station P303 is near the edge of the previously discussed large subsidence bowl centered south of El Nido (fig. 12). More than 100 mm of subsidence during mid-2005–10 was calculated from the CGPS measurements at P303 (fig. 8). Water levels in nearby shallow wells were stable on short-term and long-term scales during 1959–2010, generally deviating less than 3 m during the approximate 50-year period, (for example, 10S/11E-13H1 in fig. 16*A*); deep wells were not found near P303.

Near Mendota, CGPS P304 data indicated about 80 mm of subsidence during 2004–10 (fig. 10); nearly all of it (70 mm) occurred during 2007–10. The Fordel extensometer, about 2.3 km distant from P304 and anchored near the top of the Corcoran Clay, measured about 2 mm of (net) compaction during 2002–10 and about 11 mm during 2007–10 (fig. 14). The hydrographs for this area indicated some differences between the shallow and deeper systems and in each system but generally showed seasonal and climatic effects and some long-term variability. The lowest water levels were measured in some shallow and deep wells during the 2007–10 drought. The hydrograph for shallow well 13S/16E-32F1 reached a historical low in 2007, whereas shallow or inferred shallow wells 13S/15E-28G1, 14S/15E-5J1, and 13S/15E-31J3 did not (fig. 16*A*). Similarly, the hydrograph for deep well 13S/15E-31J6 reached a historical low in 2009, whereas 14S/15E-19N1 did not (fig. 16*A*). The shallow (13S/15E-31J3) and deep (13S/15E-31J6) wells adjacent to the Fordel extensometer showed seasonal variations superimposed on longer-term trends of recovery (2003–07) and of decline (2007–10; figs. 14, 16*A*). The seasonal variations were more pronounced in the shallow water levels, whereas the longer-term trends were more pronounced in the deep water levels.

Relation of Subsidence and Groundwater Levels

Near Bypass Curve, where 340 mm of subsidence was measured using InSAR methods during 2003–10, of which more than 220 mm occurred during 2007–10 (fig. 13*A*), water levels in shallow and deep wells declined, with only water levels in deep wells surpassing historical lows (fig. 16*A*). It is likely that most of the compaction occurred in the deep aquifer system because of the much larger water-level declines than those in the shallow system during 2007–10. Furthermore, because water levels in the deep system during 2007–10 were lower than historically low levels, the deformation measured was likely mostly inelastic. Small amounts of mostly elastic compaction may have resulted from the groundwater-level declines in the shallow system.

Similar to the Bypass Curve area, most subsidence measured at the Oro Loma extensometers and at CGPS station P303 occurred during 2007–10 (figs. 8*A*, 13*A*). Near the Oro Loma extensometers, water levels in shallow wells were fairly stable, whereas water levels in the deep aquifer surpassed historical lows during the 2007–10 drought period (fig. 16*A*). Near P303, water levels in the shallow aquifer also were fairly stable (fig. 16*A*), but deep wells could not be found. Therefore, similar to the Bypass Curve area, it is likely that most of the compaction occurred in the deep aquifer system in these two areas, and near the Oro Loma extensometers, was likely mostly inelastic. The lack of water-level for the deep aquifer system near P303 precludes comparison of historical and recent water levels; thus, the nature of compaction that may have occurred in the deep system near P303 is unknown.

The frequent monitoring and the close proximity of shallow (13S/15E-31J3) and deep (13S/15E-31J6) monitoring wells to the shallow Fordel extensometer and CGPS P304 permits a meaningful interpretation of the stresses and strains above and below the Corcoran Clay that (in 2018) is not possible in any other location in the San Joaquin Valley. As previously mentioned, the Fordel extensometer measured about 9 percent of the subsidence measured by P304 during 2004–10, indicating that about 9 percent of the compaction occurred above the Corcoran Clay and 91 percent occurred below the top of the Corcoran Clay. Both the shallow and deep wells showed seasonal variations superimposed on longer-term trends of recovery (2003–07) and of decline (2007–10; fig. 14). Water levels measured in the shallow well correspond to at least some of the stresses causing the strains measured by the extensometer, whereas water levels measured in the shallow and deep wells correspond to at least some of the stresses causing the strains measured by CGPS P304. Therefore, the larger seasonal water-level variations shown by the shallow well correspond to the seasonal strains shown by the extensometer. Because water levels in shallow well 13S/15E-31J3 remained above the historical low level measured in 1991 (fig. 16*A*), the compaction measured by the extensometer (above the Corcoran Clay) is likely mostly elastic. Similarly, the longer-term water-level changes shown by the shallow and deep wells correspond to the longer-term vertical displacements shown by CGPS P304. Although the water level in deep well 13S/15E-31J6 dropped below the historical low level (measured in 1992) for a couple of months in fall 2009, the amount of inelastic subsidence that may have occurred during that short period is likely small, such that the vertical displacement shown by CGPS P304 is likely mostly elastic. However, it should be noted again here that the measured water levels represent a relatively small part of the aquifer system (according to screened intervals), compared to the thicknesses represented by the Fordel extensometer or CGPS P304, and therefore also represent only part of the stresses acting upon the aquifer system.

In summary, long-term water levels in the shallow aquifer were fairly stable compared to declining water levels in the deep aquifer. Although water levels in shallow wells generally did not surpass the historical lows measured in the 1990s, water levels did decline, especially near P304 and the Fordel extensometer, indicating that compaction of sediments in the shallow system measured using the Fordel extensometer during this period could be largely recoverable if water levels rise in the future. The historical lows reached in the deep aquifer during the 2007–10 drought period in much of the area are consistent and concurrent with the increased subsidence rates measured in parts of this region. The spatial and temporal coincidence of historically lowest deep-groundwater levels and the increased subsidence rate indicated that the preconsolidation stress was surpassed during this period and that the resulting subsidence could be largely permanent.

Panoche Creek

The Panoche Creek area is nearly 600 km^2 and includes about 45 km of the California Aqueduct just south of the town of Oro Loma. This area also includes the extensometer 14S/15E-11D6 (Panoche) and valley-fringing CGPS stations P301 and P302 (figs. 9, 11).

Subsidence and Aquifer-System Compaction

Interferometric Synthetic Aperture Radar results for 2003–10 showed that about half of the Panoche Creek area subsided at least 15 mm and had a local maximum of about 85 mm (figs. 11, 12, 13*B*). The interferograms for the area and deformation time series for two selected locations in the Panoche Creek area—the location of the maximum subsidence in this area (Panoche area maximum) and the location of the Panoche extensometer—showed subsidence during 2003–04, uplift or stability during 2004–05 and during 2006–07, and subsidence during 2007–10 (figs. 11, 12, 13*B*; appendix 1). Because InSAR analyses at, and compaction measurements from, the Panoche extensometer were taken at different times, aquifer-system compaction and land-elevation change cannot be directly compared at this location. However, the trends of Panoche extensometer measurements were generally consistent with the trends of InSAR results at the Panoche extensometer site between 2003 and 2010 (fig. 13*B*). The InSAR-derived subsidence estimates indicated about 85 mm of subsidence occurred at the Panoche area maximum, and about 30 mm of subsidence occurred at the Panoche extensometer. Panoche extensometer measurements indicated about 40 mm of compaction during 2003–10, indicating that the Panoche extensometer measured about the same amount of compaction as InSAR-derived subsidence results (fig. 13*B*). Historical comparisons between subsidence magnitudes derived from leveling surveys and compaction magnitudes for periods during 1963–75 indicated that a range of 43–73 percent, with an average of 69 percent, of subsidence was measured by the Panoche extensometer (Ireland, 1984). The more recent percentage may be higher because recent compaction may be occurring at shallower depths (less than the 414-m depth of the extensometer) or because of errors in the InSAR, extensometer, and (or) leveling measurements.

The CGPS data from P301 indicated small amounts of seasonal or shorter-term deformation (about 10 mm) with a stable longer-term deformation trend (no inelastic subsidence) from 2005 to 2010 (fig. 10). Data from CGPS station P302 showed a similar seasonal and shorter-term deformation as station P301 but indicated a subsidence trend during 2008–10 (fig. 10).

A comparison of results from geodetic surveying along the California Aqueduct by the DWR between 2000 and 2009 and InSAR results from 2003 to 2010 along the approximately 45-km reach of the Aqueduct in this area generally indicated similar patterns of deformation, consisting of two subsiding reaches separated by a reach of lesser subsidence (figs. 15*A*, *D*). The InSAR results indicated a maximum of about 50 mm of subsidence along two Aqueduct reaches, whereas the geodetic data indicated subsidence magnitudes smaller and larger than the InSAR results. Geodetic surveys along the California Aqueduct in the Panoche Creek area indicated as much as about 110 mm of subsidence and about 20 mm of uplift from 2000 to 2009. In the geodetic-survey data, there are several reaches where fairly high subsidence gradients (large differential subsidence over short reaches) are indicated. The InSAR results do not indicate as many of these high subsidence gradient reaches (figs. 15*A*, *D*). The difference in magnitudes could be caused by (1) different periods of the datasets, (2) the comparison of point-specific geodetic surveying data and areally averaged or estimated InSAR data that represent a much larger area than the Aqueduct itself, (3) instability of the monuments, (4) errors in the InSAR or survey data, or (5) a combination of these factors.

Groundwater Levels

Groundwater levels in the Panoche Creek area are exemplified by the hydrographs of inferred shallow well 15S/14E-18R1 and deep well 14S/13E-22A1 (figs. 9, 16*B*). Groundwater levels in inferred shallow well 15S/14E-18R1, which generally is representative of shallow wells in the Panoche Creek area, showed small seasonal fluctuations superimposed on longer-term trends, albeit small, of recovery from 1971 (the historical low) to 1988, stability from 1988 to 1994, and decline of about 1 m from 2004 to 2009 (fig. 16*B*). Groundwater levels in deep well 14S/13E-22A1 generally showed longer-term trends of recovery from 1967 (the historical low) to 1975 and from 1979 to 1989; stability from 1995 to 2006; and drought-induced declines during 1975–79, 1989–94, and 2006–09. Water levels declined about 35 m during the latter period (fig. 16*B*).

Relation of Subsidence and Groundwater Levels

Water levels in the shallow system declined during 2004–09 but were above the historically lowest water level recorded in 1971 (the earliest measurement; fig. 16*B*). Water levels in the deep system were generally stable or rose during the period of uplift observed in InSAR results from 2004 to 2007. They declined about 35 m during 2007–10, when subsidence was measured using InSAR, CGPS, and the Panoche extensometer (figs. 10–12, 13*B*, 16*B*), but were tens of meters above the historically lowest water level recorded in 1967 (fig. 16*B*). It is likely that most of the compaction occurred in the deep aquifer system because of the large water-level declines during the 2007–10 period of subsidence. However, because recent water levels (in the deep and shallow systems) during 2007–10 were higher than the historically low levels measured in the 1960s and 1970s (fig. 16*B*), the deformation measured was likely mostly elastic.

San Joaquin–Huron

The San Joaquin–Huron area spans from about the town of San Joaquin in the north to about Huron in the south, and from the western edge of the San Joaquin Valley to the eastern edge of the ENVISAT track-435 InSAR data coverage near Lemoore Station and encompasses about 2,500 km^2 (figs. 7, 9). This area includes about 70 km of the Aqueduct; extensometers 16S/15E-34N1 (Cantua Creek), 18S/16E-33A1 (DWR Yard), and 20S/18E-6D1 (Rasta); and valley-fringing CGPS station P300 (figs. 9, 11).

Subsidence and Aquifer-System Compaction

The San Joaquin–Huron area is part of the large subsidence feature to the east, centered near Pixley, where 350 mm of subsidence occurred between 2008 and 2010 (fig. 13*C*). The interferograms for the area and deformation time series for four selected locations in the San Joaquin–Huron area—near Helm and the locations of the Cantua Creek, DWR Yard, and Rasta extensometers—indicated a maximum of 170 mm of subsidence occurred during 2003–10 about 3 km northeast of the town of Helm (figs. 11, 12, 13*C*; appendix 1). The four locations showed subsidence during 2003–04, uplift or stability during 2004–05 and 2006–07, and subsidence during 2007–10; the result was net subsidence at these locations.

Recent measurements from the Cantua Creek and DWR Yard extensometers were not available, but InSAR time series at these two locations show similar trends of vertical deformation as near Helm (fig. 13*C*). The Cantua Creek extensometer was destroyed in 2001 (Al Steele, California Department of Water Resources, written commun., 2009); historical data are shown in figure 3. The CGPS data from P300 indicated small amounts of seasonal or shorter-term deformation (less than 5 mm) with a nearly stable, longer-term deformation trend from 2005 to 2010 (fig. 7); this stability resulted in its selection as a reference point for PS InSAR ENVISAT track-435 processing.

Recent (2003–10) measurements from the Rasta extensometer, located along the California Aqueduct about 4 km northeast of Huron, show seasonal variation in compaction and expansion, longer-term compaction during 2003–04, expansion during 2004–06, compaction during 2006–08, and expansion during 2009–10; overall, net compaction of about 10 mm occurred during 2003–10 (fig. 13*C*). The InSAR results for 2003–08 were consistent with extensometer measurements during 2003–08 but diverge during 2009–10, when InSAR results indicated subsidence, but the Rasta extensometer indicated (net) stability (fig. 13*C*). During the period 2003–08, InSAR results at the Rasta extensometer indicated 23 mm of subsidence; the extensometer indicated 12 mm of compaction, or 52 percent of the subsidence (fig. 13*C*). Historical comparisons between subsidence magnitudes derived from leveling surveys and compaction magnitudes from the Rasta extensometer for periods during 1966–78 indicated that a range of 36 to 61 percent (with an average of 42 percent) of subsidence was measured by the Rasta extensometer (Ireland, 1984). The 2003–08 percentage was consistent with this historical percentage, indicating that about half of the subsidence that occurred during each of these periods was caused by compaction in the upper 264 m, and half occurred at greater depths. The discrepancy in InSAR results and extensometer measurements for 2009–10 indicated that all the subsidence measured during this period using InSAR was a result of compaction that occurred below the depth of the extensometer (264 m).

A comparison of results from geodetic surveys along the California Aqueduct by the DWR in 2000 and 2009, and InSAR results for 2003–10, generally indicated similar patterns of deformation for this 70-km reach, consisting of two subsiding reaches separated by a reach of lesser subsidence near the DWR Yard extensometer (figs. 15*A*, *D*). The geodetic data generally indicated larger magnitudes of subsidence along the Aqueduct than do the InSAR results. The difference in magnitudes could be caused by (1) different periods of the datasets, (2) the comparison of point-specific geodetic surveying data and areally averaged or estimated InSAR data that represent a much larger area than the Aqueduct itself, (3) instability of the monuments, (4) errors in the InSAR or survey data, or (5) a combination of these factors. The northern subsiding reach is centered south of the Cantua Creek extensometer; results from geodetic surveys indicated the maximum subsidence along this reach was 260 mm during 2000–09, and results from InSAR analysis for 2003–10 indicated a maximum subsidence of about 70 mm (figs. 15*A*, *D*). The southern subsiding reach is centered near the Rasta extensometer; results from geodetic surveys indicated that the maximum subsidence along this reach was 170 mm during 2000–09, and results from InSAR analysis indicated a maximum subsidence of about 120 mm during 2003–10

(fig. 15*D*). The geodetic survey and the InSAR data along the Aqueduct indicate several reaches that have relatively high subsidence gradients, including an abrupt change in the subsidence magnitude near the DWR Yard extensometer, which is closer to the Coast Ranges than the subsiding reaches north and south of the DWR Yard extensometer. Such abrupt changes in subsidence magnitudes often are associated with groundwater barriers (faults or facies transitions), resulting in differential drawdowns across the barrier or abrupt changes in aquifer-system thickness resulting from irregular bedrock geometry such as a bedrock ridge (Galloway and others, 1999). There are no mapped faults in the area, and differential drawdowns in wells were not observed in hydrographic analyses. Although detailed data regarding depth-to-bedrock in the area are not available, the proximity to the Coast Ranges indicates that bedrock could be closer to the land surface in this Aqueduct reach compared to adjacent reaches.

Groundwater Levels

Groundwater levels near the local maximum of InSAR-derived subsidence in the San Joaquin–Huron area, near the city of Helm, were examined using the hydrographs from wells 16S/18E-3A1 (inferred shallow), 15S/17E-36G1 (shallow), and 15S/17E-36L1 (shallow; fig. 16*C*). Data from deep wells were not available in this area after 1969, but examination of the groundwater levels from shallow and deep wells revealed similar trends and magnitudes during the late 1950s to late 1960s. Groundwater levels show small seasonal fluctuations superimposed on a longer-term trend of decline from the late 1950s to 2010, when historical lows were measured (fig. 16*C*).

Groundwater levels from the northern, central, and southern San Joaquin–Huron area along the California Aqueduct, near Cantua Creek, DWR Yard extensometer, and Rasta extensometer were examined using the hydrographs from shallow and deep wells. Because this area includes a long reach of the Aqueduct (about 70 km), hydrographs from four inferred shallow wells (18S/16E-33A2, 16S/15E-20E1, 18S/16E-22Q4, and 19S/19E-32R1) and three deep wells (17S/16E-7R1, 18S/17E-20N2, and 19S/17E-22M1) along the reach were examined (fig. 16*C*). Although these wells are distributed over a large area, the hydrographs of the inferred shallow wells are similar to each other, and the hydrographs of the deep wells are similar to each other (fig. 16*C*). Groundwater levels in inferred shallow well 18S/16E-33A2 showed small seasonal fluctuations superimposed on longer-term trends of minor recovery from 1970 (the historic low) to 1994 (fig. 16*C*). Groundwater levels in inferred shallow wells 16S/15E-20E1, 18S/16E-22Q4, and 19S/19E-32R1 showed small seasonal fluctuations superimposed on longer-term trends of minor declines from 2003 to 2010, a period during which historical lows were measured (fig. 16*C*). Groundwater levels in deep wells 17S/16E-7R1, 18S/17E-20N2, and 19S/17E-22M1 generally show a longer-term trend of recovery from historically low levels in the 1960s to 1987 that was interrupted by fairly large declines related to drought periods (1976–77, 1987–92, 2007–10), and to other periods when groundwater pumping apparently increased (late 1990s to early or mid-2000s). In summary, hydrographs in this area show seasonal and climatic effects and substantially more long-term variability in the deep aquifer than in the shallow aquifer. The lowest groundwater levels were measured in the 1960s in the deep aquifer; the lowest groundwater levels for most shallow wells were measured during 2006–10.

Relation of Subsidence and Groundwater Levels

The InSAR analysis indicated 170 mm of subsidence at the local maximum, near the town of Helm in the San Joaquin–Huron area (fig. 13*C*), which is part of a large subsidence feature centered near Pixley (fig. 12). Water levels in the shallow system persistently declined for decades, including during 2006–10 (fig. 16*C*), indicating that the preconsolidation stress was surpassed during this period and compaction that may have occurred in the shallow system may be largely permanent. The lack of longer-term hydrographs for the deep system precludes comparison of historical and recent water levels; thus, the nature of compaction that may have occurred in the deep system is unknown.

Elevation changes measured using InSAR and geodetic survey data during 2003–10 and 2000–09, respectively, indicated subsidence along and adjacent to the California Aqueduct in two reaches, separated by a reach of lesser subsidence (figs. 15*A*, *D*). Seasonal aquifer-system deformation superimposed on longer-term subsidence and compaction were measured using InSAR methods and the Rasta extensometer (fig. 13*C*). Comparison of the 2003–08 Rasta extensometer and InSAR results at the Rasta extensometer site indicated that about half of the compaction occurred in the upper 264 m and half occurred below that depth. However, comparison of the 2009–10 data indicates that compaction during this 2-year period occurred deeper than 264 m. Recent groundwater levels (2003–10) in some wells in the shallow system declined, and therefore, compaction may have occurred in the shallow system (fig. 16*C*). The lack of shallow wells near the Aqueduct with long-term records precludes direct comparison of historical and recent water levels; thus, the nature of compaction that may have occurred in the shallow system in these areas is unknown. Recent groundwater levels (2003–10) in the deep system were higher than the historical lows measured in the 1960s, indicating that recent compaction that may have occurred in the deep system was likely primarily elastic. Similarities among shallow-well hydrographs and among deep wells along the California Aqueduct in the San Joaquin–Huron area indicate that the differential subsidence magnitudes along the California Aqueduct likely were influenced by other factors, such as subsurface geology. This differential subsidence is particularly evident along the reaches near the DWR Yard extensometer, where an abrupt change in subsidence was measured by InSAR methods and geodetic surveys for periods between 2000 and 2010.

Kettleman City

The Kettleman City area consists of approximately 360 km^2 surrounding the town of Kettleman City and includes 16 km of the California Aqueduct (figs. 11, 12). This area also includes the valley-fringing CGPS station P547 near the southwestern extent of this area (figs. 9, 11).

Subsidence and Aquifer-System Compaction

The Kettleman City area is part of the large subsidence feature to the east, centered near Pixley, where 350 mm of subsidence occurred between 2008 and 2010 (fig. 13*C*). Within this area, a local maximum subsidence magnitude of 110 mm during 2003–10 occurred about 12 km north of the town of Kettleman City (figs. 11, 13*D*). The InSAR results from 2003–10 indicate a similar subsidence trend to that of other areas previously mentioned in this study: subsidence during 2003–04, uplift during 2004–05, stability during 2006–07, and subsidence during 2007–10. The CGPS station P547 showed seasonal periods of subsidence and uplift superimposed on a longer-term trend of slight uplift (fig. 10). The geodetic-survey data for 2000–09 and the InSAR results for 2003–10 along the 16-km reach of the Aqueduct in this area show that this reach had fairly small amounts (less than 30 mm) of subsidence and of uplift (figs. 15*A*, *D*), and the geodetic data generally indicate smaller magnitudes of subsidence than do the InSAR results. The difference in magnitudes could be caused by (1) different periods of the datasets, (2) the comparison of point-specific geodetic surveying data and areally averaged or estimated InSAR data that represent a much larger area than the Aqueduct itself, (3) instability of the monuments, (4) errors in the InSAR or survey data, or (5) a combination of these factors.

Groundwater Levels

Groundwater levels near the local maximum of InSAR-derived subsidence in the Kettleman City area, north of Kettleman City, were examined using the hydrographs from wells 20S/19E-32R1 (inferred shallow) and 21S/19E-7D1 (inferred deep; fig. 16*D*). Groundwater levels in inferred shallow well 20S/19E-32R1 show small seasonal fluctuations superimposed on longer-term trends of small amounts of recovery during 1991–2001 and 2005–07 and longer-term trends of small amounts of decline during 2001–05 and 2007–10. Historical lows were reached during 2008–10, which were about 2 m lower than the average water level for the period of record (fig. 16*D*). Groundwater levels in inferred deep well 21S/19E-7D1 show longer-term trends of recovery during 1978–88 and 1992–2006 and trends of decline during 1988–92 and 2006–10, indicating responses to drought periods. Water levels declined tens of meters during these periods; however, the water level in 2010 was about 20 m above the historical low reached in 1992. The declines during 2007–10 were much larger in the inferred deep well compared to the inferred shallow well.

Relation of Subsidence and Groundwater Levels

Water levels in the shallow and deep systems declined during the drought period 2007–10, when subsidence was measured just north of Kettleman City (fig. 13*D*). Water levels in the shallow system reached historical lows during this period, whereas water levels in the deep system remained substantially higher than historical lows. It is likely that more compaction occurred in the deep aquifer system because of the much larger water-level declines than in the shallow system during the 2007–10 period of subsidence. However, because recent water levels in the deep system during 2007–10 were higher than historically low levels (fig. 16*D*), the deformation measured was likely mostly elastic. Small amounts of inelastic compaction may have resulted from the relatively small groundwater-level declines below historical lows in the shallow system.

Comparison to Historical Land Subsidence

Subsidence contours for 1926–70 (Poland and others, 1975) show the area of maximum subsidence was southwest of Mendota, whereas data collected and compiled for this study for 2003–10 indicate that the area of maximum subsidence has shifted northeast, to the area south of El Nido (fig. 17). Historical maximum subsidence exceeded 8,500 mm during 1926–70 southwest of Mendota, where rates ranged 180–500 mm/yr during the 1950s and 1960s (Ireland and others, 1984; Ireland, 1986). Maximum subsidence during 2008–10 was about 540 mm, or about 270 mm/yr, in the area south of El Nido (fig. 17). A second important subsidence maximum was near Pixley, where subsidence rates were less than near El Nido, but a larger area, more than 1,600 km^2, was affected by at least 150 mm of subsidence during 2008–10 (fig. 17). Near Pixley, the maximum subsidence was 350 mm during this period, or 175 mm/yr (fig. 13*C*). The subsidence areas centered near El Nido and Pixley coalesce to form a 12,000 km^2 area affected by at least 25 mm of subsidence during 2008–10, including long reaches of the California Aqueduct and many other water conveyance facilities and other infrastructure (fig. 17).

The subsidence information gap between the late 1970s and the early 2000s, was caused by sharply reduced subsidence monitoring efforts after the delivery of water through Federal and State distribution systems appeared to have largely arrested subsidence. As the subsidence problem began to be revisited in earnest around 2010, the lack of subsidence information for the previous three decades largely precluded the construction of a regional subsidence history; researchers had few clues about how much, or where, subsidence may have occurred during that period. Had all other factors, such as population, land use, water application and other farming techniques, and cropping patterns all remained unchanged since the 1960s and 1970s, then perhaps an estimated subsidence history could have been reconstructed. However, these and many other factors influencing water use have changed and will continue to change. Had the aquifer-system response been tracked during these decades, it would not have been a surprise that large parts of the valley were subsiding at rates as high as 270 mm/yr in the 2000s.

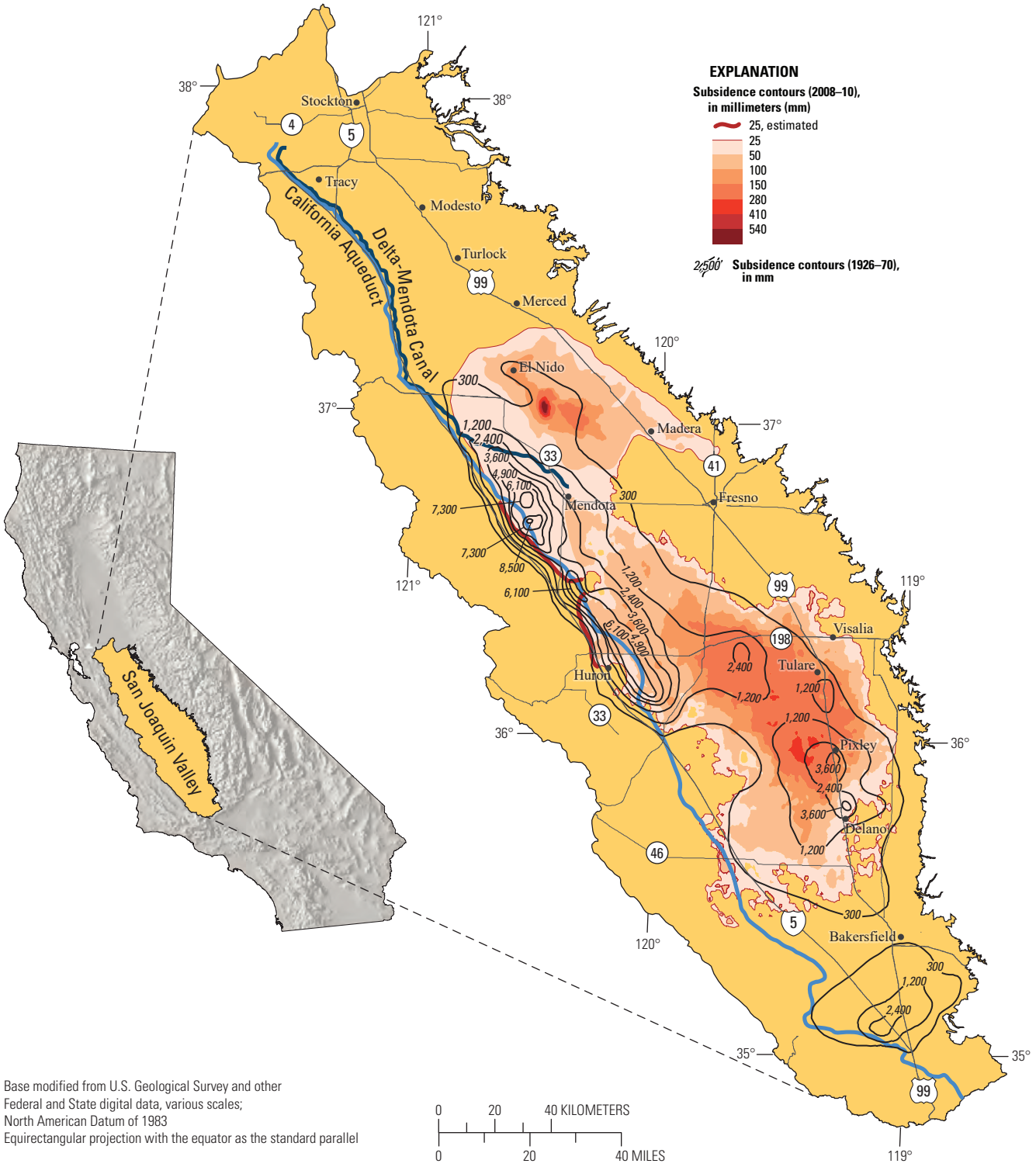

Figure 17. Land subsidence in the San Joaquin Valley, California, 1926–70 (modified from Poland and others, 1975) and 2008–10.

Oro Loma–Madera (El Nido)

The Oro Loma Deep and Shallow extensometers (305- and 107-m depths, respectively) were used to measure about 910 and 100 mm of compaction, respectively, between 1958 and 2010 (fig. 18*A*). Most of the compaction in Oro Loma Deep occurred by the mid-1970s; the maximum measured compaction, about 980 mm, occurred by 1993, following the 1987–92 drought, after which 70 mm of aquifer-system expansion was measured. The largest measured compaction rate, about 130 mm/yr, occurred during the first year of measurements; the rate generally declined thereafter, except during drought periods. Measurements at Oro Loma Shallow, on the other hand, show small amounts of compaction at fairly steady rates during the periods 1958–82, 1997–2000, and 2009–10; measurements were not taken between these periods. Although measurements at the Oro Loma extensometers were not taken between 2000 and 2008, the InSAR results indicate periods of small amounts of uplift and subsidence between 2003 and 2010, with a maximum subsidence rate of 130 mm/yr occurring during part of spring 2008—the same rate that occurred during the late 1950s. (Note: the extensometer records could be continued through the gaps because the measuring tape used to take measurements was still intact, apparently undisturbed, and attached to the reference table and the extensometer cable.)

Historical subsidence rates along Highway 152, which bisects the 2008–10 area of active subsidence in the Oro Loma–Madera area, were calculated from geodetic-survey data from 1972, 1988, and 2004. These data show that for the two 16-year periods (1972–88 and 1988–2004), an average subsidence rate of about 50 mm/yr resulted in more than 1,500 mm of subsidence south of El Nido during 1972–2004 (figs. 15*A*, *B*). The subsidence rates for the same area computed from the 2008–10 InSAR data were 50–75 mm/yr, or as much as about 50 percent higher than the historical rates.

Panoche Creek

The Panoche extensometer (414-m depth) is in the Panoche Creek area; it shows about 1,380 mm of compaction between 1961 and 2010. The majority occurred during 1961–68, when about 1,180 mm of subsidence was measured at a fairly steady rate of about 160 mm/yr (fig. 18*B*; Ireland and others, 1984). Compaction rates slowed substantially between mid-1968 and 1977, when the average rate was less than 20 mm/yr. Since 1978, small amounts of compaction were measured during drought periods, and small amounts of expansion occurred between the drought periods. However, during a 2-month period in 2008, about 55 mm of compaction was measured (figs. 13*B*, 18*B*), corresponding to a rate of about 310 mm/yr—the highest rate ever measured using the Panoche extensometer. (Note: the extensometer record could be continued through the gap because the measuring tape used to take measurements was still intact, apparently undisturbed, and attached to the reference table and the extensometer cable.)

San Joaquin–Huron

The Cantua Creek extensometer (610-m depth), in the San-Joaquin–Huron area, recorded nearly 3,600 mm of aquifer-system compaction between 1958 and 1998 (fig. 18*C*). This is the largest magnitude of compaction measured using an extensometer in the San Joaquin Valley. The Cantua Creek extensometer was destroyed in 2001 (Al Steele, California Department of Water Resources, written commun., 2009). Nearly 3,400 mm of compaction were measured by 1972, or about 250 mm/yr, after which compaction occurred generally during drought periods and expansion occurred between the drought periods. Measurements were not taken after 1998 at the Cantua Creek extensometer, but InSAR results indicate periods of small amounts of uplift and subsidence between 2003 and 2010, resulting in about 30 mm of subsidence for the 7-year period (fig. 13*C*). For a 35-day period in spring 2008, when surface-water allocations were limited to 35 percent (accessed July 5, 2018, at http://wdl.water.ca.gov/swpao/deliveries.cfm), InSAR results indicate about 25 mm of subsidence, corresponding to a rate of 250 mm/yr—a rate equivalent to the compaction rate computed for 1958–72. Notwithstanding the short period of high subsidence rates in 2008, the comparatively small amounts of subsidence measured during this study compared to historical magnitudes, and the continued dominance of agricultural land use in this vicinity, indicate that the delivery of surface water through the California Aqueduct markedly reduced dependence on groundwater in this area.

The DWR Yard extensometer (314-m depth) is in the San Joaquin–Huron area and recorded about 680 mm of aquifer-system compaction between 1965 and 1998 (fig. 18*D*). The largest rates were measured during the first years of measurements; the subsequent rates generally declined each year, except during drought periods. The 1987–92 drought period was associated with particularly large rates at this site: between 1965 and 1986 (21-year period), about 290 mm of compaction was measured, or less than 15 mm/yr; by 1995, an additional 430 mm of compaction was measured, or about 50 mm/yr. Measurements were not taken between 1998 and 2010 at the DWR Yard extensometer, but InSAR results indicate periods of small amounts of uplift and subsidence between 2003 and 2010, resulting in about 55 mm of net subsidence for the 7-year period (fig. 13*C*). During 2008–10, this location subsided at about 35 mm/yr, which was lower than the compaction rate measured during and after the 1987–92 drought period. As noted earlier, the reach of the Aqueduct that includes this extensometer subsided less than adjacent reaches, perhaps because of shallower depth to bedrock and associated thinner aquifer system. A thinner aquifer system also could have the effect of increased sensitivity to pumping stresses because there is less capacity to store water, and its juxtaposition to the Coast Ranges likely limits flow (recharge) from the west. These conditions could set the stage for rapid drawdowns and associated aquifer-system compaction; this may explain the 55-m water-level decline (fig. 16*C*) and 430 mm of compaction that were measured during 1987–95.

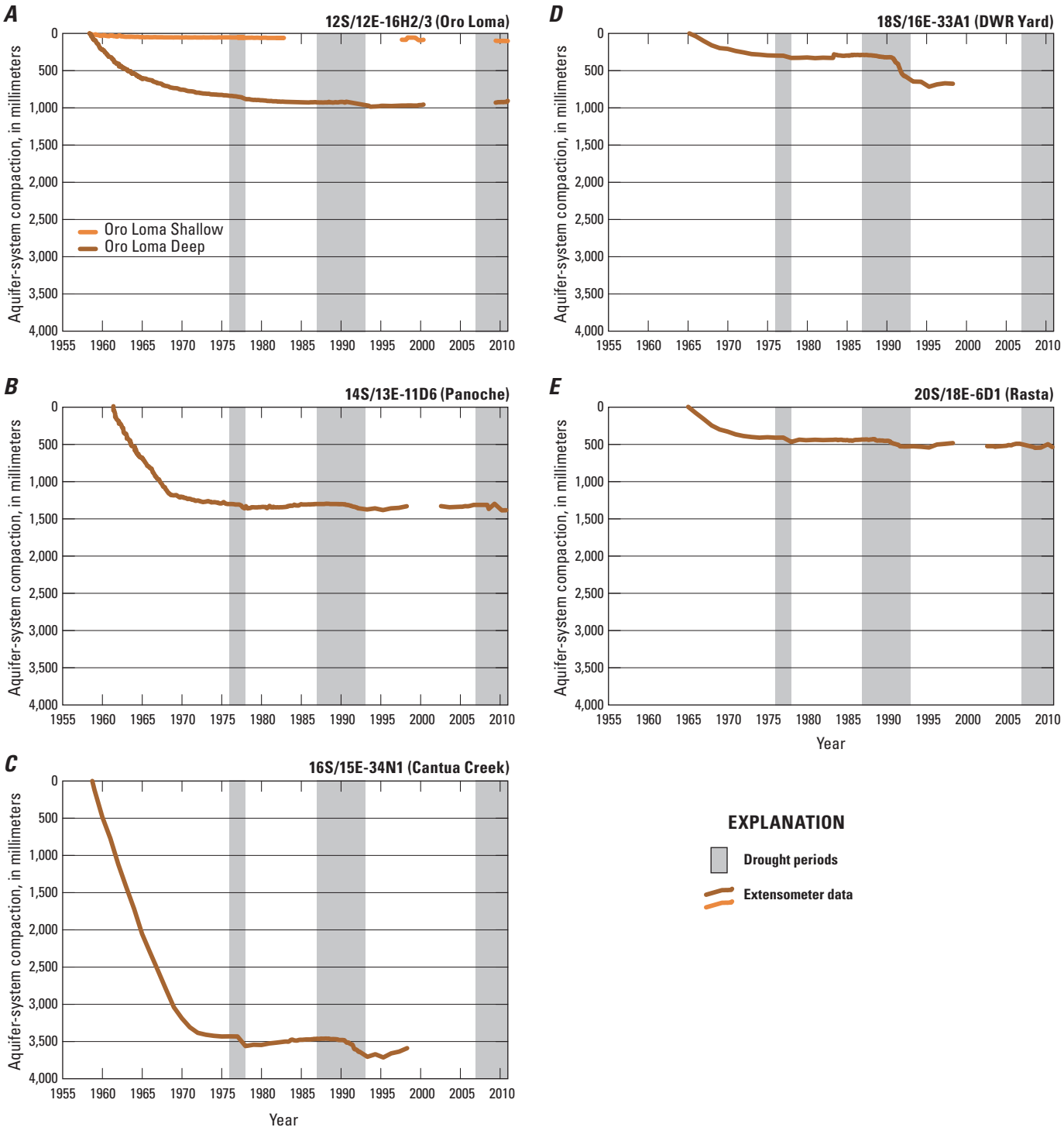

Figure 18. Aquifer-system compaction measured using *A*, the Oro Loma Deep and Oro Loma Shallow extensometers (12S/12E-16H2 and 12S/12E-16H3) for 1958–2010; *B*, the Panoche extensometer (14S/13E-11D6) for 1961–2010; *C*, the Cantua Creek extensometer (16S/15E-34N1) for 1958–98; *D*, the DWR Yard extensometer (18S/16E-33A1) for 1965–98; and *E*, the Rasta extensometer (20S/18E-6D1) for 1965–2010, San Joaquin Valley, California. A break in the compaction graph line indicates that no measurements were taken for at least 4 years. The periods shaded represent calendar years affected by increased pumping as a result of drought periods. Larger values indicate increased compaction. See figure 9 for extensometer locations.

The Rasta extensometer (264-m depth) is in the San Joaquin–Huron area and was used to measure about 540 mm of compaction between 1965 and 2010; nearly half was measured during 1965 to late 1967, a period when 250 mm of compaction was measured at a fairly steady rate of about 80 mm/yr (fig. 18*E*; Ireland, 1986). Compaction rates slowed significantly during 1968–77, after which compaction was measured only during drought periods, including the 2007–10 drought, when the extensometer measured a maximum rate of about 70 mm/yr in 2010 and InSAR measured a rate of about 50 mm/yr during 2008–10. The recent rates are similar, albeit slightly smaller, than historical rates. (Note: the extensometer record could be continued through the gap because the measuring tape used to take measurements was still intact, apparently undisturbed, and attached to the reference table and the extensometer cable.)

Historical contours for 1926–70 indicate that about 2,400 mm, or about 55 mm/yr, of subsidence occurred along Highway 198, near the town of Armona, which is about 30 km east of the California Aqueduct and 15 km east of the San Joaquin–Huron area (figs. 15*A*, 15*C*, 17). Historical subsidence rates calculated from geodetic-survey data from the late 1950s or early 1960s and 2004 show that for this 40–45-year period, a maximum subsidence magnitude of about 2,900 mm, corresponding to a rate of about 70 mm/yr, occurred in this same area. Although the location of the geodetic-survey-inferred subsidence maximum along Highway 198 was not captured by the 2003–08 InSAR data, InSAR results for 2008–10 indicate that this location subsided 235 mm during the 2-year period, or about 117 mm/yr (figs. 12, 15*A*, 15*C*, 17). Although the 2008–10 subsidence rate is substantially higher than the historical rate, the historical rate is computed for a much longer period during which rates varied substantially (for example, fig. 3).

Kettleman City

Historical contours for 1926–70 indicate that the Kettleman City area subsided as much as 2,400 mm (fig. 17), or about 55 mm/yr. Although data from valley-fringing P547 for 2006–10 in the southern part of the area indicate slight uplift (fig. 10), InSAR results indicate about 100 mm of subsidence between 2008 and 2010 in the northern part of the area (fig. 13*D*), or about 50 mm/yr, which is similar to the historical rate.

Effects of Land Subsidence on Infrastructure

Land subsidence in the San Joaquin Valley has caused damage to structures including aqueducts, levees, dams, roads, bridges, pipelines, and well casings (Galloway and Riley, 1999; Luhdorff and Scalmanini Consulting Engineers and others, 2014); costs from these damages during 1955–72 have been estimated at $1.3 billion (2013 dollars). Total subsidence and costs would be expected to be much greater at the time of this report, but few data are available to quantify total damages (Moran and others, 2014).

Aqueducts tend to be the most sensitive infrastructure to subsidence because they largely were designed to use gravity to drive flow. For gravity to drive flow through an aqueduct, the water surface upstream must be at a higher elevation than the water surface downstream. In the topographically flat San Joaquin Valley, aqueducts have been constructed to have small gradients to control the costs of construction associated with elevating the aqueduct to achieve higher gradients. If the entire aqueduct subsided at the same rate, then the gradient would be maintained, and water would flow as designed. However, because the aqueduct has subsided differentially, the gradient is disrupted in parts of the aqueduct, which causes a reduction in the conveyance capacity and freeboard of the aqueduct. As the aqueduct subsides differentially, the water-surface elevation differences, and therefore conveyance capacity, can be maintained by raising the associated infrastructure, including levees, canal liners, bridges, and check stations, which essentially increases the size and associated capacity of the aqueduct. Subsidence also damages concrete liners and causes misalignment of the water surface and liner. If aqueduct water seeps through a broken concrete liner or overtops the liner because of misalignment, the earthen levee behind the liner may erode, thereby weakening the levee.

Significant resources have been applied to mitigate subsidence-induced infrastructure damage on reaches of the California Aqueduct, the DMC, and other canals, and continued maintenance and repairs are expected (Swanson, 1998; Bob Martin, San Luis and Delta-Mendota Water Authority, oral commun., 2011; Chris White, Central California Irrigation District, oral commun., 2011; David Rennie, California Department of Water Resources, written commun., 2014; Luhdorff and Scalmanini Consulting Engineers and others, 2014; Doug DeFlitch, Friant Water Authority, written commun., 2017). On the California Aqueduct, many major repairs are being planned and are focused on bridge repairs, canal structural repairs, and check station or turnout repairs (David Rennie, California Department of Water Resources, written commun., 2014). The canal liner has been repaired in several locations since the mid-2000s. The previous major round of subsidence-related repairs on the Aqueduct occurred in 1982, when the concrete canal lining was raised between about 0.3 and 1 m at various locations (David Rennie, California Department of Water Resources, written commun., 2014). Water delivery structure (and other infrastructure) locations are at higher risk of rupture where there are high subsidence gradients from differential subsidence. Several areas of high subsidence gradients measured using InSAR and geodetic survey results coincide with recent repairs on the Aqueduct, including the southern extent of the Panoche Creek area, and between the DWR Yard and Rasta extensometers in the San Joaquin–Huron area (fig. 15*D*). Some canal-repair locations were in areas with low- to moderate-subsidence gradients, such as near CGPS station P301 near the northern extent of the Panoche Creek area (fig. 15*D*).

Flow capacity in the DMC (Oro Loma–Madera area) has essentially been maintained by extending the height of infrastructure, including check structures, raising embankments and bridges, and tolerating reduced freeboard (Seth Harris, San Luis and Delta-Mendota Water Authority, oral commun., 2012). Despite some similar mitigation efforts on other nearby canals, design flow capacity on several of these nearby canals has been reduced by as much as 50 percent (Chris White, Central California Irrigation District, oral commun., 2011). At least one irrigation district has had difficulty maintaining adequate diversions from the south end of Mendota Pool behind the Mendota Dam, even though water levels were raised to nearly the top of the dam embankment (Swanson, 1998). The repair or replacement of the Mendota Dam is being considered (Swanson, 1998).

Significant resources also have been applied to mitigate subsidence along the Eastside Bypass, the primary flood-control channel for the region. By 1995, there had been about 1.2 m of subsidence since its construction in 1965, causing erosion and deposition in this unlined channel and a 27-percent reduction in flow capacity, which required the raising of levees on the west bank (Swanson, 1998). Erosion and deposition in this channel also have recently occurred (Reggie Hill, Lower San Joaquin Levee District, oral commun., 2014). Along the San Joaquin River, resources were applied during 2011–18 to characterize the subsidence magnitudes and rates in order to mitigate substantial subsidence-related design problems of the Arroyo Canal Fish Screen and Sack Dam Fish Passage Project, which is part of the multi-agency San Joaquin River Restoration Program (accessed July 5, 2018, at http://www.restoresjr.net/science/subsidence-monitoring/).

Future Monitoring

Continued groundwater-level and land-subsidence monitoring in the San Joaquin Valley is important because (1) operational- and drought-related reductions in surface-water deliveries since 1976 have resulted in periods of increased groundwater pumping and associated land subsidence, (2) land use and associated pumping continue to change throughout the valley, and (3) subsidence management is stipulated in California's Sustainable Groundwater Management Act (SGMA) of 2014. The availability of surface water remains uncertain; even during relatively wetter years, such as 2010–11, water deliveries fell short of requests. Future subsidence is therefore of concern.

The lack of subsidence data from the late 1970s to the early 2000s degrades the capabilities of numerical models to simulate observed subsidence over large areas, and therefore, to predict future subsidence, because few calibration data are available. Periodic geodetic surveys along some canals during this period can provide useful calibration data for more constrained subsidence simulations of these structures. With the passage of SGMA, the consistency of subsidence monitoring in some areas is expected to improve, which will result in better model calibrations and future subsidence projections.

Data types with different ranges of spatial and temporal densities are complementary, and a suite of such data types are needed to understand the mechanisms that underlie the spatial and temporal subsidence patterns and improve associated subsidence simulations; the different data types reveal unique aspects of the subsidence story, as this study demonstrates. Diversification of data types increases their robustness, reliability, and redundancy. Different types of subsidence measurements also can be used to validate or ground truth each other for quality assurance and to increase depth of understanding.

Spatially detailed InSAR-derived maps of ground displacements could be processed annually or more frequently, depending on data availability. The cost of processing InSAR data can be high, and data availability and continuity uncertain, but the increasing number of satellites orbiting and planned for launch by a plethora of space agencies is driving data costs down and increasing data availability. For example, the ESA is providing free and open access to SAR data from the Sentinel-1A and -1B SAR satellites recently launched; NASA and the Indian Space Research Organization (ISRO) plan to cooperatively launch the NASA-ISRO SAR (NiSAR) mission in early 2021 and also reportedly plan free and open data access (Jet Propulsion Laboratory, 2018). However, satellite failures could result in periods when no, or very little, SAR data are available.

Temporally detailed CGPS data, depending on data availability, can be used to provide an ideal dataset by which to cross-validate InSAR results because CGPS solutions are computed daily. Hydrogeologists focused on the west coast of the United States, including the San Joaquin Valley, have enjoyed the plethora of CGPS data collected by UNAVCO since 2003; this research group investigates deformation associated with the boundary between the North American and Pacific tectonic plates. National Science Foundation funding to continue operation and maintenance of the CGPS stations is expected to expire in 2018. An improvement to these stations is the installation of corner reflectors, or ideally radar transponders, at CGPS stations to ensure that a coincident InSAR pixel is produced for dependable comparison. Corner reflectors must be specifically oriented toward the satellite line of sight, which varies; radar transponders can be used with any satellite.

Extensometers provide temporally detailed and uniquely depth-specific deformation measurements; they are typically monitored continuously by using a linear potentiometer and data logger, discretely using a dial gauge, or by using both. Extensometers can be installed singly or in clusters and can be used in conjunction with InSAR or other measurements of land-surface change to quantify the compaction of specific depth intervals. The newly developed magnetic-marker extensometer, not yet employed in the United States, can be configured to monitor deformation of multiple depth intervals using a single borehole (Hung and others, 2012). The unique capability of extensometers to delineate the depths at which compaction is occurring is instrumental for calibrating groundwater-flow and compaction models and likely will be employed as groundwater sustainability agencies wrestle with groundwater sustainability monitoring and management requirements now mandated by California law.

Spatially detailed InSAR data and temporally continuous data from CGPS and extensometers can be used to indicate when and where additional monitoring efforts should be made, such as geodetic surveys to measure and map land subsidence, or establishing new CGPS or extensometer stations. Because InSAR-detected areas of subsidence spatially overlap the CGPS network, future monitoring of the CGPS network could provide ground truth for the more spatially detailed InSAR measurements, as was done during this study.

Infrastructure, such as the California Aqueduct, is often hundreds of kilometers in length but less than 0.1 km in width—and most of that width is under the water surface. Only about 10 m on each side of the canal—the levee tops—are used to measure and map land subsidence of the canal. Precise elevation (and elevation change) measurements at specific locations on each side of the canal are critical for computing flows and flow capacities; therefore, high-resolution monitoring techniques are necessary. Most often, geodetic surveying techniques have been used, which are costly because of the long distances involved; therefore, they are not done frequently. For example, parts of the California Aqueduct were measured about every 3–6 years between 2000 and 2009. In this study, we compared InSAR results to the periodically collected geodetic data along the Aqueduct. Although the spaceborne InSAR results generally indicated patterns of subsidence along the Aqueduct similar to those indicated by the geodetic data, the spatial resolution was substantially coarser than the geodetic data, and therefore, spaceborne InSAR may not be a very useful tool for monitoring such narrow infrastructure. More recently, airborne SAR systems have been used to assess subsidence along parts of the California Aqueduct (Farr and others, 2015; 2016). Uninhabited Aerial Vehicle Synthetic Aperture Radar (UAVSAR) has a much higher signal-to-noise ratio than satellite SARs, usually achieving a factor of 100 increase in signal using a high-power instrument transmitting from a much lower altitude compared to Earth orbit. The L-band system has a higher spatial resolution than the satellite SARs, with a 1.7-m instrument ground resolution, which allows significantly higher resolution than satellite SARs when accounting for the spatial averaging that is done to reduce the phase noise. The reduction in phase noise results in increased deformation-measurement accuracy and reduced temporal decorrelation (Farr and others, 2016). Therefore, airborne SAR data combined with repeated geodetic survey data may enable precise measurements of specific locations and may be used to identify problems in other locations along and adjacent to canals and other long, narrow infrastructures.

Generally, the frequency of water-level measurements in monitoring wells has been too low to permit meaningful interpretations of shorter-term aquifer-system responses to water-level changes. In many wells, water-level measurements are taken annually in the spring; quarterly measurements would provide a much better dataset for assessing seasonal groundwater-level and storage changes. At daily or sub-daily frequencies, water-level data can be combined with other datasets to estimate aquifer-system properties (Sneed and Galloway, 2000). As a part of the recent work in the study area by the USGS, Reclamation, and SLDMWA, four extensometer sites were instrumented to collect continuous (hourly) water levels (appendix E in Sneed and others, 2013). Paired continuous-deformation and water-level data permit (1) detection of changes in the relationship between water-level change and aquifer-system deformation, (2) estimation of key hydraulic parameters that govern groundwater flow and the timing and rate of land subsidence, including the preconsolidation head (the critical head at which elastic, or recoverable, deformation converts to inelastic, or permanent, compaction), and (3) elucidation of the role of residual compaction. This information is critical not only to manage water and land resources sustainably but also to better constrain models used to evaluate aquifer-system compaction and resultant land subsidence that may result under various future management scenarios.

Summary and Conclusions

The extensive withdrawal of groundwater from the unconsolidated deposits of the San Joaquin Valley has caused widespread land subsidence—locally exceeding 8.5 meters (m) by 1970 (fig. 2) and reaching 9 m by 1981. Land subsidence from groundwater pumping began in the mid-1920s, and by 1970, there had been more than 0.3 m of land subsidence over an area of about 13,500 square kilometers

(km^2). The importation of surface water after completion of the Central Valley Project's Delta-Mendota Canal (DMC) in the early 1950s and the State Water Project's California Aqueduct in the early 1970s, and the associated decrease in groundwater pumping in some parts of the valley, was accompanied by a steady recovery of water levels and a reduced rate of aquifer-system compaction and resultant subsidence in some areas (figs. 3, 18). During the drought periods of 1976–77, 1987–92, and 2007–10, diminished deliveries of imported water prompted pumping of groundwater to meet irrigation demands. This increased groundwater pumping resulted in water-level declines and periods of renewed subsidence (figs. 3, 4, 13, 18). Subsidence has reduced the flow capacity and freeboard of several channels that deliver irrigation water to farmers and transport floodwater out of the valley.

The U.S. Geological Survey, in cooperation with the California Department of Water Resources, assessed more recent land subsidence near a 145-kilometer reach of the California Aqueduct from about the town of Oro Loma to about Kettleman City in the west-central part of the San Joaquin Valley, as part of an effort to minimize future subsidence-related damages to the California Aqueduct. This report presents the status of land subsidence, compaction, and water-level trends along the Aqueduct and adjacent areas in the west-central San Joaquin Valley from 2003 through 2010. Measured groundwater-level changes during 2003–10 were examined and compared with measurements of compaction and land subsidence to evaluate their relation, including determinations of stress-strain regimes (elastic or inelastic). The location, magnitude, and stress regime of land-surface deformation during 2003–10 in the west-central part of the San Joaquin Valley traversed by the California Aqueduct were determined by using data and analyses associated with extensometers, Global Positioning System (GPS) surveys, Interferometric Synthetic Aperture Radar (InSAR), spirit-leveling surveys, and groundwater wells. The InSAR measurements were useful for detailed mapping of areas affected by subsidence during multiple periods, and along with geodetic data, were used to subdivide the California Aqueduct into four reaches showing similar subsidence characteristics by which to organize discussions in this report (figs. 11, 12, 15). Continuous Global Positioning System (CGPS) measurements were useful for constructing continuous time series at a few locations and also for constraining the InSAR results (figs. 8, 10). Repeat GPS- and spirit-leveling-survey data were useful for identifying areas near highways and canals affected by subsidence and for computing longer-term rates of subsidence, which were compared to subsidence rates computed using InSAR results (fig. 15). Extensometer data were useful in determining specific depth intervals of aquifer-system compaction and comparing to InSAR and CGPS results (figs. 13, 14, 18). Water-level data were useful in postulating whether the aquifer-system deformation was predominantly elastic or inelastic in some areas (fig. 16).

Generally, InSAR, GPS, and extensometer analysis in the study area indicate that much of the San Joaquin Valley subsided from 2003 to 2010. Temporally, there were periods of subsidence during 2003–04 and 2007–10 and a period of slowed subsidence and (or) uplift during 2004–07. In areas where groundwater levels in the shallow and (or) deep systems declined during 2003–10 but remained above historical lows, such as along the California Aqueduct in the Panoche Creek and Kettleman City areas (figs. 16*B*, *D*), primarily elastic subsidence likely occurred. In areas where groundwater levels in the shallow system surpassed historical lows, but groundwater levels in the deep system remained above historical lows, such as along the California Aqueduct in the San Joaquin–Huron area (fig. 16*C*), primarily inelastic subsidence may have occurred in the shallow system, and primarily elastic deformation may have occurred in the deep system. In areas where water levels in shallow and deep wells declined to historical lows, such as near El Nido and Bypass Curve, large magnitudes of primarily inelastic subsidence were measured (fig. 16*A*).

The differential rate of subsidence is particularly important where infrastructure is located. As a result, the study area was subdivided into four areas showing similar deformation patterns of subsidence along the California Aqueduct—Oro Loma–Madera, Panoche Creek, San Joaquin–Huron, and Kettleman City (figs. 11, 12, 15*D*). The analyses indicate that the Oro Loma–Madera area subsided as part of a large subsidence feature centered south of the town of El Nido, which is about 40 km northeast of the California Aqueduct (fig. 12). The area affected by 25 millimeters (mm) or more of net subsidence during 2008–10 extends from near Los Banos to Madera, and from near Merced to near Mendota, including parts of the California Aqueduct; the maximum subsidence was at least 540 mm during this period. There were seasonal variations in elevations given by CGPS stations on the fringes of the area of most rapid subsidence (figs. 8, 10–12), but these variations were small compared to the large and longer-term subsidence magnitudes measured in this area. Water levels in many deep wells in this area reached historical lows during 2007–10 (fig. 16*A*), indicating that some of the subsidence measured in this area likely was inelastic. Calculations of subsidence rates indicate increases in 2008 in much of the area. The GPS survey data from 2008 and 2010 corroborated the high subsidence rate computed using InSAR results during that period, and GPS survey data collected biannually since 2011 indicate that the high rate of subsidence continued through 2016. Results of data comparison from the Fordel extensometer (anchored near the top of the Corcoran Clay) and CGPS P304, the historically low water levels in deep wells during 2007–10, and water levels in shallow wells that remained above historically low levels indicate that most of the aquifer-system compaction occurred below the Corcoran Clay (fig. 14), which also was the conclusion of historical investigations.

The InSAR results indicate that portions of the Panoche Creek area (including about 45 km of the California Aqueduct) had periods of subsidence and of uplift, which resulted in a maximum net loss in elevation of 85 mm during 2003–10 (figs. 11, 12, 13*B*). The InSAR results indicate a maximum of about 50 mm of subsidence along two California Aqueduct reaches, which was likely mostly elastic because water levels in many wells in this area did not reach historical lows during 2003–10.

The InSAR results indicate that parts of the San Joaquin–Huron area (including about 70 km of the California Aqueduct) had periods of subsidence and of uplift, which resulted in a maximum net loss of 170 mm in elevation during 2003–10 near Helm (figs. 11, 12, 13*C*). The results indicate that the San Joaquin–Huron area subsided as part of a large subsidence feature centered near the town of Pixley, which is about 40 km east of the California Aqueduct (figs. 12, 13*C*). The proximity to the Coast Ranges is associated with changes in subsidence magnitude, such that relatively larger magnitudes of subsidence along the California Aqueduct occurred in areas where it extends farther into the valley. The 120 mm or less of InSAR-measured subsidence along the California Aqueduct was likely mostly elastic because water levels in many wells in this area did not reach historical lows during 2003–10 (fig. 16*C*). However, data from the eastern part of the San Joaquin–Huron area, such as near the town of Helm, indicate subsidence with periods of minor uplift resulting in a net loss of elevation of about 170 mm (fig. 13*C*). Water levels in many deep wells in this area reached historical lows during 2006–10, indicating that at least some of the subsidence measured in this area likely was inelastic (fig. 16*C*).

The InSAR results indicate that the Kettleman City area had periods of subsidence and uplift during 2003–10, resulting in a maximum net elevation loss of 110 mm (figs. 11, 12, 13*D*). Similar to the San Joaquin–Huron area, parts of the Kettleman City area subsided as part of the large subsidence feature centered near Pixley. Groundwater levels in shallow and deep wells declined in response to the 2007–10 drought, but only the shallow water levels reached historical lows during this period (fig. 16*D*). Although water levels in deep wells remained tens of meters above historical lows, the drawdowns were much larger than those in the shallow wells. Consequently, it is likely that most of the compaction measured using InSAR occurred in the deep aquifer system and was elastic, whereas small amounts of inelastic compaction may have resulted from the relatively small groundwater-level declines below historical lows in the shallow system.

Continued groundwater-level and land-subsidence monitoring in the San Joaquin Valley is important because (1) operational and drought-related reductions in surface-water deliveries since 1976 have resulted in increased groundwater pumping and associated water-level declines and land subsidence, (2) land use and associated pumping continue to change throughout the valley, and (3) subsidence management is stipulated in California's Sustainable Groundwater Management Act (SGMA). The availability of surface water remains uncertain; even during relatively wetter years, such as 2010–11, water deliveries fell short of requests. Future subsidence therefore remains a concern. Furthermore, even when surface water has been plentiful such as during 2017, the reduced conveyance capacities of canals owing to subsidence may hinder the ability to deliver it, as has occurred in the Friant-Kern Canal.

Continued data collection and integration can leverage the different spatial, temporal, and depth scales to improve conceptual models and numerical simulations of subsidence. Spatially detailed InSAR-derived maps of ground displacements could be processed annually, or more frequently (depending on data availability), to provide the spatial extent of the subsidence and to help guide the design of ground-based monitoring. Data from the extensometers (Oro Loma, Panoche, Fordel, Yearout, DWR Yard, and Rasta) could continue to be collected continuously with the potentiometers and data loggers, discretely with the associated dial gauges, or both, to provide depth-specific time series of compaction at specific locations. Data from the CGPS stations could continue to be collected and analyzed regularly, depending on data availability, to provide time series of subsidence at specific locations. Airborne InSAR data and geodetic surveys could be used to periodically monitor long and narrow infrastructure such as the California Aqueduct. The CGPS and extensometer data paired with continuous water-level data could continue to improve analysis of aquifer-system response and could be useful in detecting changes in the relationship between aquifer-system compaction and water levels and in identifying or calculating aquifer-system properties controlling subsidence.

Subsidence and compaction data, and aquifer-system storage properties derived from that data, can be used to improve numerical model simulations of groundwater flow and aquifer-system compaction. These data could be used as observations and as constraints for calibration of the numerical simulations. Numerical simulations can be used to examine water-level changes, storage changes, aquifer-system compaction, and subsidence. Often these simulations are used to make future projections based on various climatic or water-use scenarios. The projections can be used to test and (or) optimize various water-management alternatives, particularly those considering land subsidence as a management criterion, as required by the SGMA.

References

Bawden, G.W., Sneed, M., Stork, S.V., and Galloway, D.L., 2003, Measuring human-induced land subsidence from space: U.S. Geological Survey Fact Sheet 069–03, 4 p.

Belitz, K., and Heimes, F.J., 1990, Character and evolution of the ground-water flow system in the central part of the western San Joaquin Valley, California: U.S. Geological Survey Water-Supply Paper 2348, 28 p.

Bertoldi, G.L., 1989, Ground-water resources of the Central Valley of California: U.S. Geological Survey Open-File Report 89–251, 2 p.

Bertoldi, G.L., Johnston, R.H., and Evenson, K.D., 1991, Ground water in the Central Valley, California—A summary report: U.S. Geological Survey Professional Paper 1401–A, 44 p.

Borsa, A.A., Agnew, D.C., and Cayan, D.R., 2014, Ongoing drought-induced uplift in the western United States: Science, v. 345, no. 6204, p. 1587–1590, https://doi.org/10.1126/science.1260279.

Brandt, J.T., Bawden, G., and Sneed, M., 2005, Evaluating subsidence in the San Joaquin Valley, California, using InSAR [abs.]: Transactions of the American Geophysical Union, Fall Meeting 2005 Supplement, v. 85, no. 52.

Bull, W.B., 1964, Alluvial fans and near-surface subsidence in western Fresno County, California: U.S. Geological Survey Professional Paper 437–A, p. A1–A71.

Bull, W.B., 1972, Prehistoric near-surface subsidence cracks in western Fresno County, California: U.S. Geological Survey Professional Paper 437–C, 84 p.

Bull, W.B., 1975, Land subsidence due to ground-water withdrawal in the Los Banos–Kettleman City area, California; Part 2, Subsidence and compaction of deposits: U.S. Geological Survey Professional Paper 437–F, 90 p.

Bull, W.B., and Miller, R.E., 1975, Land subsidence due to ground-water withdrawal in the Los Banos–Kettleman City area, California; Part 1, Changes in the hydrologic environment conducive to subsidence: U.S. Geological Survey Professional Paper 437–E, 70 p.

Bull, W.B., and Poland, J.F., 1975, Land subsidence due to ground-water withdrawal in the Los Banos–Kettleman City area, California; Part 3, Interrelations of water-level change, change in aquifer-system thickness, and subsidence: U.S. Geological Survey Professional Paper 437–G, 61 p.

California Department of Water Resources, 1998, California water plan update: California Department of Water Resources, Bulletin 160–98, v. 1, chap. 3, accessed March 1, 2018, at https://www.water.ca.gov/LegacyFiles/pubs/planning/california_water_plan_1998_update__bulletin_160-98_/b16098_vol1.pdf.

California Department of Water Resources, 2003, California's ground water update 2003: California Department of Water Resources, Bulletin 118, 246 p.

Davis, G.H., Green, J.H., Olmsted, F.H., and Brown, D.W., 1959, Ground-water conditions and storage capacity in the San Joaquin Valley, California: U.S. Geological Survey Water-Supply Paper 1469, 287 p.

Farr, T.G., Jones, C.E., and Liu, Zhen, 2015, Progress report—Subsidence in the Central Valley, California: California Department of Water Resources, 34 p., accessed July 26, 2017, at https://water.ca.gov/groundwater/docs/NASA_REPORT.pdf.

Farr, T.G., Jones, C.E., and Liu, Zhen, 2016, Progress report—Subsidence in California, March 2015–September 2016: California Department of Water Resources, 37 p., accessed July 26, 2017, at https://www.water.ca.gov/waterconditions/docs/2017/JPL%20subsidence%20report%20final%20for%20public%20dec%202016.pdf.

Farrar, C.D., and Bertoldi, G.L., 1988, Region 4, Central Valley and Pacific Coast Ranges, *in* Back, W., Rosenstein, J.S., and Seaber, P.R., eds., Hydrogeology: Boulder, Colo., Geological Society of America, Geology of North America, v. O–2, p. 59–67.

Faunt, C.C., ed., 2009, Groundwater availability of California's Central Valley: U.S. Geological Survey Professional Paper 1766, 225 p.

Freeman, L.A., 1996, Time-series ground-water-level and aquifer-system compaction data, Edwards Air Force Base, Antelope Valley, California, January 1991 through September 1993: U.S. Geological Survey Open-File Report 96–186, 32 p.

Galloway, D.L., Jones, D.R., and Ingebritsen, S.E., 1999, Land subsidence in the United States: U.S. Geological Survey Circular 1182, 175 p.

Galloway, D.L., and Riley, F.S., 1999, San Joaquin Valley, California—Largest human alteration of the Earth's surface, *in* Galloway, D.L., Jones, D.R., and Ingebritsen, S.E., eds., Land subsidence in the United States: U.S. Geological Survey Circular 1182, p. 23–34, accessed February 2, 2008, at http://pubs.usgs.gov/circ/circ1182/.

Hanson, R.T., 1989, Aquifer-system compaction, Tucson Basin and Avra Valley, Arizona: U.S. Geological Survey Water-Resources Investigations Report 88–4172, 69 p.

Helm, D.C., 1978, Field verification of a one-dimensional mathematical model for transient compaction and expansion of a confined aquifer system, *in* Verification of Mathematical and Physical Models in Hydraulic Engineering, Proceedings 26th Hydraulic Division Specialty Conference: American Society of Civil Engineers, p. 189–196.

Holzer, T.L., 1998, The history of the aquifer-drainage model, *in* Borchers, J.W, ed., Land subsidence case studies and current research: Proceedings of the Dr. Joseph F. Poland Symposium on Land Subsidence [Sacramento, Calif., October 4–5, 1995]: Association of Engineering Geologists, Special Publication no. 8, p. 7–12.

Hung, W.C., Hwang, C., Liou, J.C, Lin, Y.S., and Yang, H.L, 2012, Modeling aquifer-system compaction and predicting land subsidence in central Taiwan: Engineering Geology, v. 147–148, p. 78–90, https://doi.org/10.1016/j.enggeo.2012.07.018.

Inter-Agency Committee on Land Subsidence in the San Joaquin Valley, 1958, Progress report—Land subsidence investigations in the San Joaquin Valley, California, through 1957: Sacramento, Calif., Inter-Agency Committee on Land Subsidence in the San Joaquin Valley, 160 p., 45 pls.

Ireland, R.L., 1986, Land subsidence in the San Joaquin Valley, California, as of 1983: U.S. Geological Survey Water-Resources Investigations Report 85–4196, 50 p.

Ireland R.L., Poland, J.F., and Riley, F.S., 1984, Land subsidence in the San Joaquin Valley, California, as of 1980: U.S. Geological Survey Professional Paper 437–I, 93 p., accessed August 18, 2008, at https://pubs.er.usgs.gov/usgspubs/pp/pp437I.

Isaaks, E.H., and Srivastava, R.M., 1989, An introduction to applied geostatistics: New York, N.Y., Oxford University Press, 561 p.

Jet Propulsion Laboratory, 2018, NASA-ISRO SAR (NISAR) Mission Science Users' Handbook: California Institute of Technology, v.1, 320 p., accessed October 4, 2018, at https://nisar.jpl.nasa.gov/files/nisar/NISAR_Science_Users_Handbook.pdf.

Johnson, A.I., Moston, R.P., and Morris D.A., 1968, Physical and hydrologic properties of water-bearing deposits in subsiding areas in central California: U.S. Geological Survey Professional Paper 497–A, 71 p., 14 pls.

Langbein, John, 2008, Noise in GPS displacement measurements from Southern California and Southern Nevada: Journal of Geophysical Research, v. 113, no. B5, 12 p., https://doi.org/10.1029/2007JB005247.

Leake, S.A., and Prudic, D.E., 1991, Documentation of a computer program to simulate aquifer-system compaction using the modular finite-difference groundwater flow model: U.S. Geological Survey Techniques of Water-Resources Investigations, no. 6, chap. A2, 68 p.

Lofgren, B.E., 1961, Measurement of compaction of aquifer systems in areas of land subsidence, *in* Short papers in the geologic and hydrologic sciences, articles 1–146: U.S. Geological Survey Professional Paper 424–B, p. B49–B52.

Lofgren, B.E., 1975, Land subsidence due to ground-water withdrawal, Arvin-Maricopa area, California: U.S. Geological Survey Professional Paper 437–D, 55 p.

Lofgren, B.E., 1976, Hydrogeologic effects of subsidence, San Joaquin Valley, California: International Symposium on Land Subsidence, 2nd, Anaheim, California, December 13–17, program and abstracts, no. 12, unnumbered pages.

Lofgren, B.E., and Klausing, R.L., 1969, Land subsidence due to ground-water withdrawal, Tulare-Wasco area, California: U.S. Geological Survey Professional Paper 437–B, 103 p.

Luhdorff and Scalmanini Consulting Engineers, Borchers, J.W., and Carpenter, M., 2014, Land subsidence from groundwater use in California: California Water Foundations report, 193 p., accessed December 2, 2015, at https://water.ca.gov/LegacyFiles/waterplan/docs/cwpu2013/Final/vol4/groundwater/13Land_Subsidence_Groundwater_Use.pdf.

Meade, R.H., 1964, Removal of water and rearrangement of particles during the compaction of clayey sediments—Review: U.S. Geological Survey Professional Paper 497–B, 23 p.

Meade, R.H., 1967, Petrology of sediments underlying areas of land subsidence in central California: U.S. Geological Survey Professional Paper 497–C, 83 p.

Meade, R.H., 1968, Compaction of sediments underlying areas of land subsidence in central California: U.S. Geological Survey Professional Paper 497–D, 39 p.

Meinzer, O.E., 1928, Compressibility and elasticity of artesian aquifers: Economic Geology, v. 23, no. 3, p. 263–291.

Miller, R.E., Green, J.H., and Davis, G.H., 1971, Geology of the compacting deposits in the Los Banos–Kettleman City subsidence area, California: U.S. Geological Survey Professional Paper 497–E, 46 p.

Moore, S.B., Winckel, J., Detwiler, S.J., Klasing, S.A., and Gaul, P.A., 1990, Fish and wildlife resources and agricultural drainage in the San Joaquin Valley, California: Sacramento, Calif., San Joaquin Valley Drainage Program, 974 p.

Moran, T., Choy, J., and Sanchez, C., 2014, The hidden costs of groundwater overdraft, *in* Understanding California's groundwater: Palo Alto, Calif., Stanford University, Water in the West, 11 p., accessed August 2, 2017, at http://waterinthewest.stanford.edu/groundwater/overdraft/.

National Geodetic Survey, variously dated, NGS survey marks: National Geodetic Survey Data Sheets, accessed September 7, 2018, at https://www.ngs.noaa.gov/datasheets/.

Page, R.W., 1986, Geology of the fresh ground-water basin of the Central Valley, California, with texture maps and sections: U.S. Geological Survey Professional Paper 1401–C, 54 p.

Page, R.W., and Bertoldi, G.L., 1983, A Pleistocene diatomaceous clay and a pumiceous ash: California Geology, v. 36, no. 1, p. 14–20.

Phillips, S.P., Carlson, C.S., Metzger, L.F., Howle, J.F., Galloway, D.L., Sneed, Michelle, Ikehara, M.E., Hudnut, K.W., and King, N.E., 2003, Analysis of tests of subsurface injection, storage, and recovery of freshwater in Lancaster, Antelope Valley, California: U.S. Geological Survey Water-Resources Investigations Report 03–4061, 122 p.

Planert, Michael, and Williams, J.S., 1995, Ground water atlas of the United States—Segment 1, California, Nevada: U.S. Geological Survey Hydrologic Atlas 730–B, 1 atlas, 28 p.

Poland, J.F., 1984, Guidebook to studies of land subsidence due to ground-water withdrawal, vol. 40 *of* Studies and reports in hydrology: Paris, France, United Nations Educational, Scientific, and Cultural Organization (UNESCO), 305 p., 5 appendixes.

Poland, J.F., Lofgren, B.E., Ireland, R.L., and Pugh, A.G., 1975, Land subsidence in the San Joaquin Valley, California, as of 1972: U.S. Geological Survey Professional Paper 437–H, 78 p.

PRISM Climate Group, 2006, Precipitation data from PRISM data: PRISM Climate Group, Oregon State University, accessed June 4, 2018, at http://www.prism.oregonstate.edu/.

Quinn, N.W.T., and Faghih, J.A., 2008, WESTSIM—Groundwater conjunctive use, agricultural drainage and wetland return flow simulation on the west-side of the San Joaquin Basin, *in* Brush C.F., Miller N.L., eds., Proceedings of the California Central Valley Groundwater Modeling Workshop, July 10–11, 2008, Lawrence Berkeley National Laboratory, Berkeley, Calif.: California Water and Environmental Modeling Forum, p. 26–32.

R Development Core Team, 2008, R—A language and environment for statistical computing (ver. 2.8.1): Vienna, Austria, R Foundation for Statistical Computing, http://www.R-project.org/.

Riley, F.S., 1969, Analysis of borehole extensometer data from central California, *in* Tison, L.J., ed., Land subsidence: International Association of Hydrological Sciences Publication 89, v. 2, p. 423–431.

Riley, F.S., 1970, Land-surface tilting near Wheeler Ridge, southern San Joaquin Valley, California: U.S. Geological Survey Professional Paper 497–G, 29 p.

Riley, F.S., 1998, Mechanics of aquifer systems—The scientific legacy of Joseph F. Poland, *in* Borchers, J.W., ed., Land subsidence case studies and current research: Proceedings of the Dr. Joseph F. Poland Symposium on Land Subsidence [Sacramento, Calif., October 4–5, 1995]: Association of Engineering Geologists, Special Publication no. 8, p. 13–27.

Sandwell, D.T., Myer, D., Mellors, R., Shimada, M., Brooks, B., and Foster, J., 2008, Accuracy and resolution of ALOS interferometry: Vector deformation maps of the Father's Day Intrusion at Kilauea: IEEE Transactions on Geoscience and Remote Sensing, v. 46, no. 11, p. 3524–3534, https://doi.org/10.1109/TGRS.2008.2000634.

Sneed, M., 2001, Hydraulic and mechanical properties affecting ground-water flow and aquifer-system compaction, San Joaquin Valley, California: U.S. Geological Survey Open-File Report 01–35, 26 p.

Sneed, M., and Galloway, D.L., 2000, Aquifer-system compaction and land subsidence—Measurements, analyses, and simulations—the Holly site, Edwards Air Force Base, Antelope Valley, California: U.S. Geological Survey Water-Resources Investigations Report 00–4015, 65 p.

Sneed, M., and Brandt, J.T., 2013, Detection and measurement of land subsidence using global positioning system and interferometric synthetic aperture radar, Coachella Valley, California, 1996–2005 (ver. 2.0, June 2013): U.S. Geological Survey Scientific Investigations Report 2007–5251, 31 p.

Sneed, M., Brandt, J., and Solt, M., 2013, Land subsidence along the Delta-Mendota Canal in the northern part of the San Joaquin Valley, 2003–10: U.S. Geological Survey Scientific Investigations Report 2013–5142, 87 p.

Sneed, M., and Phillips, S.P., 2012, Recently measured rapid land subsidence in Eastern San Joaquin Valley, California [abs]: Proceedings from the 2012 National Ground Water Association Summit, Anaheim, Calif., May 7–9, 2012.

Strozzi, T., Wegmüller, U., Werner, C., Teatini, P., and Tosi, L., 2005, SAR interferometric point target analysis and application to the monitoring of land subsidence in the Venice lagoon: Proceedings of the Seventh International Symposium on Land Subsidence, p. 417.

Swanson, A.A., 1998, Land subsidence in the San Joaquin Valley, updated to 1995, *in* Borchers, J.W., ed., Land subsidence case studies and current research: Proceedings of the Dr. Joseph F. Poland Symposium on Land Subsidence [Sacramento, Calif., October 4–5, 1995]: Association of Engineering Geologists, Special Publication no. 8, p. 75–79.

Terzaghi, K., 1925, Principles of soil mechanics—IV; Settlement and consolidation of clay: Erdbaumechanic, v. 95, no. 3, p. 874–878.

Thomas, H.E., and Phoenix, D.A., 1976, Summary appraisal of the Nation's ground-water resources—California region: U.S. Geological Survey Professional Paper 813–E, 51 p.

Wentworth, C.M., Fisher, G.R., Levine, P., and Jachens, R., 2012, The surface of crystalline basement, Great Valley and Sierra Nevada, California—A digital map database: U.S. Geological Survey Open-File Report 95–96, version 1.11, 18 p.

Werner, C., Wegmüller, U., Strozzi, T., and Wiesmann, A., 2003, Interferometric point target analysis for deformation mapping: IGARSS 2003, Institute of Electrical and Electronics Engineering, v. VII, p. 4362–4364.

Williams, S.D.P., Bock, Y., Fang, P., Jamason, P., Nikolaidis, R.M., Prawirodirdjo, L., Miller, M., and Johnson, D.J., 2004, Error analysis of continuous GPS position time series: Journal of Geophysical Research, v. 109, B03412, 19 p.

Williamson, A.K., Prudic, D.E., and Swain, L.A., 1989, Ground-water flow in the Central Valley, California: U.S. Geological Survey Professional Paper 1401–D, 127 p.

Zebker, H.A., Rosen, P.A., and Hensley, S., 1997, Atmospheric effects in interferometric synthetic aperture radar surface deformation and topographic maps: Journal of Geophysical Research, v. 102, p. 7547–7563.

Zerbini, S., Richter, B., Negusisi, M., Romagnoli, C., Simon, D., Domenichini, F., and Schwahn, W., 2001, Height and gravity variations by continuous GPS, gravity and environmental parameter observations in the southern Po Plain, near Bologna, Italy: Earth and Planetary Science Letters, v. 192, no. 3, p. 267–279.

Appendix 1. Interferometric Synthetic Aperture Radar (InSAR) Interferograms For The California Aqueduct In West-Central San Joaquin Valley, California

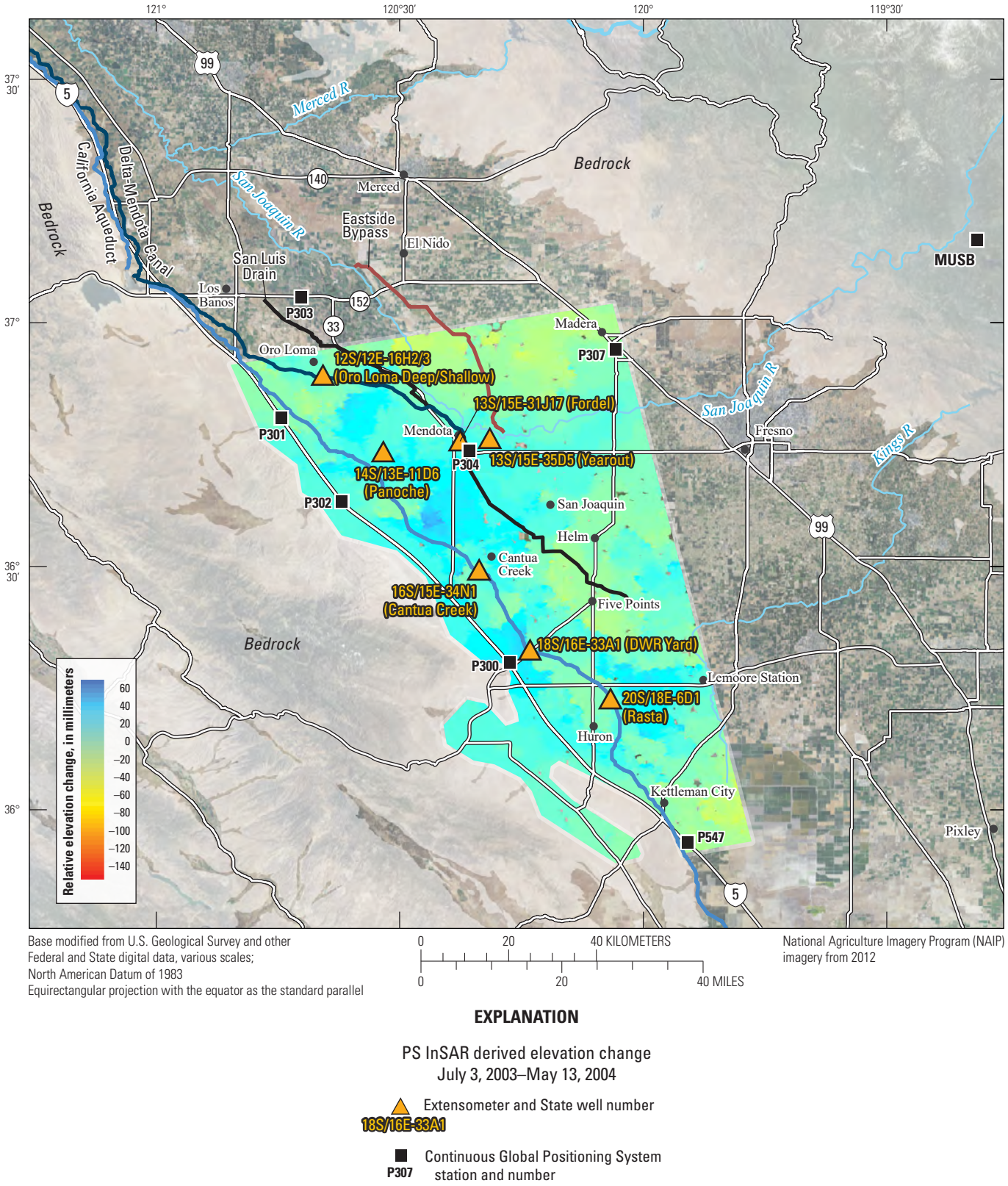

Base modified from U.S. Geological Survey and other Federal and State digital data, various scales; North American Datum of 1983 Equirectangular projection with the equator as the standard parallel

National Agriculture Imagery Program (NAIP) imagery from 2012

EXPLANATION

PS InSAR derived elevation change
July 3, 2003–May 13, 2004

Extensometer and State well number
18S/16E-33A1

P307 Continuous Global Positioning System station and number

Figure 1–1. Persistent scatterer Interferometric Synthetic Aperture Radar (PS InSAR) interferogram derived from Environmental Satellite (ENVISAT) data, July 3, 2003–May 13, 2004, for the California Aqueduct, west-central San Joaquin Valley, California. Negative relative elevation-change values indicate subsidence, and positive values indicate uplift. DWR, California Department of Water Resources.

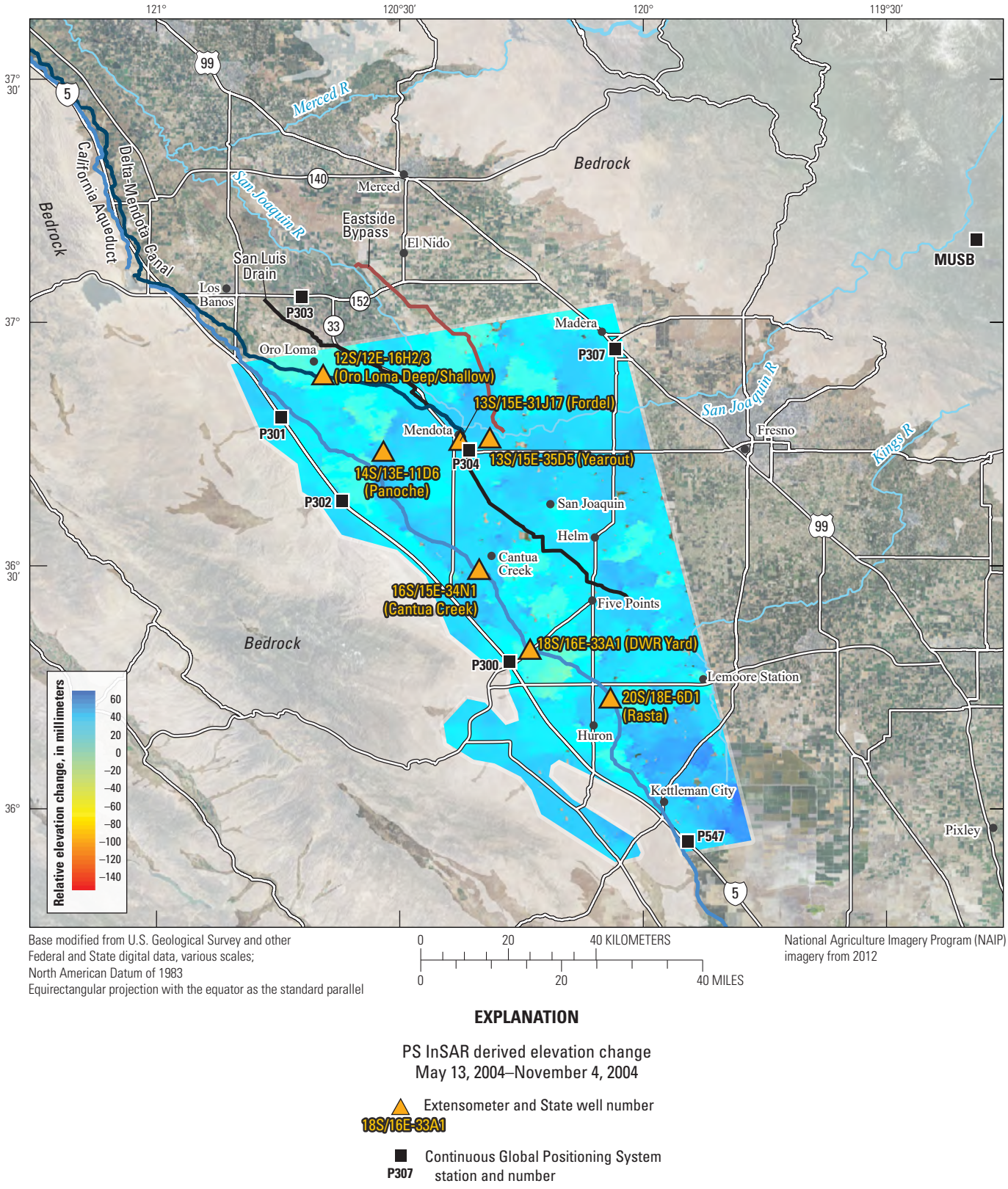

Base modified from U.S. Geological Survey and other Federal and State digital data, various scales; North American Datum of 1983 Equirectangular projection with the equator as the standard parallel

National Agriculture Imagery Program (NAIP) imagery from 2012

EXPLANATION

PS InSAR derived elevation change
May 13, 2004–November 4, 2004

Extensometer and State well number
18S/16E-33A1

Continuous Global Positioning System station and number
P307

Figure 1–2. Persistent scatterer Interferometric Synthetic Aperture Radar (PS InSAR) interferogram derived from Environmental Satellite (ENVISAT) data, May 13–November 4, 2004, for the California Aqueduct, west-central San Joaquin Valley, California. Negative relative elevation-change values indicate subsidence, and positive values indicate uplift. DWR, California Department of Water Resources.

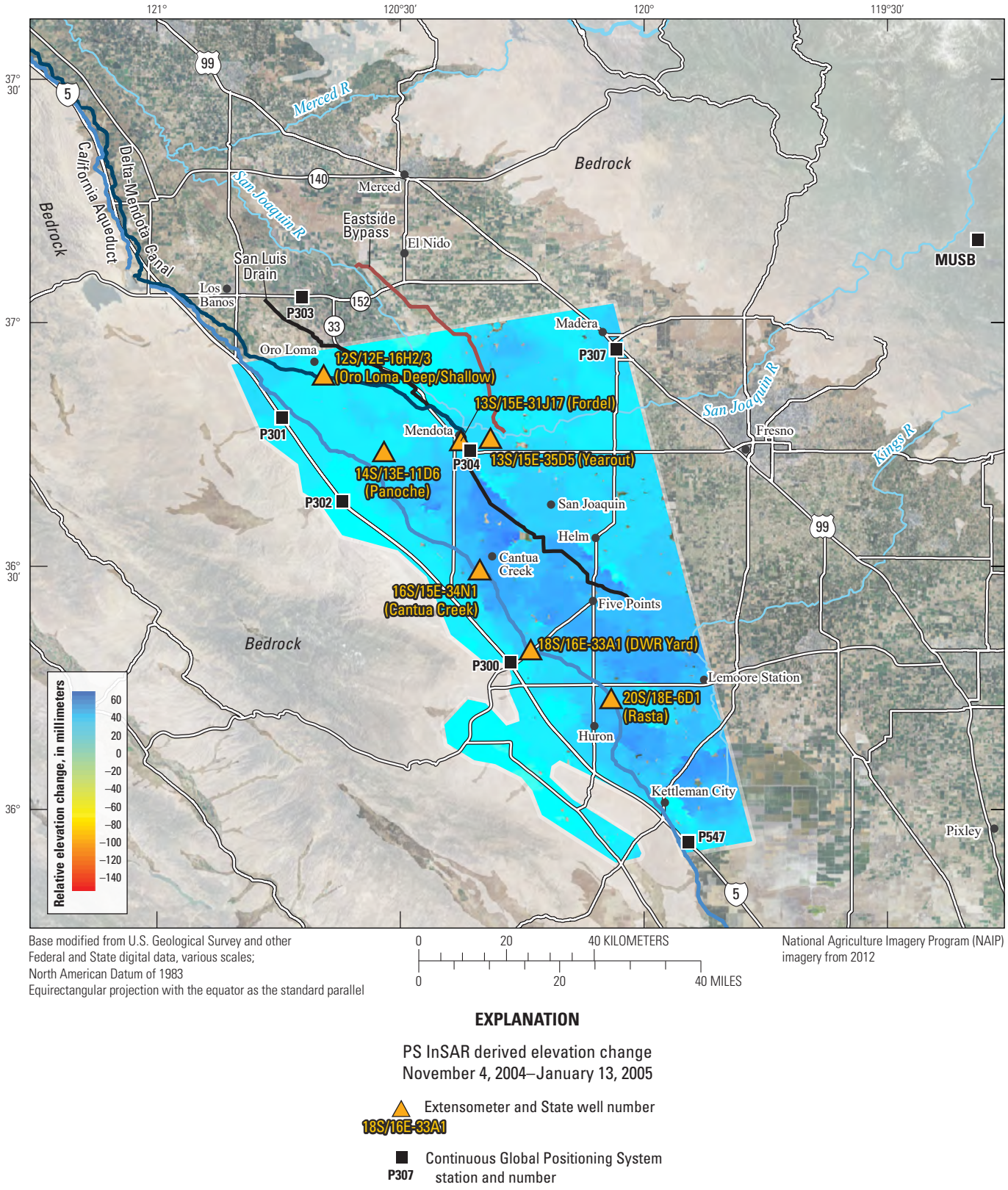

Figure 1–3. Persistent scatterer Interferometric Synthetic Aperture Radar (PS InSAR) interferogram derived from Environmental Satellite (ENVISAT) data, November 4, 2004–January 13, 2005, for the California Aqueduct, west-central San Joaquin Valley, California. Negative relative elevation-change values indicate subsidence, and positive values indicate uplift. DWR, California Department of Water Resources.

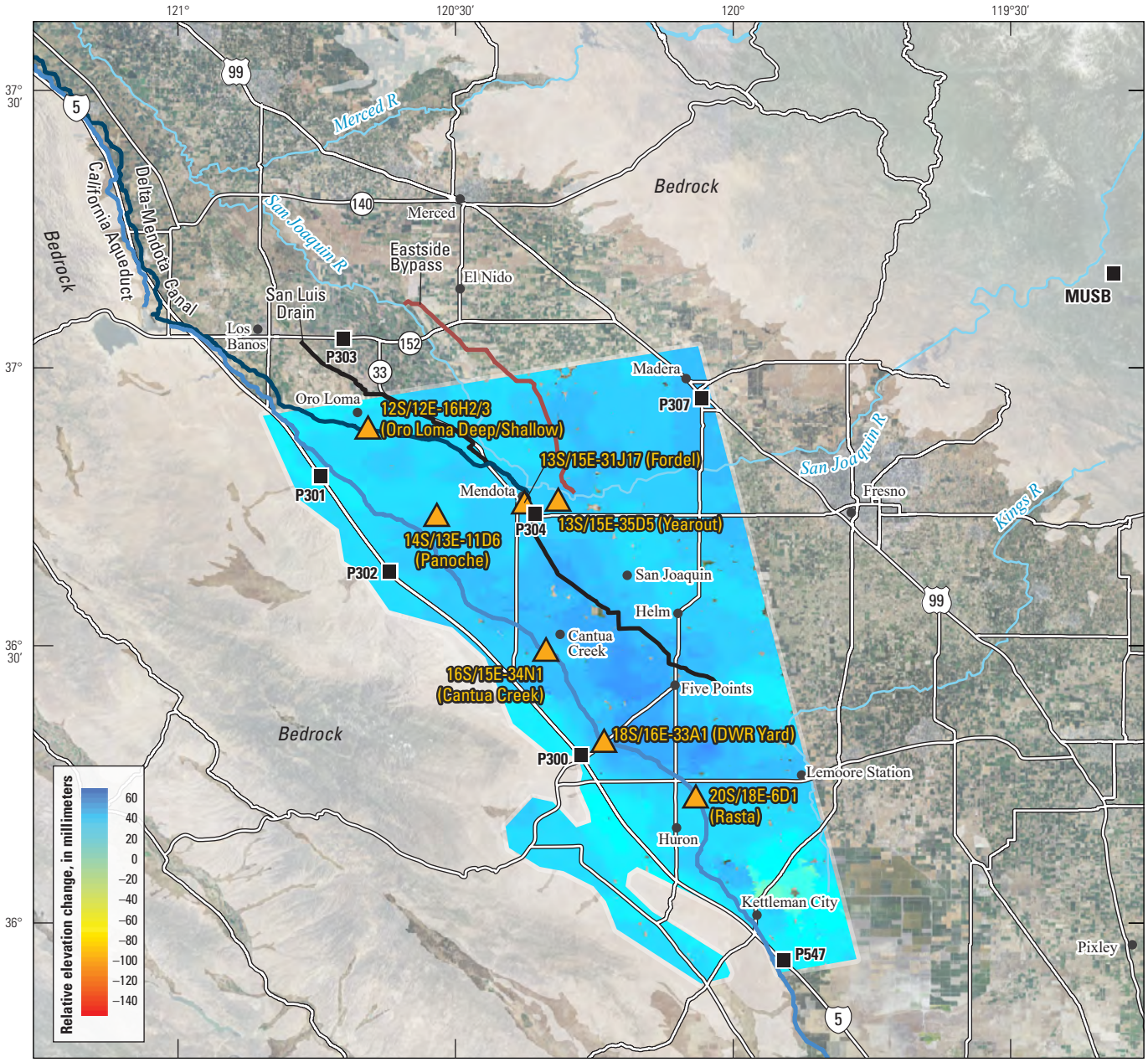

Base modified from U.S. Geological Survey and other Federal and State digital data, various scales; North American Datum of 1983 Equirectangular projection with the equator as the standard parallel

National Agriculture Imagery Program (NAIP) imagery from 2012

EXPLANATION

PS InSAR derived elevation change
January 13, 2005–March 24, 2005

Extensometer and State well number
18S/16E-33A1

Continuous Global Positioning System station and number
P307

Figure 1–4. Persistent scatterer Interferometric Synthetic Aperture Radar (PS InSAR) interferogram derived from Environmental Satellite (ENVISAT) data, January 13–March 24, 2005, for the California Aqueduct, west-central San Joaquin Valley, California. Negative relative elevation-change values indicate subsidence, and positive values indicate uplift. DWR, California Department of Water Resources.

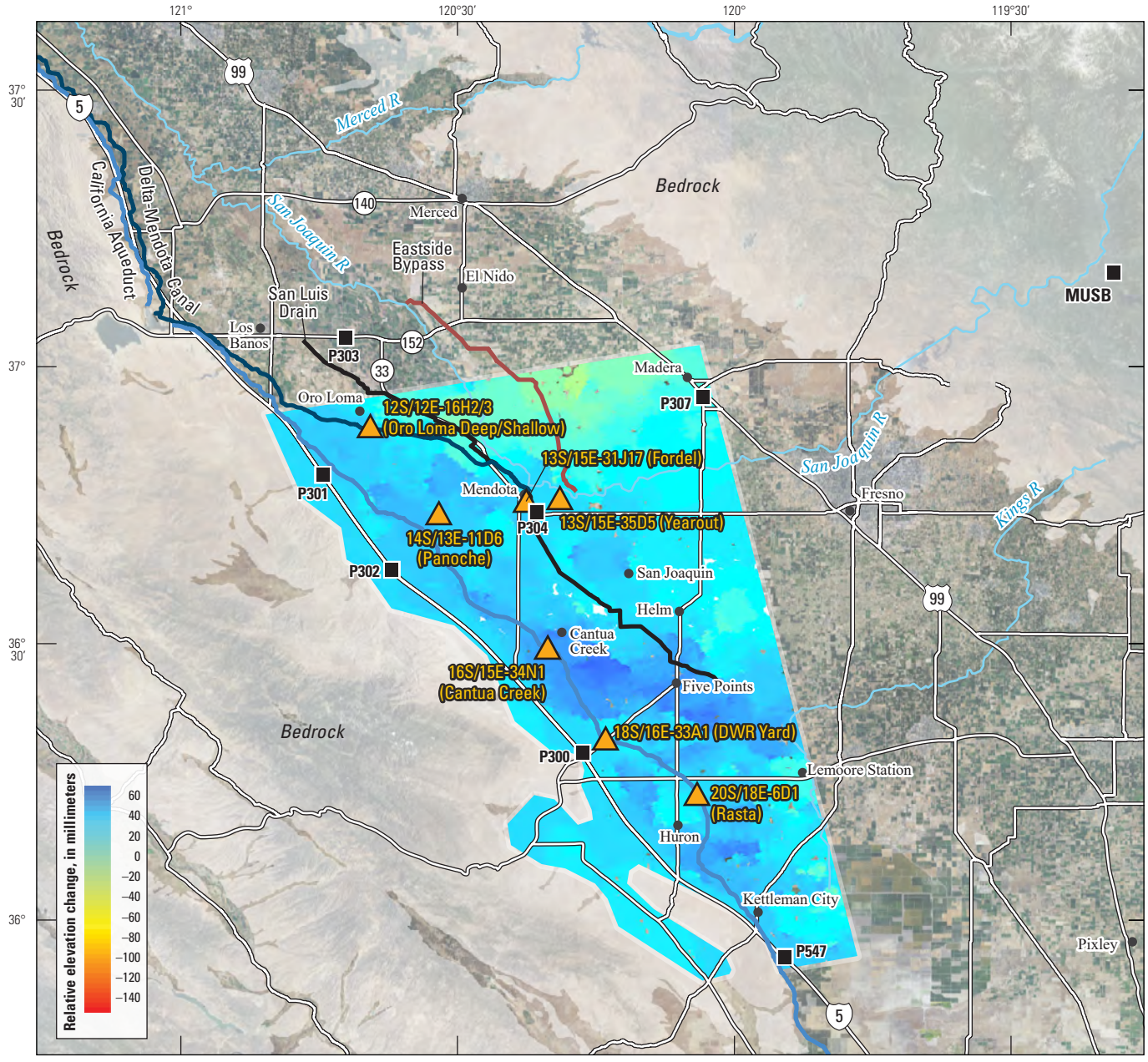

Base modified from U.S. Geological Survey and other Federal and State digital data, various scales; North American Datum of 1983 Equirectangular projection with the equator as the standard parallel

0 20 40 KILOMETERS
0 20 40 MILES

National Agriculture Imagery Program (NAIP) imagery from 2012

EXPLANATION

PS InSAR derived elevation change March 9, 2006–January 18, 2007

Extensometer and State well number
18S/16E-33A1

P307 Continuous Global Positioning System station and number

Figure 1–5. Persistent scatterer Interferometric Synthetic Aperture Radar (PS InSAR) interferogram derived from Environmental Satellite (ENVISAT) data, March 9, 2006–January 18, 2007, for the California Aqueduct, west-central San Joaquin Valley, California. Negative relative elevation-change values indicate subsidence, and positive values indicate uplift. Negative relative elevation-change values indicate subsidence, and positive values indicate uplift. DWR, California Department of Water Resources.

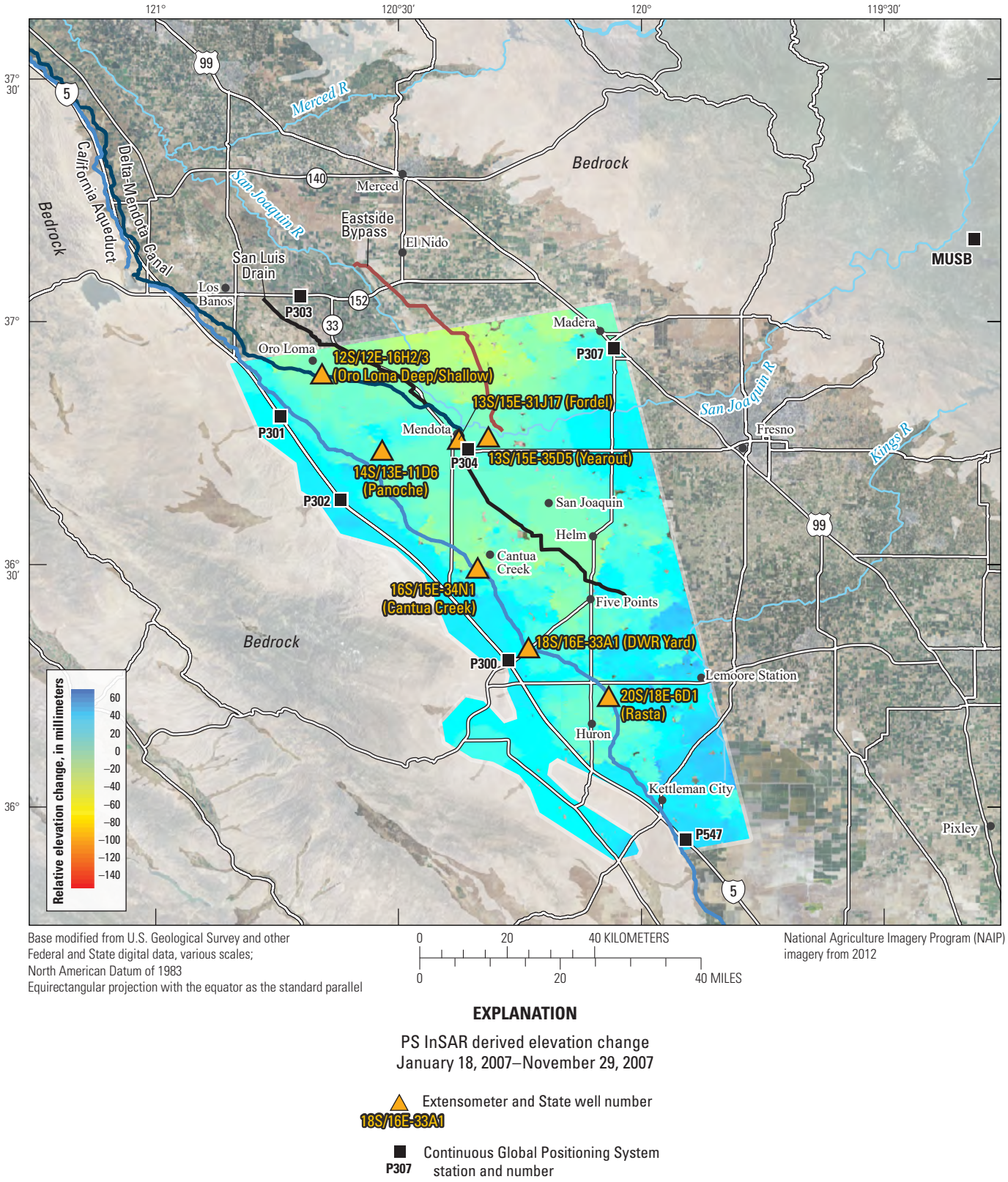

Figure 1–6. Persistent scatterer Interferometric Synthetic Aperture Radar (PS InSAR) interferogram derived from Environmental Satellite (ENVISAT) data, January 18–November 29, 2007, for the California Aqueduct, west-central San Joaquin Valley, California. Negative relative elevation-change values indicate subsidence, and positive values indicate uplift. DWR, California Department of Water Resources.

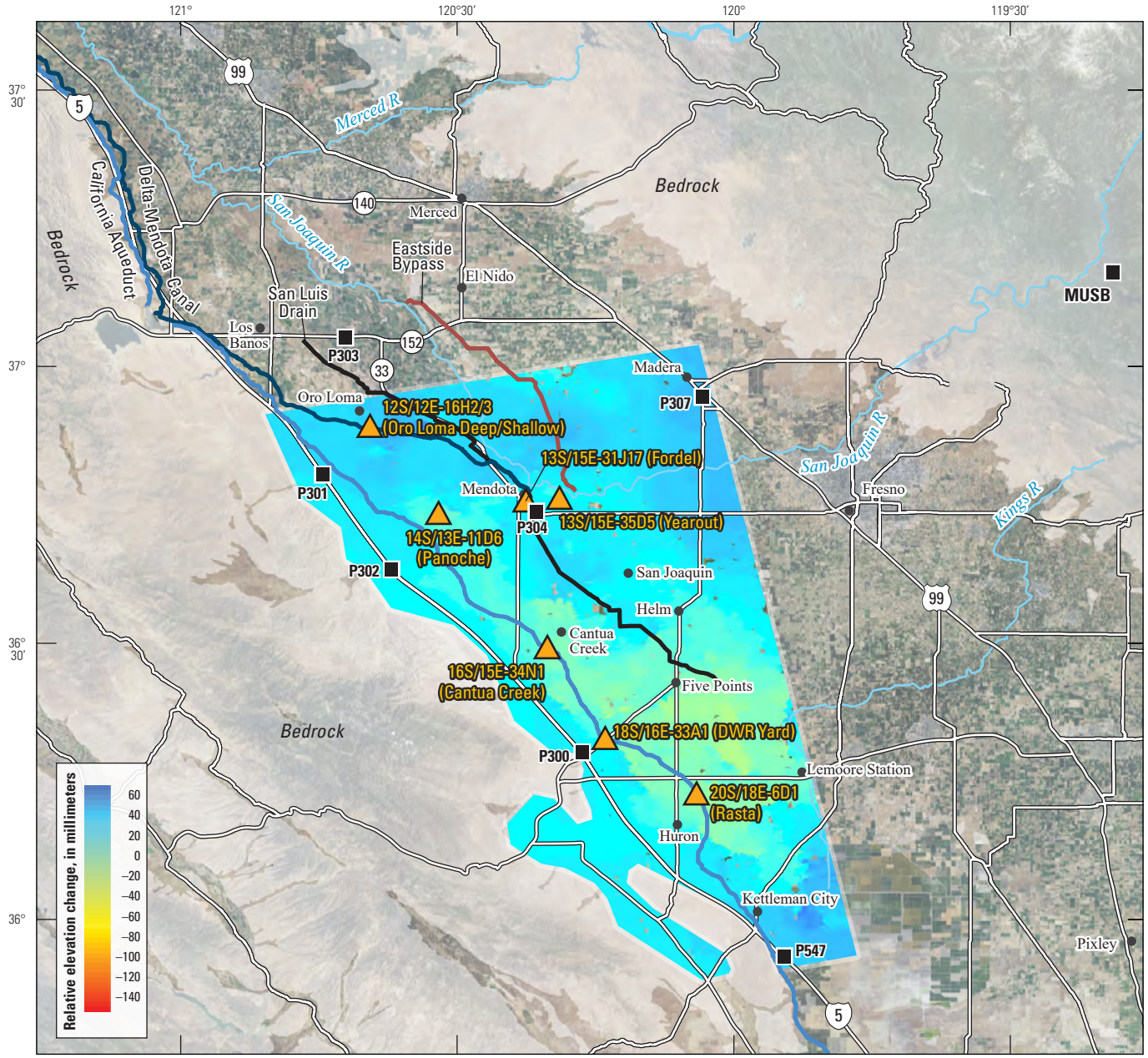

Figure 1–7. Persistent scatterer Interferometric Synthetic Aperture Radar (PS InSAR) interferogram derived from Environmental Satellite (ENVISAT) data, November 29, 2007–April 17, 2008, for the California Aqueduct, west-central San Joaquin Valley, California. Negative relative elevation-change values indicate subsidence, and positive values indicate uplift. DWR, California Department of Water Resources.

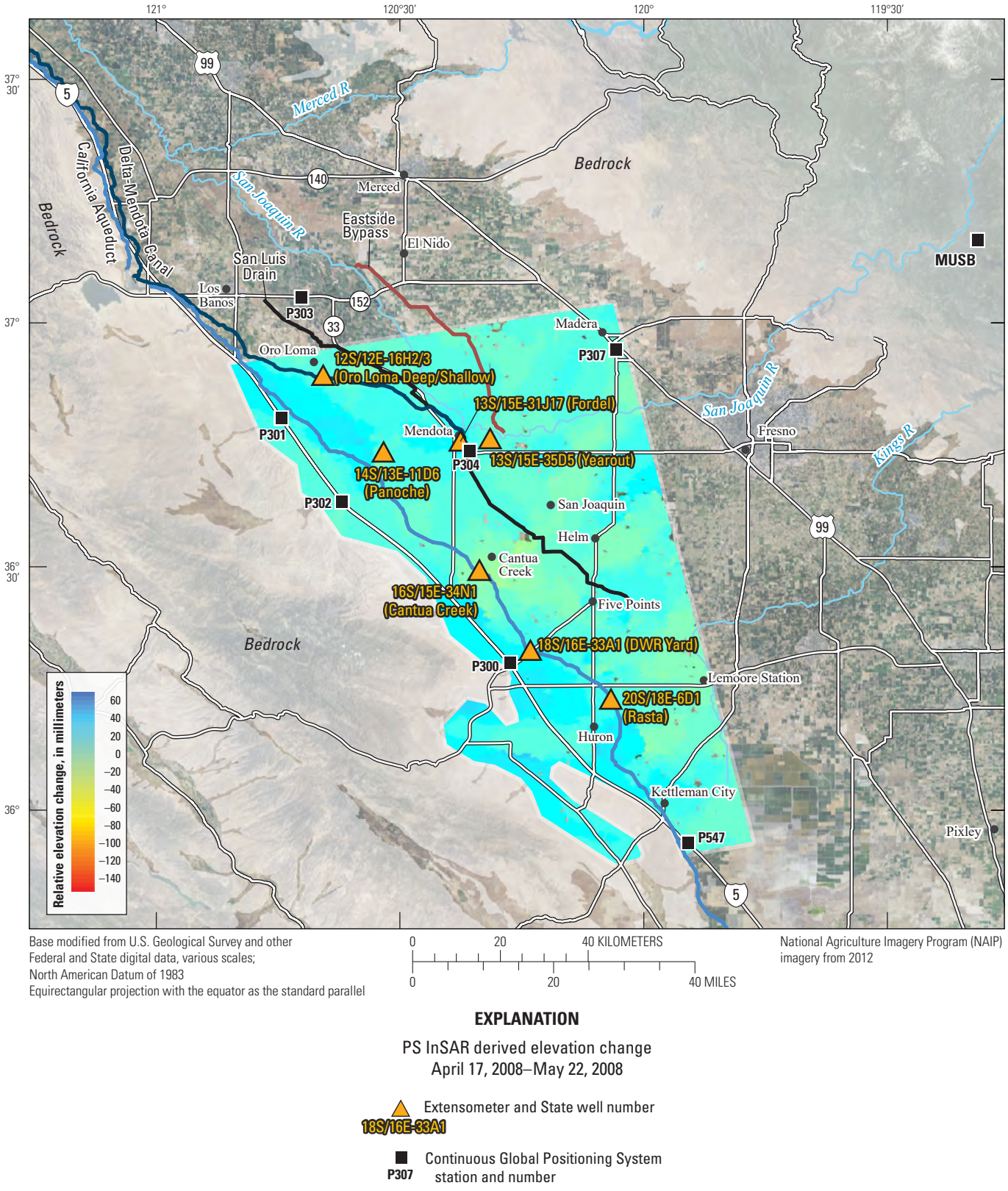

Figure 1–8. Persistent scatterer Interferometric Synthetic Aperture Radar (PS InSAR) interferogram derived from Environmental Satellite (ENVISAT) data, April 17–May 22, 2008, for the California Aqueduct, west-central San Joaquin Valley, California. Negative relative elevation-change values indicate subsidence, and positive values indicate uplift. DWR, California Department of Water Resources.

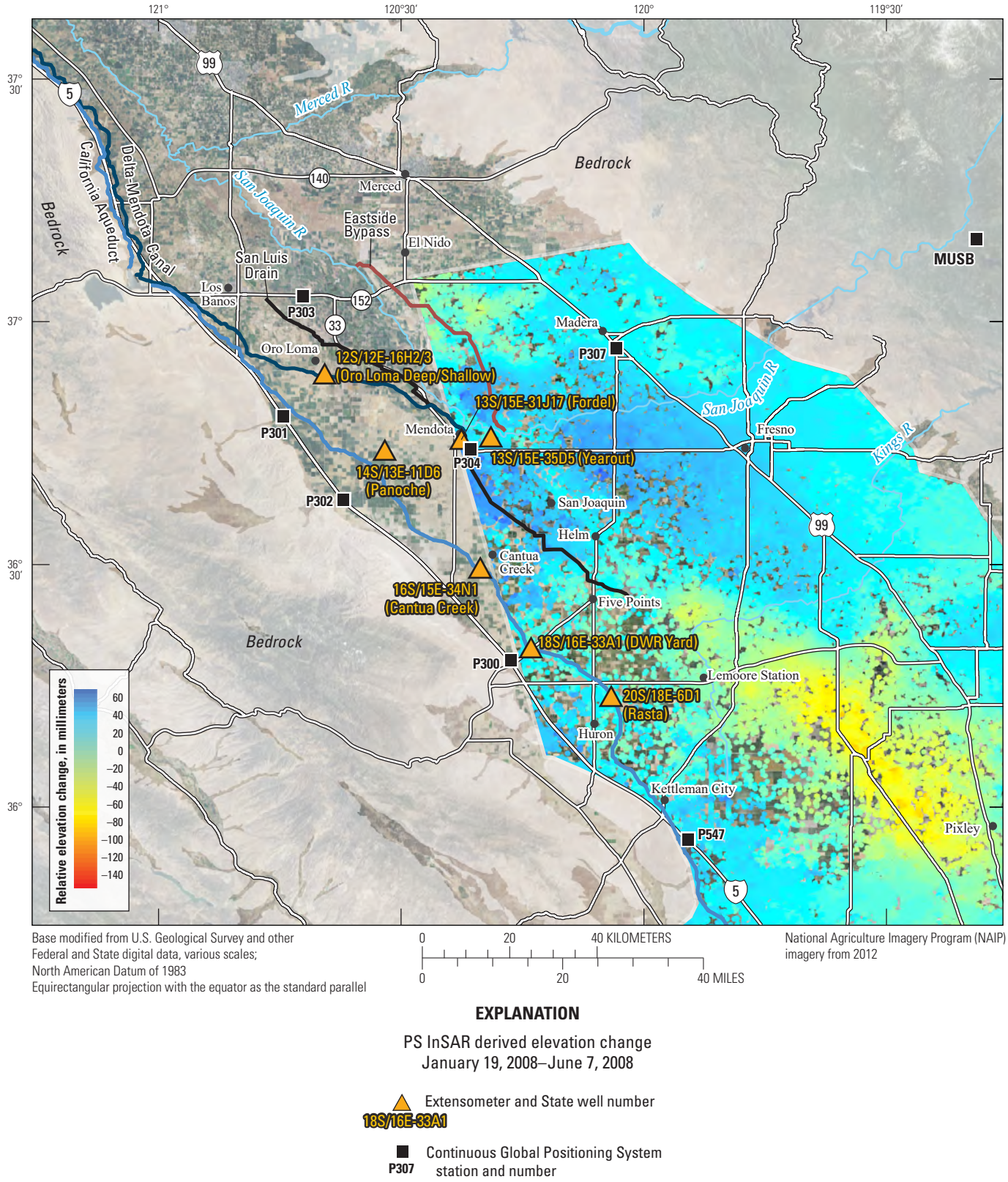

Base modified from U.S. Geological Survey and other Federal and State digital data, various scales; North American Datum of 1983 Equirectangular projection with the equator as the standard parallel

National Agriculture Imagery Program (NAIP) imagery from 2012

EXPLANATION

PS InSAR derived elevation change January 19, 2008–June 7, 2008

Extensometer and State well number
18S/16E-33A1

Continuous Global Positioning System station and number
P307

Figure 1–9. Persistent scatterer Interferometric Synthetic Aperture Radar (PS InSAR) interferogram derived from Environmental Satellite (ENVISAT) data, January 19–June 7, 2008, for the California Aqueduct, west-central San Joaquin Valley, California. Negative relative elevation-change values indicate subsidence, and positive values indicate uplift. DWR, California Department of Water Resources.

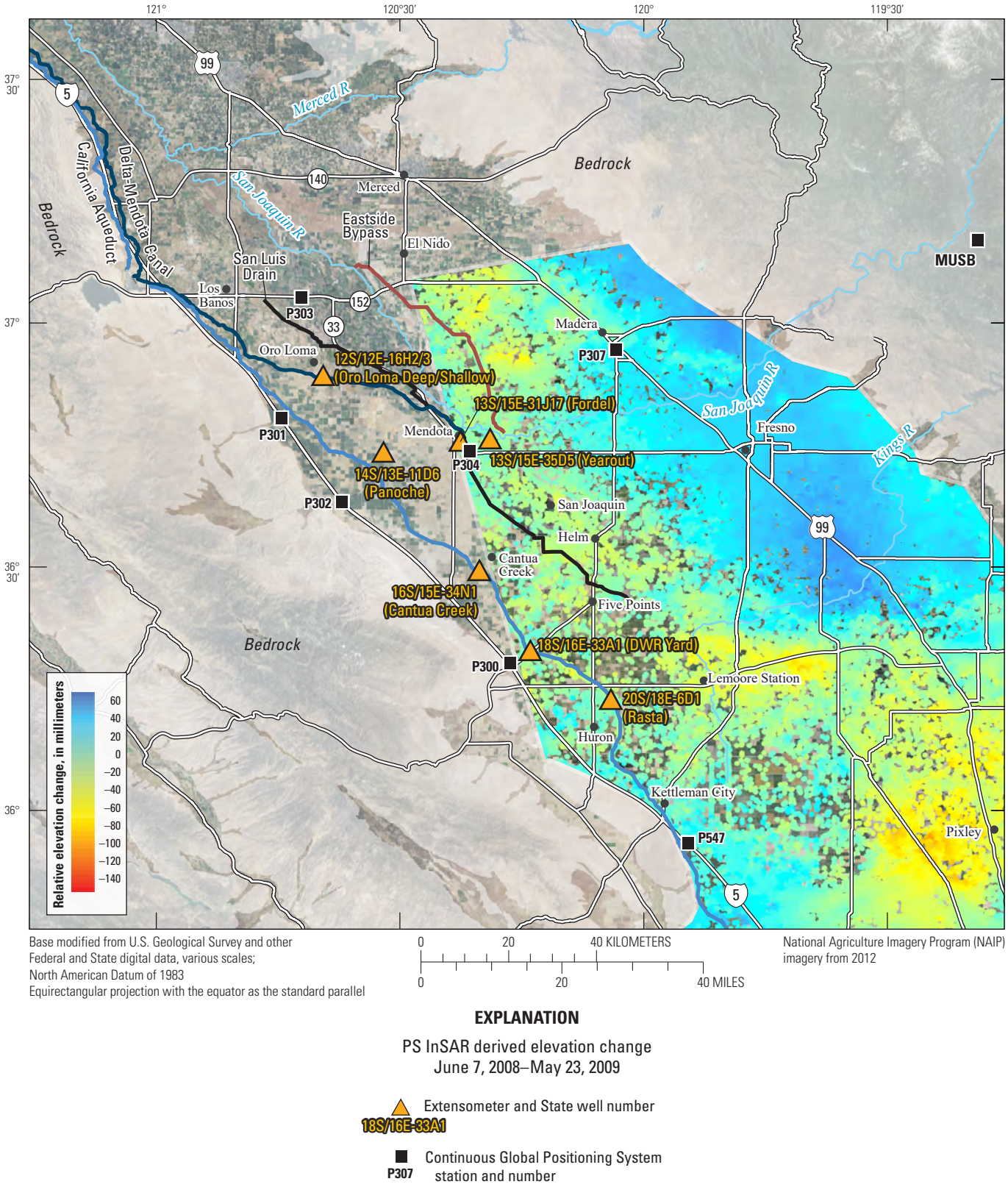

Figure 1–10. Persistent scatterer Interferometric Synthetic Aperture Radar (PS InSAR) interferogram derived from Environmental Satellite (ENVISAT) data, June 7, 2008–May 23, 2009, for the California Aqueduct, west-central San Joaquin Valley, California. Negative relative elevation-change values indicate subsidence, and positive values indicate uplift. DWR, California Department of Water Resources.

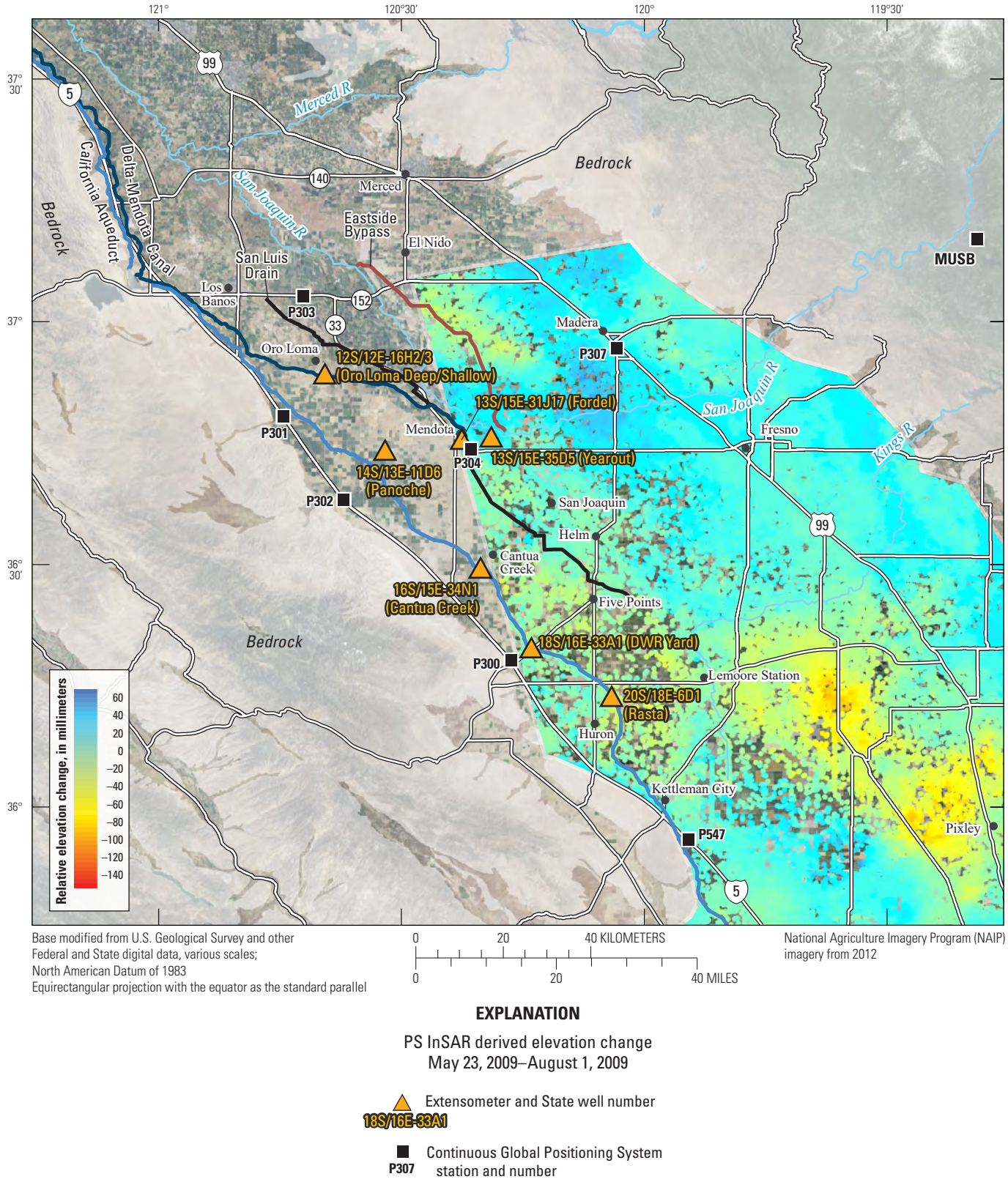

Figure 1–11. Persistent scatterer Interferometric Synthetic Aperture Radar (PS InSAR) interferogram derived from Environmental Satellite (ENVISAT) data, May 23–August 1, 2009, for the California Aqueduct, west-central San Joaquin Valley, California. Negative relative elevation-change values indicate subsidence, and positive values indicate uplift. DWR, California Department of Water Resources.

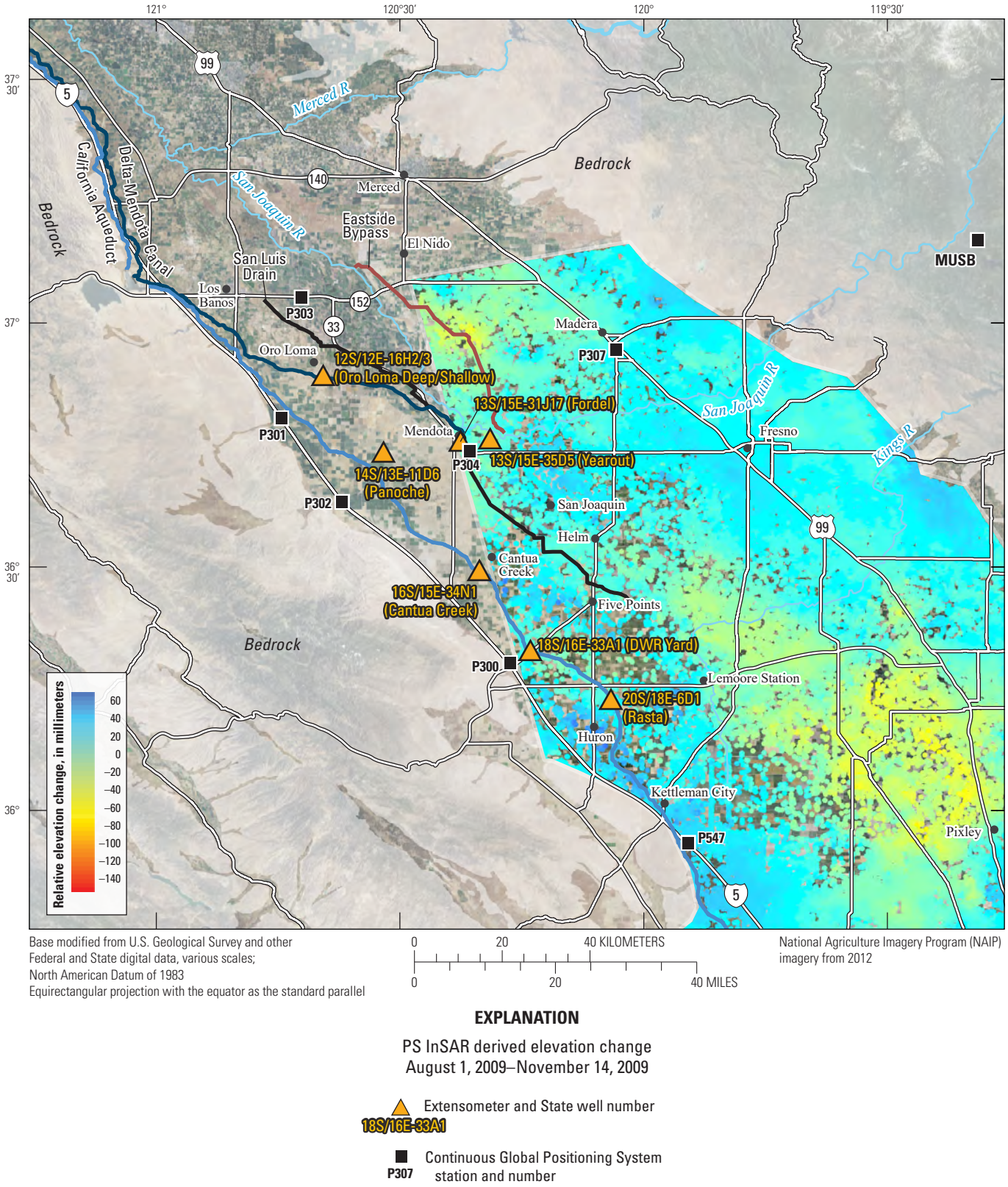

Figure 1–12. Persistent scatterer Interferometric Synthetic Aperture Radar (PS InSAR) interferogram derived from Environmental Satellite (ENVISAT) data, August 1–November 14, 2009, for the California Aqueduct, west-central San Joaquin Valley, California. Negative relative elevation-change values indicate subsidence, and positive values indicate uplift. DWR, California Department of Water Resources.

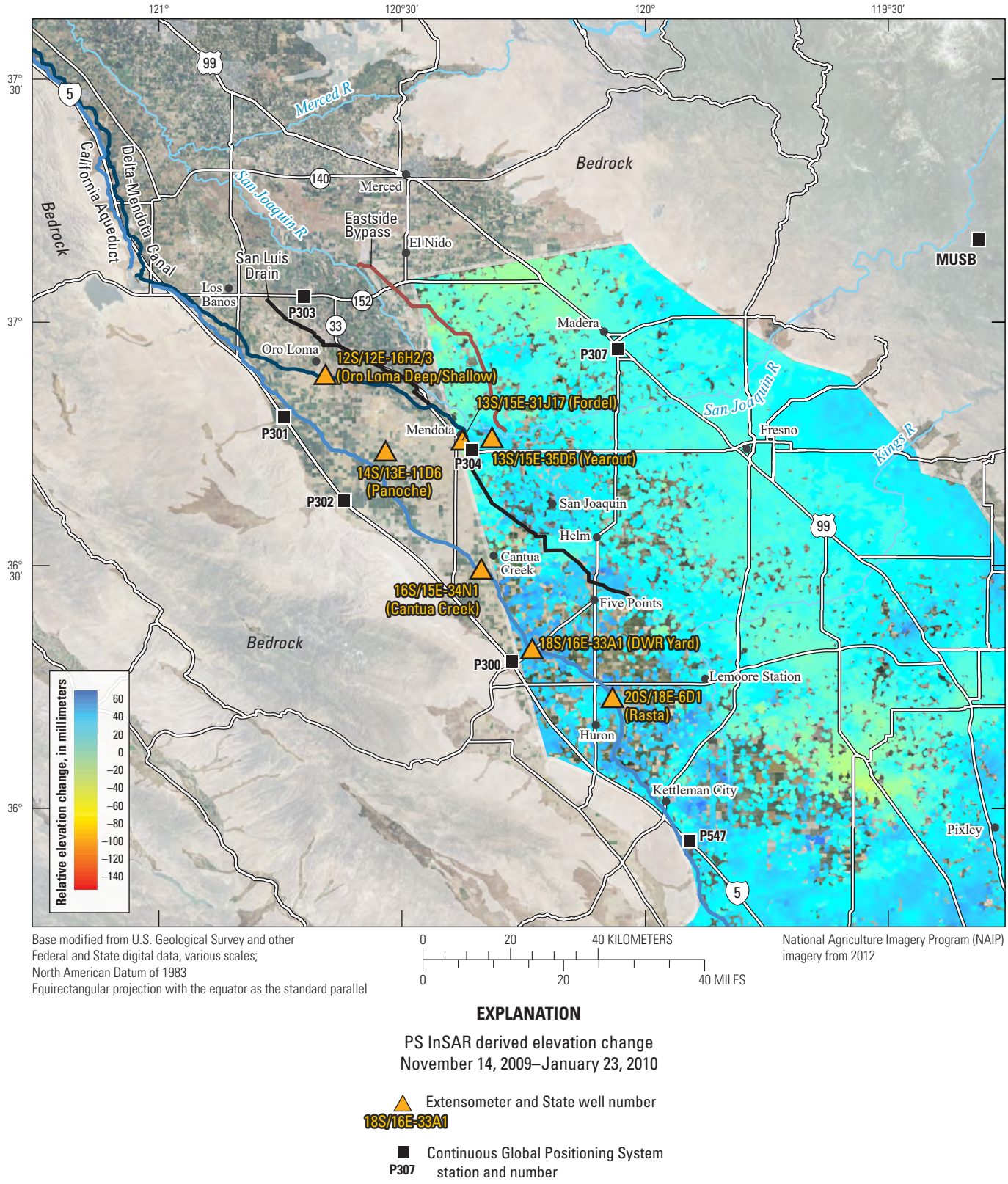

Figure 1–13. Persistent scatterer Interferometric Synthetic Aperture Radar (PS InSAR) interferogram derived from Environmental Satellite (ENVISAT) data, November 14, 2009–January 23, 2010, for the California Aqueduct, west-central San Joaquin Valley, California. Negative relative elevation-change values indicate subsidence, and positive values indicate uplift. DWR, California Department of Water Resources.

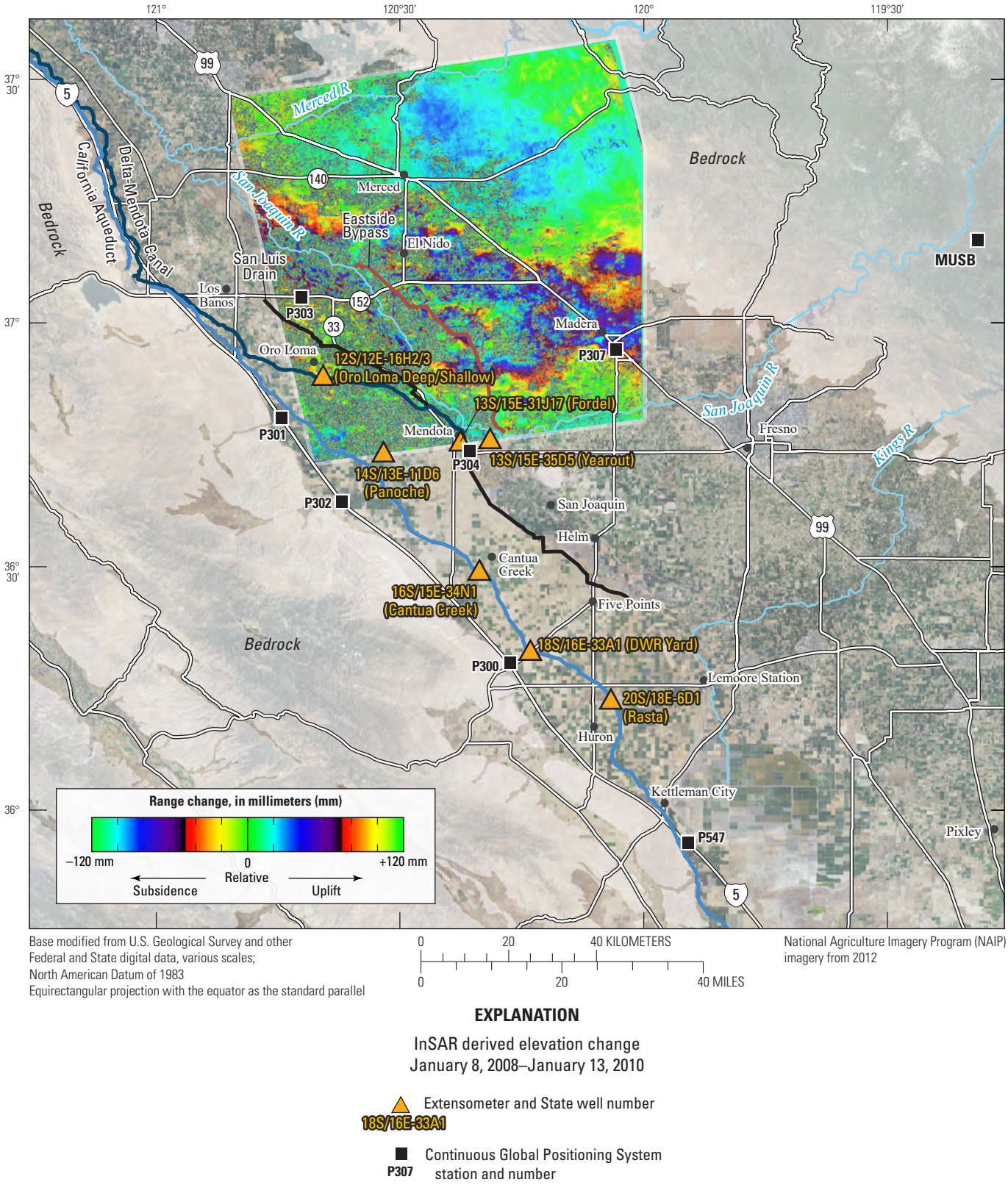

Figure 1–14. Interferometric Synthetic Aperture Radar (InSAR) interferogram derived from Advanced Land Observing Satellite (ALOS) data, January 8, 2008–January 13, 2010, for the Oro Loma–Madera area, San Joaquin Valley, California. The color progression purple-blue-cyan-green-yellow-red indicates relative subsidence; the opposite progression indicates relative uplift. See table 1 for more information about the interferograms. DWR, California Department of Water Resources.

Publishing support provided by the U.S. Geological Survey
Science Publishing Network, Sacramento Publishing Service Center

For more information concerning the research of this report, contact the
Director, California Water Science Center
U.S. Geological Survey
6000 J Street, Placer Hall
Sacramento, California 95819
http://ca.water.usgs.gov

ISSN 2328-0328 (online)
https://doi.org/10.3133/sir20185144